Growth and characterization by x-ray topography of highly perfect crystals

Majed Saeed Alourfi

GROWTH AND CHARACTERIZATION BY X-RAY TOPOGRAPHY OF HIGHLY PERFECT CRYSTALS

by

MAJED SAEED ALOURFI

(King Abdalaziz University, Jeddah, Saudi Arabia)

A thesis submitted to the University of Durham
for the Degree of Doctor of Philosophy

Department of Physics,
University of Durham, U.K.

November, 1989.

TO MY PARENTS

DECLARATION

I declare that this thesis is original. No part of it has been submitted previously for a degree at any other University. Work contained in Chapters three and four has been accepted for publication in "Journal of Crystal Growth".

CONTENTS

ABSTRACT

Single nickel crystals were grown from the melt by the Czochralski technique. Domain wall movements under applied magnetic fields were observed by using the Lang technique for X-ray topography. Magnetization measurements at room temperature were recorded and the variation of coercivity as a function of temperature was examined. Although low dislocation-density crystals were obtained, dislocation free growth was not achieved, copper single crystals were grown to compare the perfection with that of nickel. The effect of geometrical dimensions of crystal, neck, seed and neck angle on the temperature gradient at the interface of crystal and melt was examined theoretically using the model developed by Buckley-Golder and Humphreys. The model was extended to consider conical crystal and seed. It was found that for nickel the diameter had little effect on the thermal gradient. Increase of crystal cone angle led to a significant decrease in the thermal gradient at the interface. Real time movement of haematite domains under applied magnetic fields has been studied by synchrotron X-ray radiation topography.

PREFACE

The intrinsic properties of materials cannot be defined until a high perfect crystal has been grown. Single crystals can be grown by Solid, Vapour, Solution and Melt growth. High perfect metal crystals can be grown from the melt by the Czochralski technique. While the growth of large zero dislocation semiconductor crystals is by now well established, growth of zero dislocation metals single crystals still remains a problem. This is because dislocation formation in metal requires less energy than in semiconductors. Despite this difficulty, the conditions for the growth of dislocation - free copper and silver - have been established.

Chapter one is a review of X-ray topography with a brief examination of its application. Chapter two is a review of crystal growth from melt and solid state growth. Chapter three describes the perfection of single crystals of nickel and copper by the Czochralski technique. Domain movement and magnetization measurements for nickel, and the growth conditions for both nickel and copper are presented. Chapter four describes theoretical modelling to study the effect of the seed, neck, crystal dimensions and neck angle on reduction of temperature gradient and consequently the dislocation density. In Chapter five in real time magnetic domain were observed moving under an applied magnetic field by synchrotron radiation topography. Chapter six comprises the conclusions.

ACKNOWLEDGEMENTS

I would like to express deep gratitude and sincere appreciation to my supervisor Dr. B.K. Tanner for his guidance, encouragement, and assistance throughout my study at Durham and for introducing me to many other scholars from whom I have benefited.

I wish to thank all my colleagues in the Solid State group, both past and present for their interest in my work and their help in various ways. In particular I would like to thank Dr. D.B. Lambrick, Dr. G.S. Green and Miss S.M. Thompson for many constructive discussions. I would like to thank Dr. A.A. Joherji for assistance with the computation.

I wish to thank Professor A.W. Wolfendale, FRS, and Professor B.H. Bransden for the use of the Physics Department's facilities. The staff of the Electronics Workshop and the staff of the Student Workshop are thanked for their help and I wish to thank Mr. P. Foley and Mr. J. Scott for their helpful technical assistance. I would like to thank Mrs. M. Norman for typing this thesis.

I am deeply indebted to King Abdulaziz University in Jeddah for their financial support. I would like to thank the Saudi Arabian Educational office in London for taking care of my affairs in the U.K.

Last, but not least, my sincere thanks go to my parents, brother and sister for their support and encouragement from the very beginning and throughout my study.

CHAPTER 1

X-RAY DIFFRACTION TOPOGRAPHY

1.1 Introduction

X-ray topography is a non-destructive method of structural characterisation for studying lattice imperfections in a nearly perfect crystal. The technique is very similar to transmission electron microscopy since it reveals defects. X-ray diffraction is more sensitive to strain than is electron microscopy, this being due to the fact that the scattering of X-rays by a crystal is weaker than that by electrons. Thus the resolution is very poor compared with that of electron microscopy. The size of the X-ray image is a few micrometers whereas the electron microscopy image is a few hundred Ång stroms, therefore almost perfect crystals are required to reveal individual defects by this technique. A large area of thick crystal can be examined by this technique whereas only a small area of a thin crystal must be prepared for electron microscopy.

As crystal growth techniques improve and crystals with high perfection are produced, X-ray topography plays an important role in understanding the perfection of crystals and the relation to conditions of growth. The first book to cover all X-ray topography techniques was written by Tanner (1976).

1.2 Orientation Contrast

Orientation contrast arises in two ways: in monochromatic beams, diffraction occurs in one area: in polychromatic beams, diffraction will occur in different directions for different areas. It can be expressed by a simple geometrical relation (Figure 1.1) without using dynamical theory. Extinction contrast happens in an imperfect region which has a diffraction intensity different to that in a perfect region. The image can be interpreted only by the dynamical theory (Tanner, 1976).

1.3 The dynamical theory of X-ray diffraction

X-ray technique is concerned with recording the different intensity diffracted from deformed regions which differ from perfect regions of the crystal. It is clear from Bragg's Law -

$$\lambda = 2d \sin\theta_B$$

where λ is the radiation wavelength,

θ_B is the angle between incident beam and lattice plane and

d is the lattice spacing -

that this relation cannot be applied to both the perfect and the imperfect regions simultaneously. Thus there will be a difference in intensity between the two regions providing the image of the defect. The interpretation of this image requires a theory of X-ray diffraction. There are two basic diffraction theories: the kinematical theory and the dynamical theory.

The kinematical theory assumes that the amplitude of the

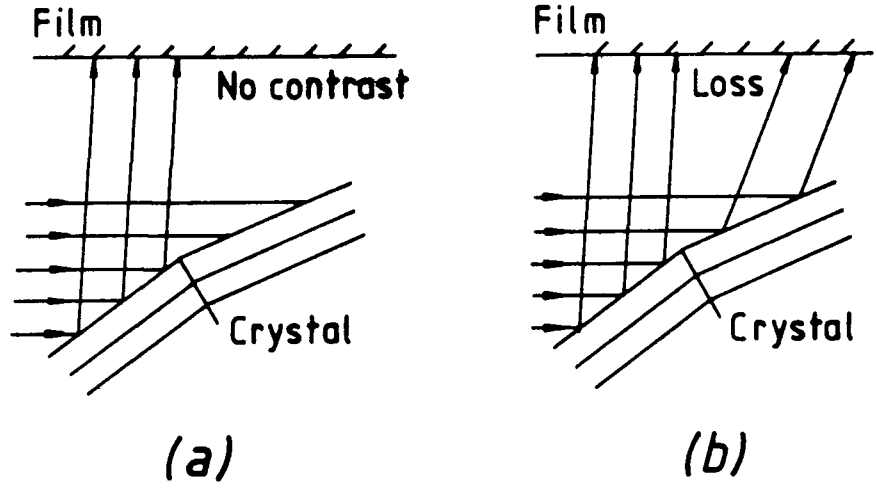

Fig. 1.1 (a) Orientation contrast from a monochromatic beam.

(b) Orientation contrast from a polychromatic beam (after Tanner, 1976).

diffracted beams are small compared with the incident beam amplitude. This theory is valid for small or imperfect crystals with mosaic structures.

When dealing with large single and highly perfect crystals, the amplitude of the diffracted beam becomes comparable with that of the incident beam. The interaction between the diffracted and incident beams is taken into account by the dynamical theory. The dynamical theory has been reviewed by Authier (1970) and Batterman and Cole (1964).

A solution of Maxwell's equation is required in a medium with periodic susceptibility (Tanner, 1977). The solution

$$\underline{D} = \exp \iota\omega t \; \Sigma \; \underline{D}_g \exp (-2\pi\iota \underline{K}_g . \underline{r})$$

is a satisfactory one and the component of the diffracted wave vector $\underline{K}_g$ is linked to the component wave vector of the incident beam $\underline{K}_o$ in reciprocal space corresponding to the reciprocal lattice vector $\underline{g}$ by the Laue equation

$$\underline{K}_g = \underline{K}_o + \underline{g}$$

The solution $\underline{D}$ inside the crystal represents a superposition of plane waves which form a wavefield. In X-ray diffraction usually we need only to consider the two waves which are associated with the refracted wave $\underline{K}_o$ and the Bragg reflected wave $\underline{K}_g$. We have a wavefield of the form

$$\underline{D} = \underline{D}_o \exp (-2\pi\iota \underline{K}_o . \underline{r}) + \underline{D}_g \exp (-2\pi\iota \underline{K}_g . \underline{r})$$

Substitution of this equation back into Maxwell's equation and the requirement for a non-trivial solution yields a relation between $\underline{K}_g$ and $\underline{K}_o$ and the amplitude ratio R

= $\underline{D}_g/\underline{D}_o$ in terms of $\underline{K}_g$ and $\underline{K}_o$, where $\underline{D}_g$ and $\underline{D}_o$ are the amplitude of the direct and diffracted wave component <u>inside</u> the crystal

$$\alpha_o\alpha_g = \frac{1}{4} k^2c^2\chi_g\chi_{\bar{g}} \; ; \; \chi_g \text{ is the fourier component of susceptibility.}$$

where

$$\alpha_o = \frac{1}{2k} (\underline{K}_o.\underline{K}_o - k^2 (1 + \chi_o)) \; ; \; \chi_o \text{ is the susceptibility}$$

$$\alpha_g = \frac{1}{2k} (\underline{K}_g.\underline{K}_g - k^2 (1 + \chi_o))$$

C is a polarisation factor = 1 for σ polarization, and = $\cos2\theta_B$ for π polarization, and $k = 1/\lambda$.

The relation between $\underline{K}_g$ and $\underline{K}_o$ when plotted graphically is known as the dispersion surface (Figure 1.2). Close to the Bragg reflection the degeneracy of the dispersion surface is raised. There are four branches, two for each polarization state. A point P on the dispersion surface is called the tie point. Each tie point on the dispersion surface defines the wave vector and the wave amplitude in the crystal.

When an incident wave excites two Bloch waves with different wave vectors, the interference between the Bloch waves gives rise to Pendellosung fringes. The depth corresponding to one period is known as the extinction distance. For the symmetric Laue geometry this is

$$\xi_g = \Lambda_o^{-1} = \pi V_c \cos\theta_B/r_e\lambda C \; (F_gF_{-g})$$

where

Λ_o diameter of dispersion surface,

V_c volume of unit cell,

r_e classical electron radius,

C polarization factor, and

F_g structure factor.

1.4 Anomalous transmission

The intensity of the wavefield is given by

$$I = D^2_o [1 + R^2 + 2RC \cos (2\pi \underline{g}.\underline{r})]$$

This shows that the intensity is modulated in correspondence with the cosine term, we have maximum at $\underline{g}.\underline{r}$ = n and minimum at $\underline{g}.\underline{r} = (2n + 1)/2$ with n integral.

On one branch of the dispersion surface, the wavefield has a maximum intensity at the atom planes on the other the minimum occurs. Since absorption takes place through the photoelectric effect, and since the electron density is greatest at the atomic planes, the wavefield with maximum intensity at the atomic planes is absorbed while the other is transmitted (Tanner, 1976). For example, in Figure (1.3), the branch 2 wave will be absorbed more than branch 1 wave. This is known as anomalous transmission or the Borrmann effect, which appears in perfect crystals. The presence of any imperfection will reduce or destroy it.

1.5 Lang's technique

The Lang technique (Lang, 1958) is the most commonly used topographic technique. The essential features of the method are explained in Figure (1.4).

Double images arising from Kα doublet can be avoided by collimating the incident beam by the first slit; the second slit will stop the transmitted beam from falling onto the potographic plate. If the crystal and the film are fixed and the incident beam is narrow, the image recorded on the plate

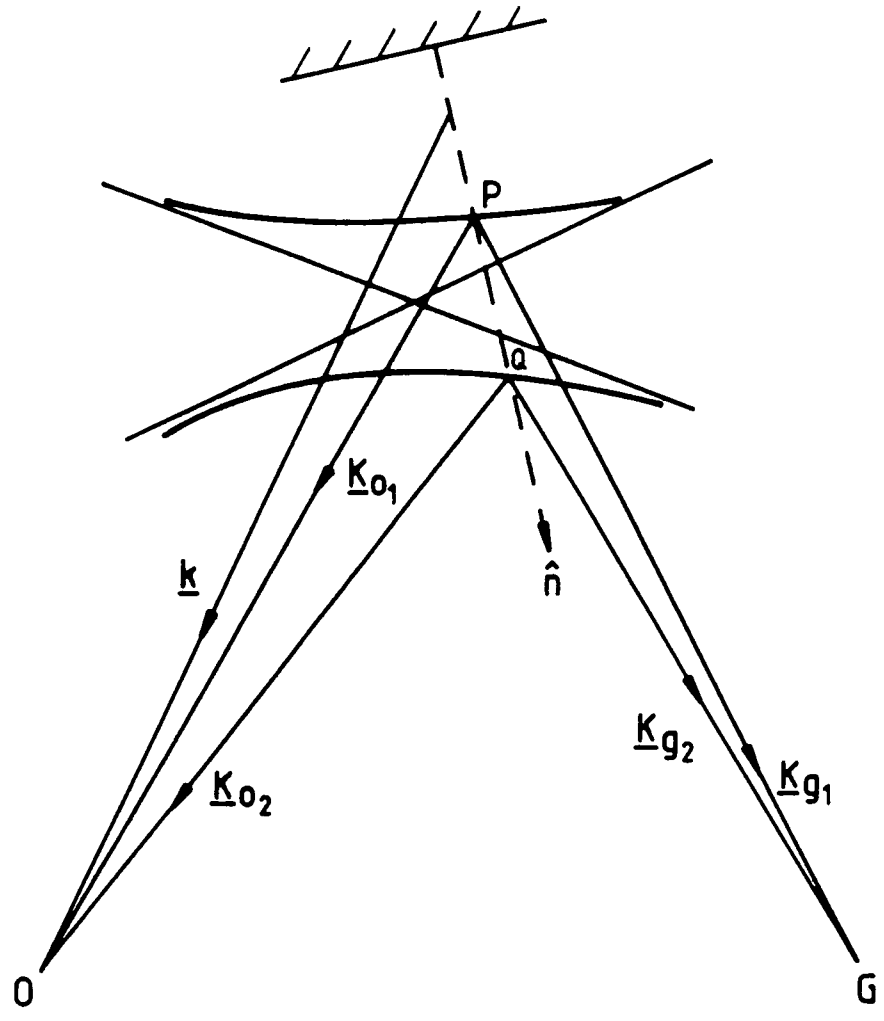

Fig. 1.2 The dispersion surface construction (after Tanner, 1977).

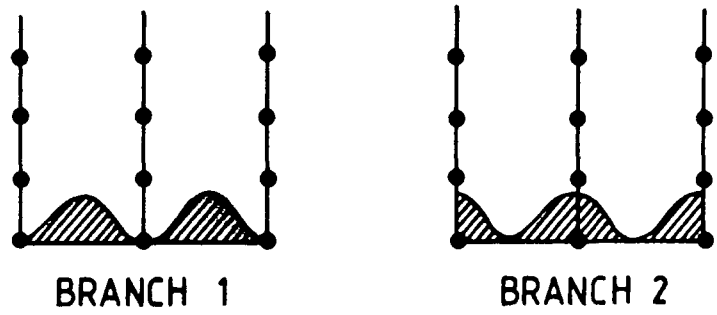

Fig. 1.3 Intensity of the two wavefields at the exact Bragg condition (after Tanner, 1976).

is called a section topograph. If the crystal and the topographic plate are traversed together the recorded image is called a projection topograph, (Lang, 1959).

A section topograph can be used to locate the position of the defect in the crystal. As a projection topograph is equivalent to a superposition of many section topographs, a large area of the crystal may be imaged in one setting. However, some of the information available in the fundamental section topograph will be blurred.

A modification of the projection topograph known as the limited projection topograph was developed by Lang (1963). It is a useful technique for studying the imperfections within crystals when it is undesirable to remove the strained surface (Figure 1.5).

1.6 X-ray topography using synchrotron radiation

The main complaint about X-ray topography (Tanner, 1976) has been the inordinate length of exposure time. With synchrotron radiation, however, the extremely high photon flux reduces exposure times to several seconds. Since the radiation is continuous each crystal plane selects its own wavelength for diffraction. All the crystal will thus be imaged at once; furthermore, imperfect crystals may also be used. The ability to increase the distance between the photograph plate and the specimen without undue loss of resolution enables the researcher to perform new experiments.

1.7 Some applications of X-ray topographic techniques

X-ray topography is a powerful method by which to reveal the defects in crystals and thus to determine their quality.

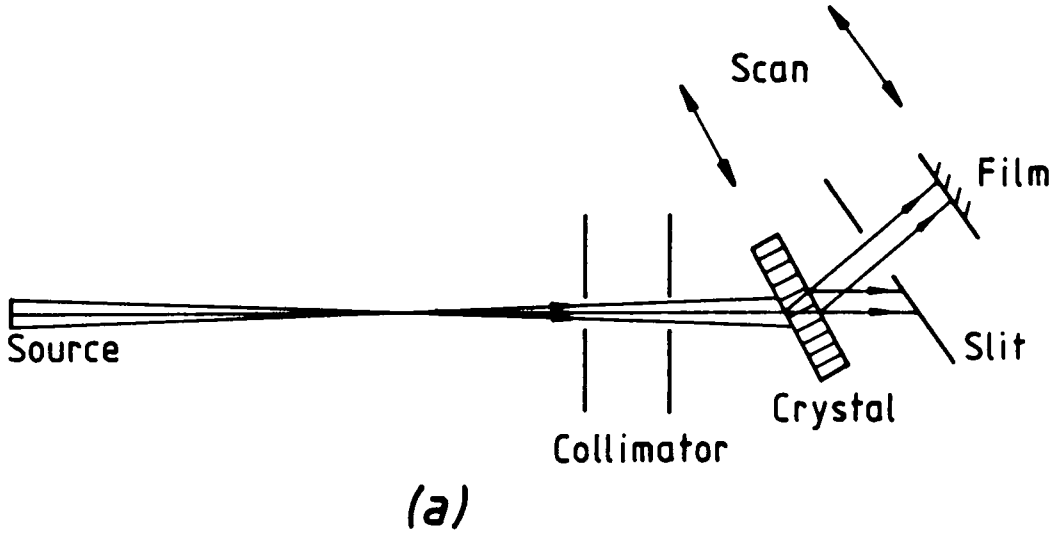

Fig. 1.4 Lang's transmission technique (after Tanner, 1976).

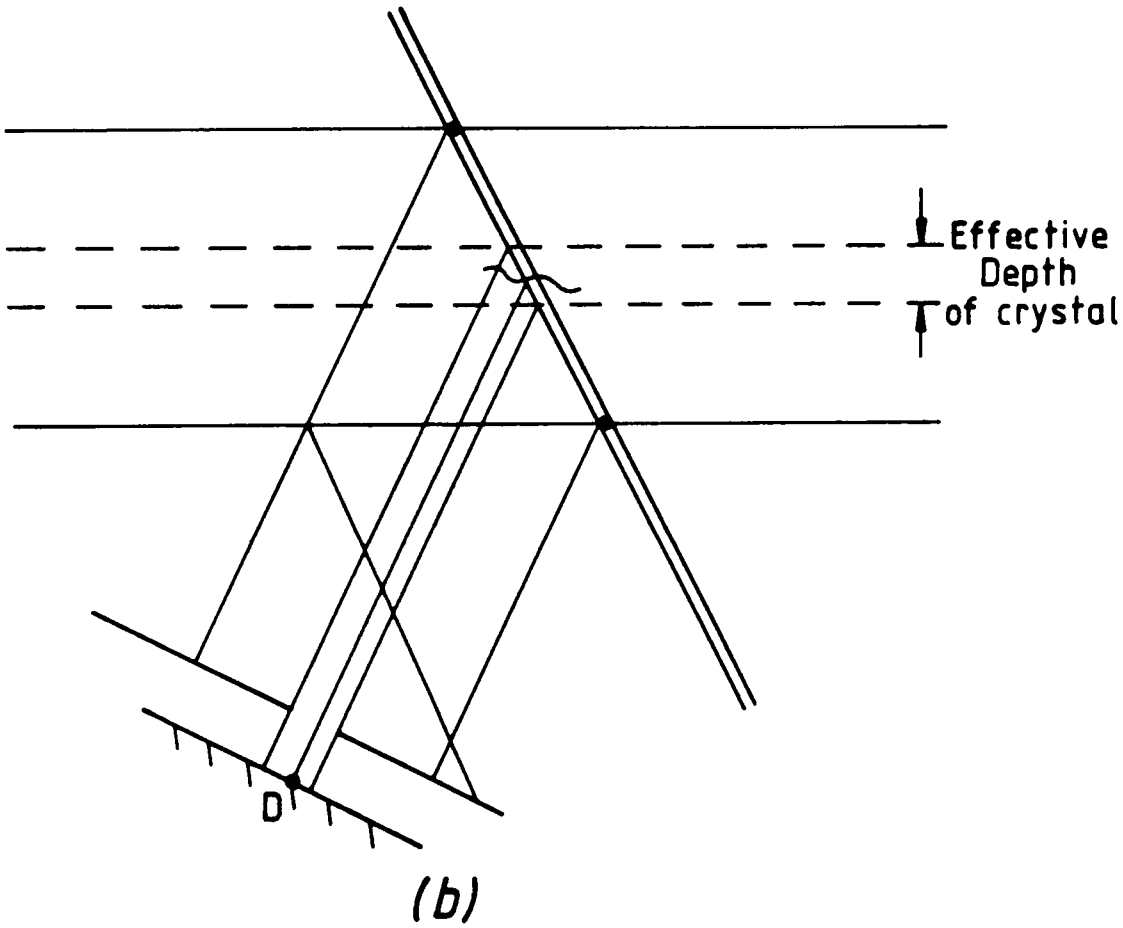

Fig. 1.5 The limited projection technique (after Tanner, 1976).

This non destructive technique enables the researcher to determine the best conditions in which to obtain a high quality crystal. The book edited by Tanner and Bowen (1980) reviews the techniques and their application.

1.7.1 Lang's technique

This technique was used by Badrick and Puttick (1971). They found that the cooling rate is an important factor in improving crystal quality. The topographs taken for slices of cadmium crystals after annealing reveal dislocation loops within sub-grains. The first observation of magnetic domains by this method was by Polcarova and Lang (1962). The domain structure of Fe-Si single crystals moved after an external magnetic field was applied.

Dislocation configurations were studied by Nes and Nøst (1966). They report that the dislocation density of a single aluminium crystal increases by stepping up the cooling rate. A small resistance furnace was built on Lang's camera to record direct changes in dislocation density in a single aluminium crystal up to 400^{o}C during annealing treatment, Nøst and Sørensen (1966).

1.7.2 Synchrotron white beam technique

The topographs taken by Tanner et al. (1977) shows that the image taken by synchrotron radiation is similar to that obtained by Lang's technique except for the fact that small cracked regions appear in the former method because the beam has a continuous spectrum.

Large distortions in SiC specimen have been studied by

this technique whereas it is impossible to study them by the Lang technique. This is because white radiation allows each structure to image simultaneously, Fisher and Barnes (1984).

Since step-by-step domain observations require a short exposure time synchrotron radiation is a very useful tool. Magnetic domains in an iron-silicon specimen are shown by Stephenson et al. (1979) to move under the influence of magnetic fields.

Jordan and Gastaldi (1979) used synchrotron radiation to study the boundary migration in aluminium during recrystallisation. They found that obstacles bent the grain boundaries which generated dislocations after they met each other.

1.8 Topographic resolution

In Lang's topograph there is no diffraction in the vertical plane, i.e. in the direction perpendicular to the plane of the incident and diffracted rays, and the resolution in the vertical direction is given approximately by

$$\delta = \frac{hX}{L}$$

where

L is the specimen - source distance,

X is the specimen - film distance, and

h is the projected high of the source.

Since L cannot be increased without loss of X-ray intensity X should always be small for a high quality topograph, (Figure 1.6).

The topographic resolution in the plane of the incident

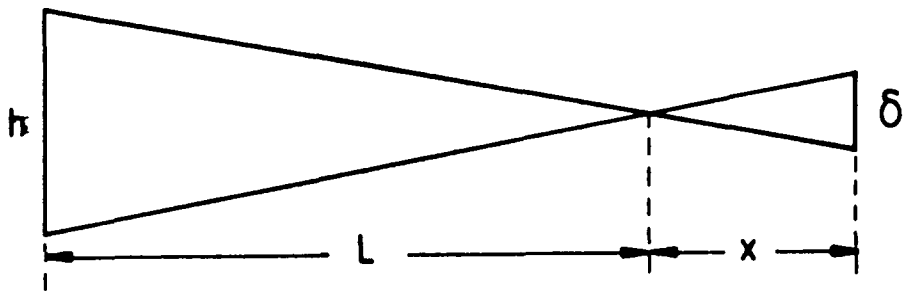

Fig. 1.6 Vertical resolution criteria (after Tanner, 1976).

and diffracted rays, the horizontal resolution, depends on the wavelength spread, the intrinsic angular range of reflection of the crystal, and vibration of the crystal during exposure.

The effect of the wavelength spread can be shown by differentiation of Bragg's Law

$$\Delta \theta_B = \tan \theta_B \frac{\Delta\lambda}{\lambda}$$

where

$\Delta\lambda$ is the wavelength spread, and

$\Delta\theta_B$ is the Bragg angle spread.

Each point in the image will be spread horizontally by

$$\Delta x = L \Delta\phi_{\alpha_1\alpha_2}$$

$\Delta\phi$ is the angular separation of the diffracted beam due to $K\alpha_1$ and $K\alpha_2$ lines. As a result of simultaneous diffraction of both $K\alpha_1$ and $K\alpha_2$ lines, double images will occur; for high resolution one image should be recorded.

In synchrotron radiation, the whole source contributes to the intensity diffracted by each point in the sample, and thus the resolution depends upon the effective source size. The horizontal and vertical resolutions are given by

$$r_H = XH/L$$

$$r_v = XV/L$$

where H and V are the horizontal and vertical dimensions of the source.

The processes involving exposure, developing and magnifying effect the resolution. X-ray topographs are usually recorded on Ilford L4 nuclear emulsion. It contains a very high concentration of silver halide and thus has a high

stopping power with minimum thickness of the emulsion. Thin emulsions suffer from poor absorption of X-rays, while thick emulsions suffer from the long processing time and loss of the resolution if the beam does not pass normally through the emulsion. Thus a compromise between efficiency and quality of resolution should be obtained. The average grain size of developed nuclear emulsion is about 0.25 micron, which is below the X-ray topographic resolution.

The details of the experimental procedure and processing of the nuclear plate have been given by Lang (1978).

1.9 Contrast of dislocations

There are three types of dislocation image in X-ray topography. The articles by Authier (1967, 1978) review the defect image formation.

In the deformed region (Tanner, 1976) some rays of the divergent direct beam do not satisfy Bragg's Law since the perfect crystal may be diffracted. Since there is no extinction they produce a high diffracted intensity which appears as a black point. This is the direct image (Figure 1.7). When the wavefields propagate within the Bormann fan ABC, along AQ, the dislocation intercepts the path at Q and they decouple into their incident and reflected wave components. When they re-enter a perfect crystal region they excite new wavefields. Intensity is removed from the direction AQ and the dislocation line gives rise to a dynamical image. This appears as a thick white line because the intensity is less than the background. The newly created

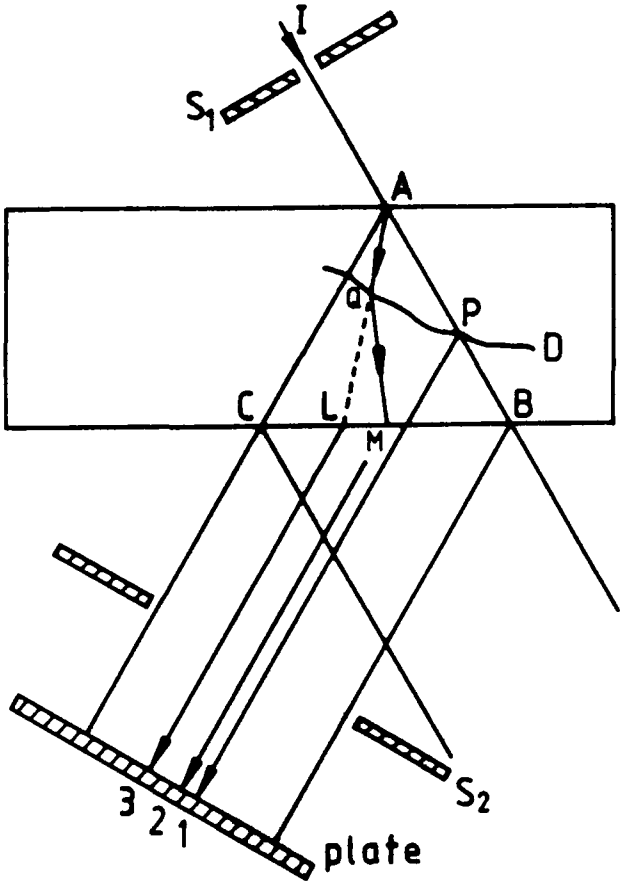

Fig. 1.7 Formation of dislocation images in section and projection topographs.

(1) Direct image,

(2) Intermediary image,

(3) Dynamical image (after Authier, 1978).

wavefields propagates along QM and this gives rise to the intermediary image. This intermediary image appears as a series of black and white fringes. The fringes are a result of the interference between the newly created wavefield and the normal wavefield propagation along AM, which was not intercepted by the dislocation.

1.10 Contrast of magnetic domains

X-ray topography is an important tool for revealing magnetic domains inside bulk crystals. The contrast of domains arises through the magnetostrictive deformation.

Polcarova (1961) states that 90^{o} wall visibility for Fe-Si crystal depends on $(\underline{m}_2 - \underline{m}_1).\underline{g}$, where $\underline{m}_1$ and $\underline{m}_2$ are unit vectors parallel to the direction of magnetization in adjacent domains and $\underline{g}$ is the diffraction vector. She also asserts that the contrast will appear as a dark band when $(\underline{m}_2 - \underline{m}_1).\underline{g} > 0$ and as a bright band when $(\underline{m}_2 - \underline{m}_1).g < 0$. Since the magnetostrictive deformation is the same on both sides of a 180^{o} wall no image will be visible. The wall image width depends on the tilt of the sample around the diffraction vector (Figure 1.8). It is equal to

$t \sin \alpha$ where α is the angle of rotation and t is the thickness of the sample.

The contrast depends on the magnitude of the magnetostriction. When the magnetostriction is large, orientation contrast can be observed; when the magnetostriction is small both domains diffract simultaneously and no orientation contrast is observed.

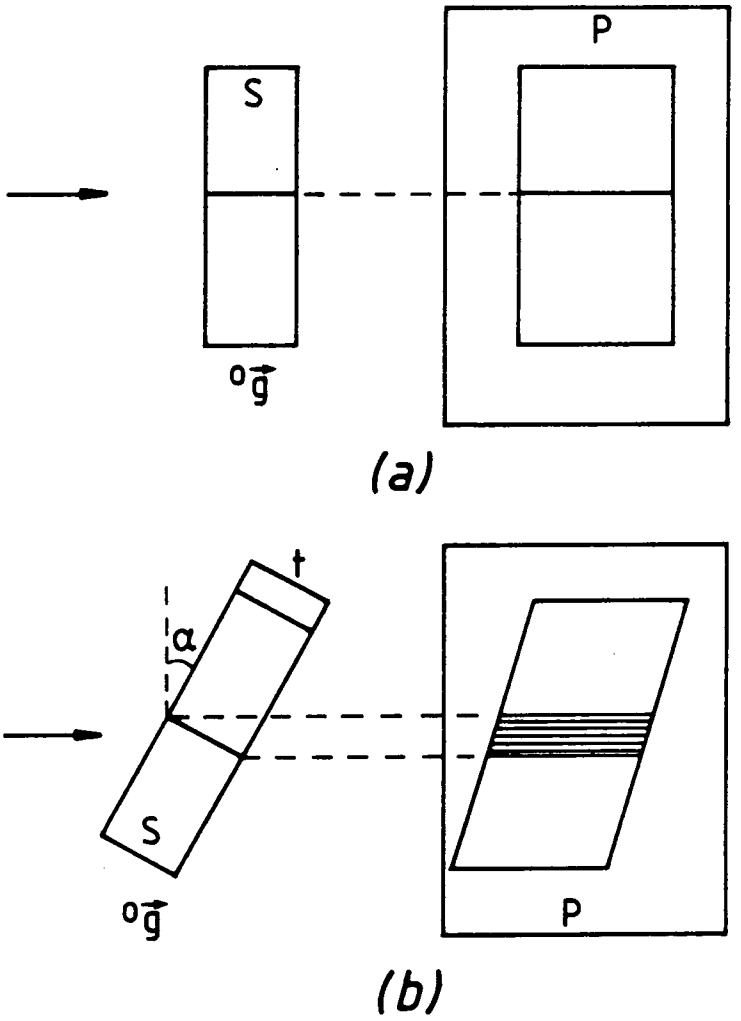

Fig. 1.8 Image of wall on photographic plate P depending on rotation of sample S around the g vector. Arrow indicates direction of incident X-ray beam (after Polcarova, 1969).

CHAPTER 2

MELT AND SOLID STATE GROWTH

2.1 Melt growth

Single crystals grown from the melt have been produced mainly by the Czochralski, Bridgman and float zone techniques. The criteria that must be fulfilled for material to grow are as follows:-

(a) It should melt congruently and not decompose before melting.

(b) The vapour pressure should be low at the melting point.

(c) Crucible material should not react with the material. If it does interact, as in the case of nickel, a non interacting crucible is arranged in an indirectly heated graphite suscepter.

(d) The melting point is obtainable by a variable heater.

The Czochralski technique is the most widely used technique because it is fast. Seed, neck and crystal geometry are controllable. The growth procedure is carried out from a free surface. Thus the crystal does not touch anything during the growth, a factor which is absent from the Bridgman technique. Large crystals can be grown whereas the float zone method is limited to small crystals.

2.1.1 The Czochralski technique

The basic process is shown schematically in Figure

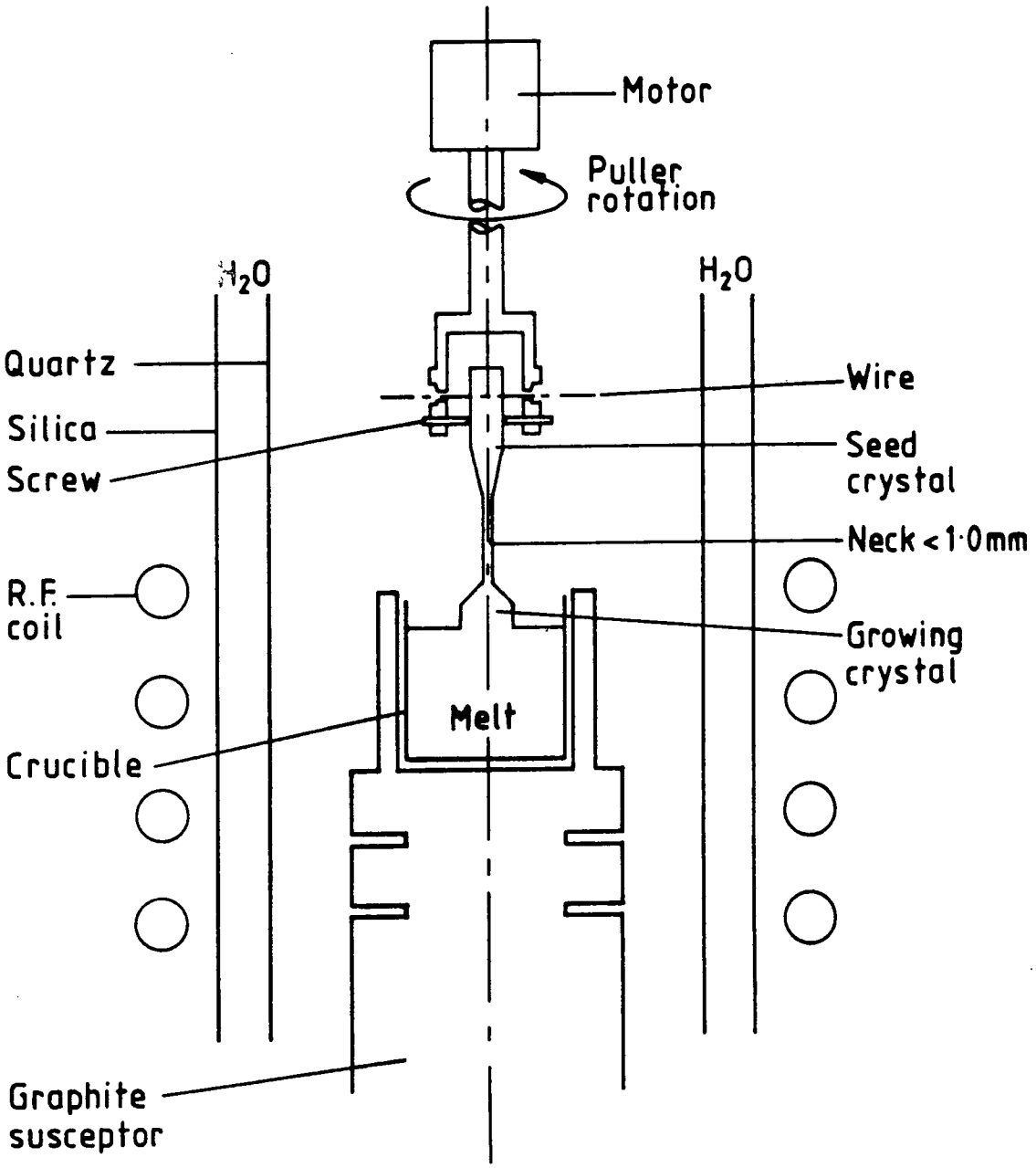

Fig. 2.1 Schematic diagram of Czochralski system.

(2.1). The equipment required for the Czochralski technique is:

(a) A means of containing the melt. Firstly, the crucible material should have a high melting point to ensure safe containment of the melt; often it is high purity graphite. Secondly, it should not interact with the melt. If it does, an alumina, tantalum or platinum crucible is placed inside a graphite susceptor. Finally, high quality crucible material is essential to ensure no impurity transfer to the melt.

(b) A means for holding and rotating the seed while withdrawing it from the melt. To avoid any mechanical fluctuation the rotation and pulling should be stable during the experiment.

(c) A means for preventing the melt from reacting with the atmosphere by surrounding the growth region by an inert gas or a vacuum. High purity inert gas should be used in order to reduce impurity, incorporation in the crystal. The top and sides of the inert growth chamber should be protected from dust and cleaned before placing the charge in the chamber. The chamber walls are cooled by water running between them to prevent cracking and to reduce the contamination caused by material vaporised by heating the walls during the experiment.

(d) A means of heating the melt:

Since the radio frequency heating induces a current flow in the crucible, the latter should be conductive. The advantages of using radio frequency heating are stirring the melt, visibility which leads to good geometrical control, use

of an after heater and a large range of temperatures.

2.1.1.1 Crystal growth of metals

(i) The charge should be cleaned with diluted nitric acid (30% nitric acid + 70% water), washed in running water and finally in methanol before being transferred to the crucible. Gloves should be worn in order to avoid introducing any contamination to the charge. The material to be grown is heated above its melting temperature in a high purity crucible. If the melt contains any impurity it will float on the surface and its collision with the growing crystal will create dislocation sources in the crystal surface (Okkerse, 1959).

(ii) A seed crystal is dipped partially into the melt. Dash (1959) stated that dislocations can be introduced to the crystal from the seed by

(a) Propagation of dislocations which are initially present in the seed.

(b) Imperfections formed by poor epitaxy between the crystal and the seed.

(c) Multiplication of dislocations present in the seed by thermal stress and propagation into the crystal, and

(d) Generation from surface damage.

These sources can be minimised by selecting a seed that is as free of defects as possible. Thus careful etching and handling of the seed before the growth are required. Sufficient time should be given to ensure uniform melting of the seed surface.

The diameter of the growing crystal is reduced to a very small neck by raising the temperature of the melt. The pulling should be vertical to the melt surface in order to obtain a long thin neck. Rotation is required to stir the melt for uniform thermal and solute distribution (Brice, 1968). Buckley-Golder and Humphreys (1979), in their calculation of the temperature distribution in copper crystals grown by this technique, found that the neck radius has a remarkable effect in reducing the temperature gradient. Sworn and Brown (1972), in their work to produce a dislocation - free copper crystal, stated that in order to get a perfect crystal with a diameter 0.5 - 1.5 mm the neck radius should be less than 0.4 mm and less than 0.3 mm for a larger diameter 2-3 mm. This points to the great effect of producing the neck before growing crystal.

(iv) After the necking procedure has been done, the melt temperature is then lowered so as to increase the crystal size to the required value. The perfection at this stage depends mainly on the pulling speed and cooling rate. A low pulling speed is required since Tanner (1973), in his experiment to grow dislocation-free silver single crystals, found that reducing the pulling speed from 1.5 cm/hour to 0.85 cm/hour gave dislocation-free growth. The latter speed produced a dislocation-free single crystal, whereas at the former speed the dislocation density is low but not zero. The diameter of the crystal is reduced again before removing the crystal from the melt. Paige (1983) described methods of controlling the crystal diameter. Thermal strain is an

important factor in determining the quality of the crystal. When the crystal is brought back to room temperature during or after growth, rapid cooling will introduce a high and non-uniform temperature gradient in the crystal which leads to dislocation formation. When the crystal grown has zero dislocation density it requires a very high stress to create new dislocations. When the crystal grown has dislocations the thermal stress will generate dislocations by multiplication. In metals the stress required to produce plastic flow is much lower than in semiconductors. it is therefore expected that the dislocation density produced by thermal strain in metal crystals will be higher than in semiconductors. The presence of an after-heater (Sworn and Brown, 1972), is an important factor in the reduction of heat emitted from the surface of the growing crystal. Thus the crystal is cooled slowly while still in the heater region. The crystal should be handled very carefully so as to avoid damage.

2.1.1.2 Growth Direction Dependence

Kuriyama et al. (1977) found that a nickel crystal grown in the [111] direction is more perfect than a crystal grown in either [110] or [100] directions. In spite of copper having the same structure of nickel (face center cubic), the optimum growth direction was found to be [100] by Fehmer and Uelhoff (1972). Their results showed that for a large copper crystal (5-10 mm) the growth direction [100] gave a good quality crystal, better than a crystal grown in the [110]

direction. The perfection for small diameter (less than 4 mm) was found by Sworn and Brown (1972) to be independent for the [321], [110] and [100] growth direction.

2.1.2 Liquid encapsulation Czochralski

The Czochralski technique has been developed to overcome one of the main material limitations, namely that the material should have a low vapour pressure (Figure 2.2). The melt surface and the crystal are covered with a liquid layer and thus there is no vapour phase. Growth proceeds similar to the normal Czochralski method. The material to be grown and the encapsulant are placed in the crucible. As the charge temperature is increased the encapsulant melts first,

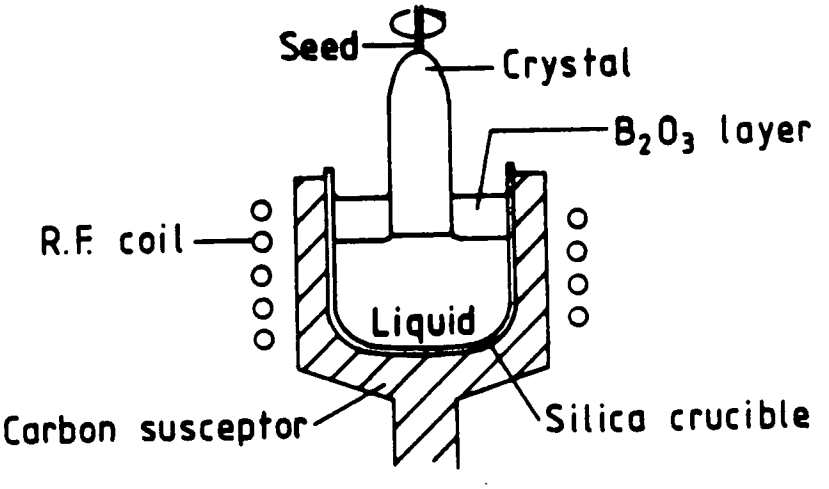

Fig. 2.2 LEC crystal pulling arrangement (after Brandle, 1980).

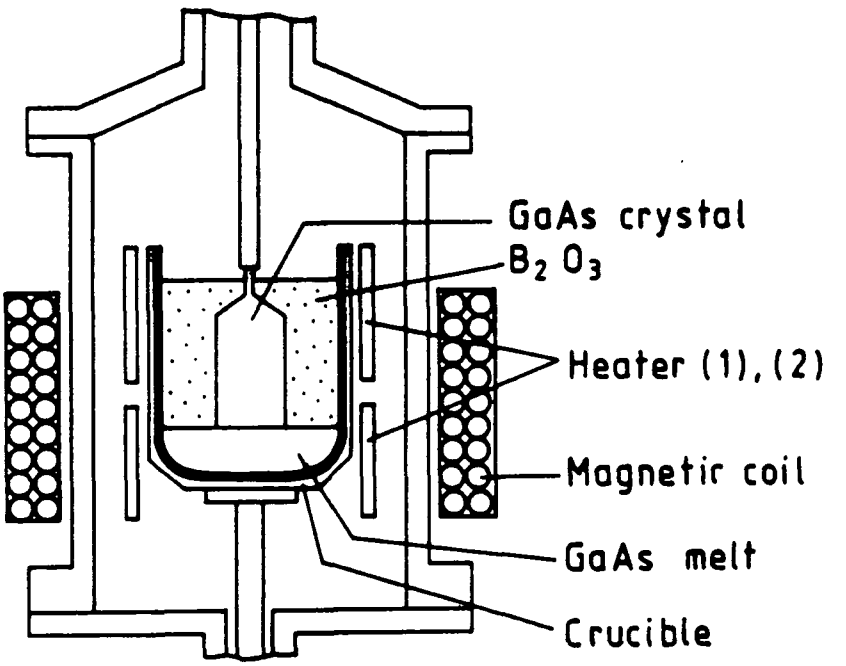

Fig. 2.3 Growth apparatus for the VM-FEC method (after Kohada, 1985).

and thus a layer of encapsulant covers the charge. After the charge is melted a seed is dipped partially into the melt and the crystal is grown as usual by the pulling technique.

Dislocation-free GaAs single crystals were grown by the fully encapsulated Czochralski method (Figure 2.3). The stress arising from arsenic evaporation was suppressed by fully encapsulated Czochralski but could not be avoided by liquid encapsulation Czochralski. In this technique, the crystal grown is totally encapsulated. This technique was used by Kohda (1985) to grow GaAs single crystals free from dislocation. A dislocation free seed was used in the experiment. The presence of a magnetic field tends to smother the surface and suppress the oscillating thermal convection in the melt (Osaka, 1984).

2.1.3 The Bridgman technique

In this method the charge is melted by increasing the temperature to above its melting point (Figure 2.4). Then the vertically placed crucible is lowered through a furnace so that solidification may start at the lowest point in the crucible. Since the crystal size is fixed by the crucible geometry, various sizes of crystal can be produced repeatedly. This method cannot be used for materials which expand on solidification. This expansion leads to stress, which affects the crystal perfection. This technique can be used in either a vertical or horizontal arrangement. In the horizontal arrangement the furnace is usually moved as in the vertical arrangement. The advantage of this arrangement lies in its simplicity; on the other hand with a large open

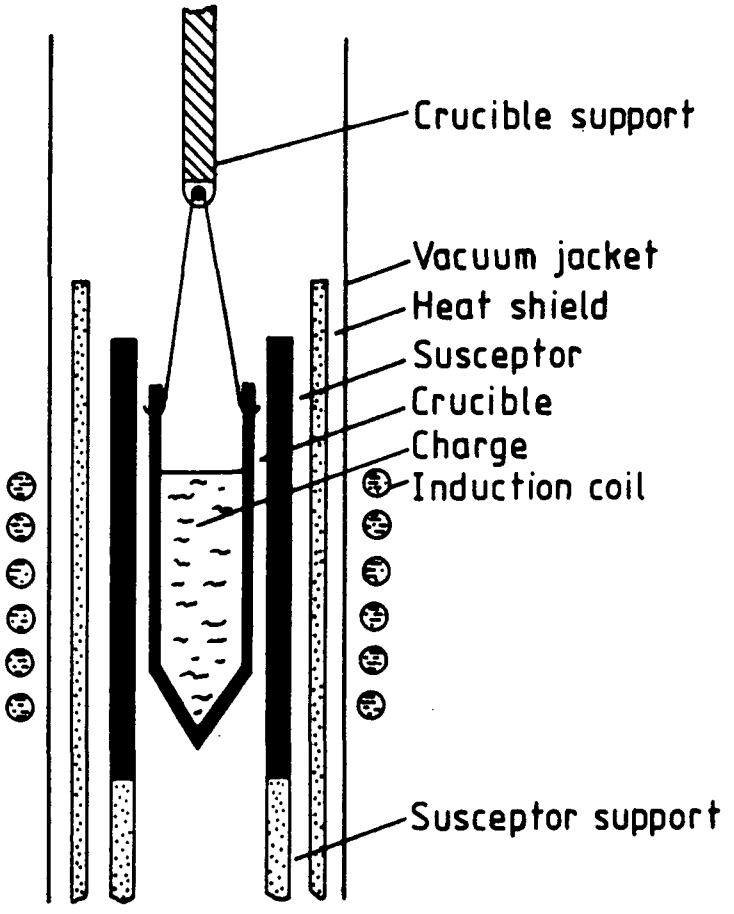

Fig. 2.4 Induction heated Bridgman apparatus (after Jones, 1974).

surface the possibility of contamination increases. Horizontal Bridgmann grown crystals of GaAs, InP and InSb are available commercially.

The temperature lowering rate should be small; Wernick and Davies (1956) produced a high purity copper single crystal at a physical lowering rate of 2 inches per hour. By the same technique Esin et al. (1981) grew aluminium single crystals. They found that in general an increase in growth rate increases dislocation density, and the dislocation density depends on the orientation. With <111> orientation the dislocation density was very small. In a horizontal arrangement single crystals of copper and nickel were produced by Gow and Chalmers (1951).

2.1.4 The Floating Zone technique

One of the important things for growing crystals from the melt is that the melt should not react with the crucible. Thus growing crystals by this technique has the advantage of limiting the contamination arising from the crucible. In this method the polycrystalline ingot is supported vertically inside the furnaces which is evacuated or has an inert gas atmosphere (Figure 2.5). To grow a single crystal, a seed is positioned in such a way that it is almost touching the lower end of the ingot. A molten zone is formed in the ingot. The seed is brought to touch the molten zone, which is then moved through the ingot to allow the single crystal to grow. The stability of the zone melting was studied by Keck et al. (1953). They found that for a given diameter the length

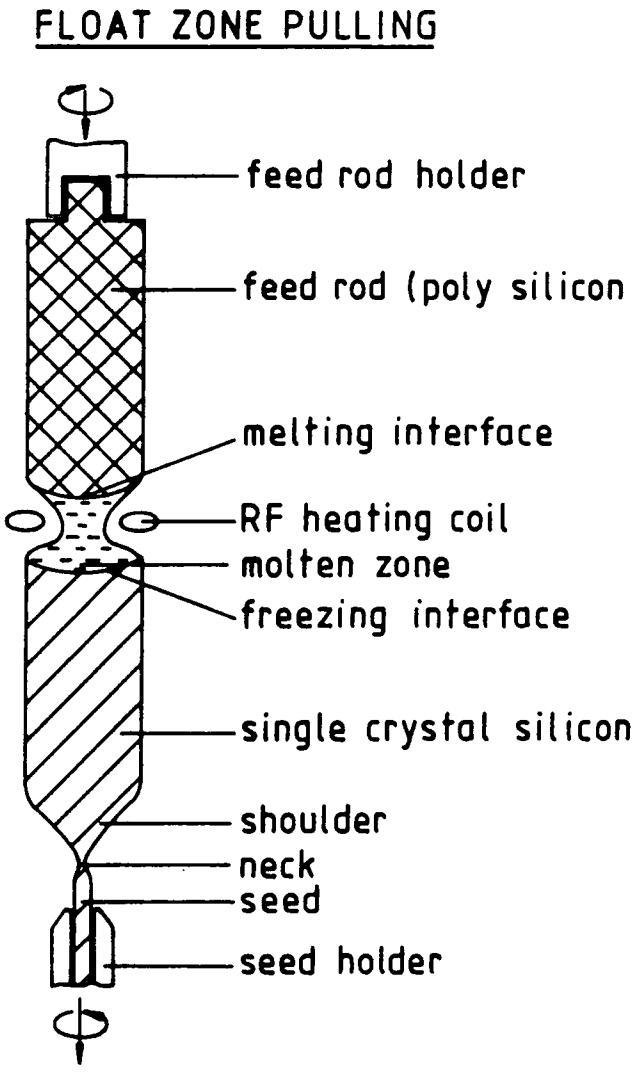

Fig. 2.5 Principle of float-zone (after Zulehner, 1983).

decreases as the diameter increases. In a vertical arrangement single crystals of tungsten, tantalum, rhenium, molybdenum, vanadium, silicon, nickel and copper have been produced by Calverly et al. (1957), with size from 2 mm to 1 cm in diameter and up to 16 cm in length. Single crystals of iron and titanium were not obtained because of the phase change on cooling.

2.2 Solid state growth

Metal crystals can be prepared from the solid state by the strain anneal method and by phase transformation. The latter method (Aust, 1963) is preferred for the preparation of crystals of materials which undergo a phase change between the melting point and room temperature. Materials prepared by this method emerge in the form of thin sheets which can be used as they stand, although the thickness is limited and the orientation is troublesome. This technique was reviewed by Aust, (1963).

2.2.1 The strain anneal method:-

In this method (Nøst, 1965), single aluminium crystals are prepared at a very slow cooling rate. The aluminium bars were rolled down to 1 mm in thickness. After being pre-annealed for a short time, the specimens were strained and cut. They were then electro-polished to remove the oxide layer on the surface and suspended vertically in the furnace. The temperature increased rapidly to 300^{o}C then more slowly at 14^{o}C per hour to 440^{o}C. It was then reduced very slowly to room temperature.

Deguchi and Kamigaki (1978) found that in order to grow

low dislocation aluminium crystals by this technique, the cooling rate must be low.

Recrystallization of iron-silicon crystals has been reported by MacCormack and Tanner (1978). The radial growth rate was found to be more or less constant and nearly equal for all grains studied.

2.2.2 Phase transformation

This method has been used to produce titanium by Jourdan (1972). In this technique, rolled strips of 0.2 mm thickness were annealed in a high vacuum at a temperature only slightly below the transition point. Several cycles around transformation points were used to permit the growth of large crystals. The furnace was slowly cooled to room temperature.

CHAPTER 3

DOMAIN OBSERVATION AND MAGNETIC MEASUREMENT IN NICKEL SINGLE CRYSTALS

3.1 Introduction

Metal single crystals of copper (Sworn and Brown, 1972) and Silver (Tanner, 1973) have been grown with zero dislocation density by Czochralski. There are no reports in the literature of zero dislocation density growth of nickel and low dislocation of nickel was reported by Kuriyama et al. (1977). They stated that the domain configuration in slices cut from nickel single crystal was observed to be removed under an external magnetic field.

3.2 Growth Procedure

Nickel single crystals have been grown by the Czochralski technique from a melt of 99.999% pure nickel contained in alumina crucible. The crucible was discarded after each use due to the fact that alumina is porous and metal keys into its surface and the subsequent contraction tends to crack the alumina. A silica after-heater was incorporated into the graphite susceptor. Crystals were grown from either <111> and <110> orientation single crystal seeds in an argon atmosphere. The grown crystals were about 11 mm long with diameter of less than 1 mm pulling rate of 2 mm/minute were used with crystal rotation rate of 2 r.p.m. Tables (3.1, 3.2) show growth conditions used while Table (3.3) presents crystal and neck dimensions. X-ray Lang

topography was used to characterise the grown crystals.

3.3 Domain movement under applied magnetic field

Figure (3.1a) shows a 220 reflection topograph of a <111> axis nickel single crystal taken by the Lang technique. As shown in Figure (3.1b) when an external field of 20 mT is applied parallel to the growth axis the image disappeared completely. When the field is removed a structure very similar to the original reappears. In this magnetic field, the crystal appears to be saturated to a single domain. The image, s, related to the strain in the crystal remained unchanged. Figure 3.2 shows the domain structure in the 440 reflection. Appendix A shows the calibration for the coil used in this experiment.

Magnetic domains within the second crystal could be seen in surface reflection in Figure (3.3). When the magnetic field of 0.2T was applied perpendicular to the growth direction, <110>, the domains disappeared.

While low dislocation density nickel single crystals could be grown reproducibly a zero extended dislocation density could not be achieved. The lack of anomalous transmission indicated that we have been unsuccessful in reducing the dislocation density to zero. The reason for this we believe that the technique of pulling extremely narrow necks as used for Ag and Cu is inappropriate for Ni. It is suggested in Chapter four that for low dislocation density growth of Ni, there should be a rapid increase in the crystal diameter from the neck region.

Table 3.1

The pulling, rotation and voltage used during growth

Pulling mm/min	Rotation r.p.m.	volt (in R.F. generator)
2.0	2.0	218
2.0	2.0	219
2.0	2.0	218
2.0	2.0	213
2.0	2.0	213
2.0	2.0	214
2.0	2.0	215
2.0	2.0	215

Table 3.2

The pulling, rotation and voltage used during growth

Pulling mm/min	Rotation r.p.m.	volt (in R.F. generator)
4.0	2.0	227
2.0	2.0	227
2.0	2.0	219
2.0	2.0	220

Table (3.3)

Growth Direction	Neck length mm	Neck radius mm	crystal length mm	crystal radius mm
<111>	3	0.3	8.5	3
<110>	11	0.2	12	2.5

Fig. 3.1 X-ray topographs of nickel crystal
(a) zero field, (b) 0.02 tesla and (c) zero field.
220 reflection, MoKα radiation.

Fig. 3.2 X-ray reflection topograph revealing domains and a large misorientation region apears as a light band. 440 reflection, MoKα radiation.

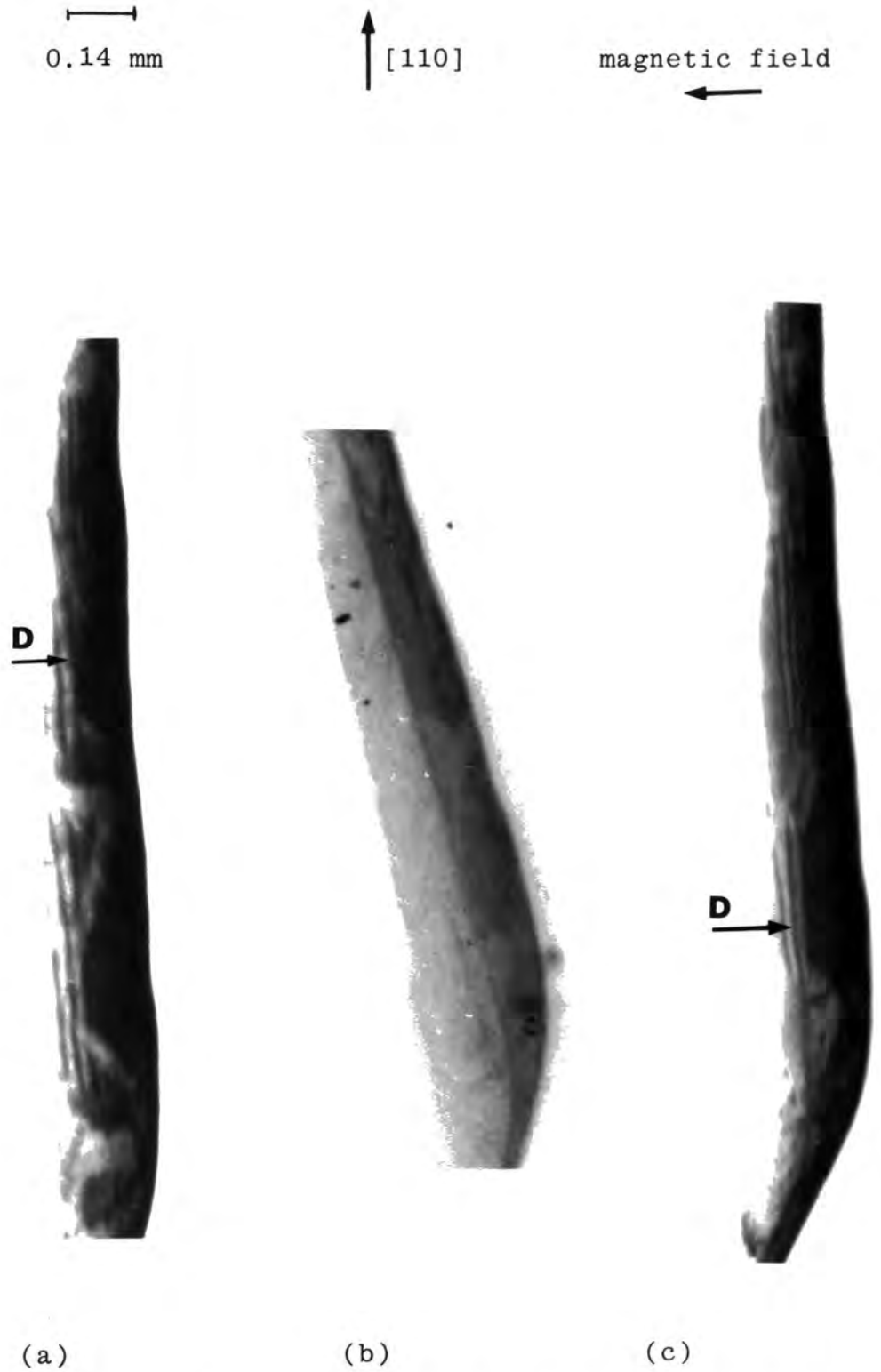

Fig. 3.3 Lang reflection topograph of nickel crystal showing magnetic domain,
(a) zero field,
(b) 0.2 tesla, and
(c) zero field. $2\bar{2}0$ reflection, MoKα radiation.

No improvement in crystal perfection was found in crystal with different growth axis.

3.4 The magnetization process and domain hypothesis

During the magnetization process in ferromagnetic material, two mechanisms are generally believed to take place. The first mechanism is domain movements for small fields and the second one is magnetization rotation within domains for large fields.

When an external magnetic field is applied to the crystal, the change in the initial portion of the magnetization curve, Figure 3.4, is due to the fact that domains having magnetization directions nearly parallel to the field direction will grow at the expense of unfavourably aligned domains. For small fields the magnetization is due to the domain boundary movement. They will return, if the applied field is sufficiently small, to their original positions if the magnetic field is gradually reduced to zero. With further increase of field the domains aligned nearest to the field direction will grow till saturation is reached. Further changes in magnetization are due to the rotation of the direction of magnetization until its magnetization is almost parallel to the external field. At this point, as the field increases the magnetization tends towards the fixed point defined as the saturation magnetization. When the external field is reduced to zero from this state, the magnetization will pass through the B-axis at a point defined as the remanence. Applying a reverse field will eventually reduce the magnetization to zero at a field denoted the

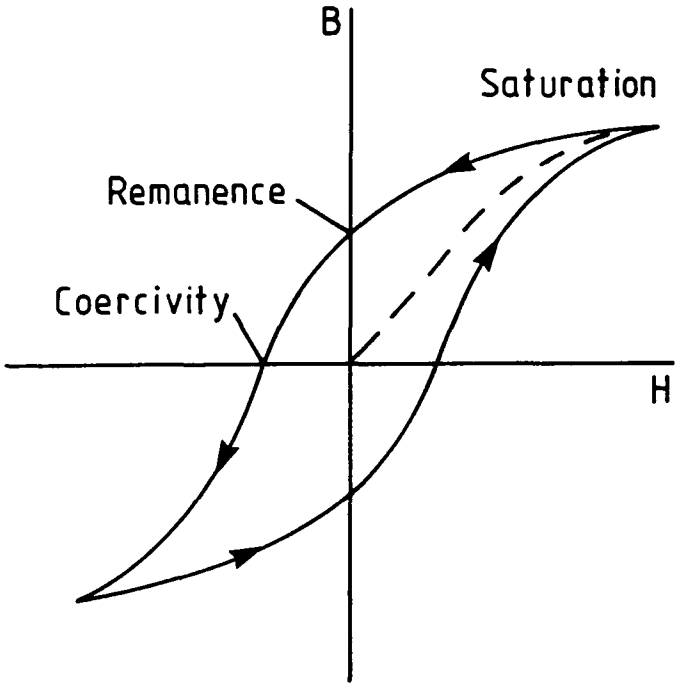

Fig. 3.4 The magnetization curve showing saturation magnetization, remanence and coercivity.

coercivity, H_c. As a result of increasing the reverse field the magnetization reaches the value - B_r as the reverse field reduced to zero. The magnetization will reach the positive saturation if a sufficiently large positive field is applied. A review of ferromagnetic theory have been given by Kittel (1949).

3.5 Magnetization measurement

The magnetization curves for single crystals grown by the Czochralski technique have been measured at room temperature using a vibrating sample magnetometer (v.s.m.) described by Hoon and Willcock (1988). Magnetization measurements to investigate the behaviour of the coercivity as a function of temperature was performed under the guidance of Miss S. Thompson. The measurements were performed with the field parallel and perpendicular to the growth axis <111>.

3.5.1 Saturation magnetization

Magnetisation curves (Figures 3.5, 3.6) show that both crystals have the same saturation magnetization value. The susceptibility is greater when the crystals are parallel to the applied field than when vertical, due principally to the lower demagnetising factor in this direction. The magnetic field required to magnetise the crystal in the easy direction <111>, for nickel, is also easier than in other directions. This is in agreement with the previous results, Figure (3.7).

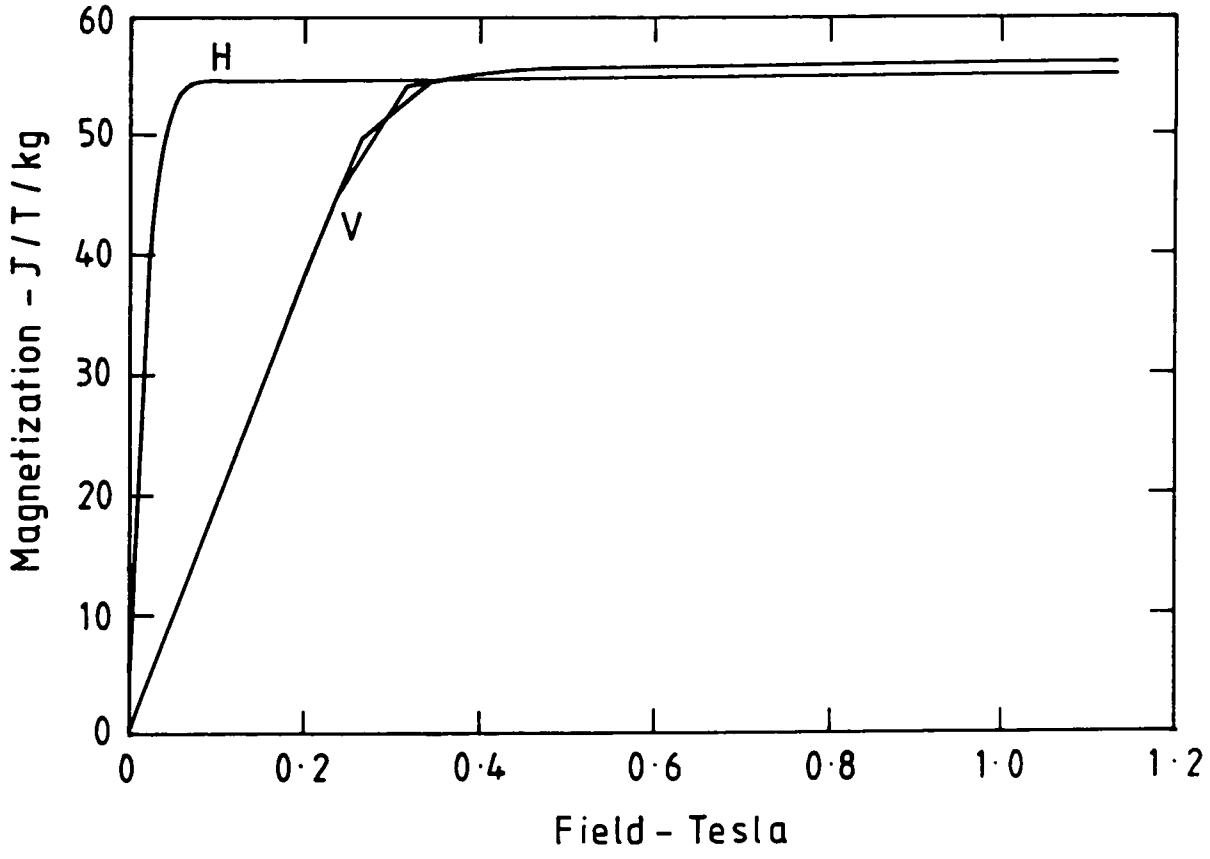

Fig. 3.5 Magnetization curve for single crystal of nickel. H, parallel to growth direction <111> V, perpendicular to growth direction <111>.

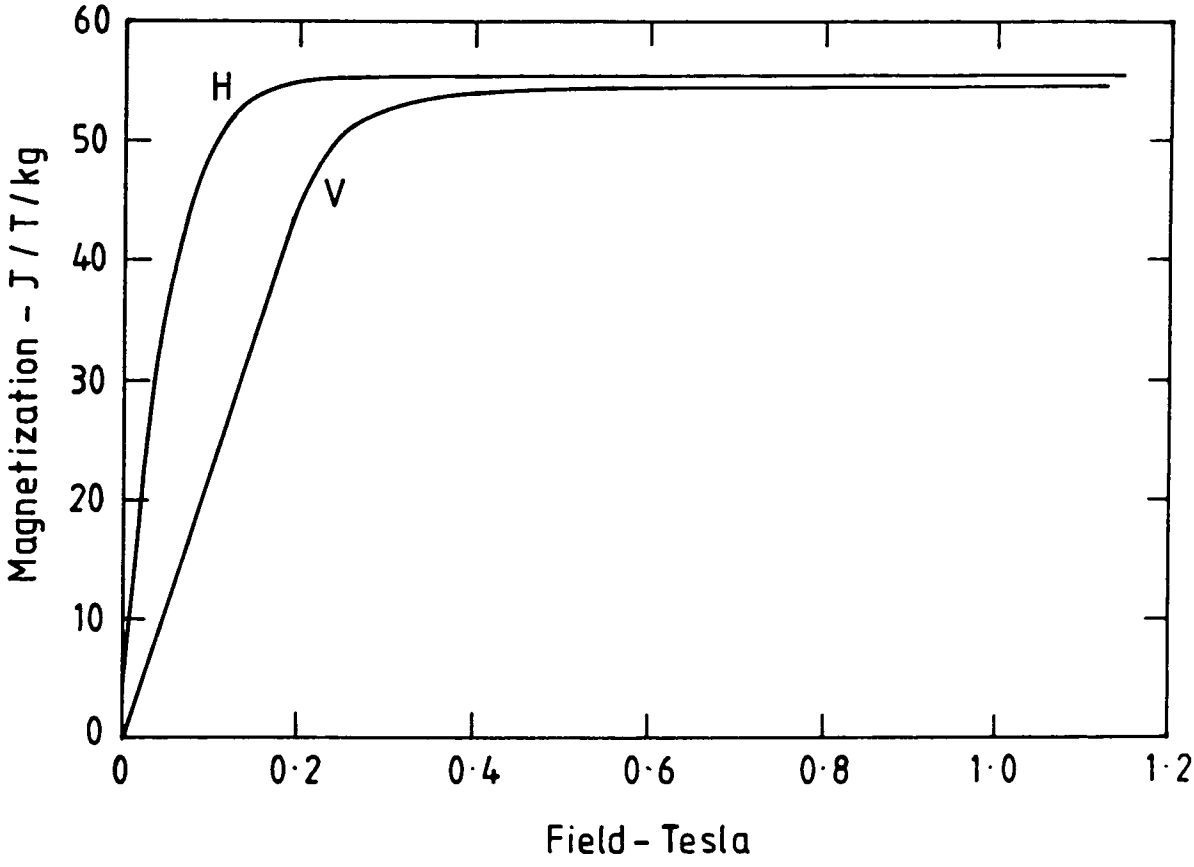

Fig. 3.6 Magnetization curve for single crystal of nickel. H, parallel to growth direction <111> V, perpendicular to growth direction <111>.

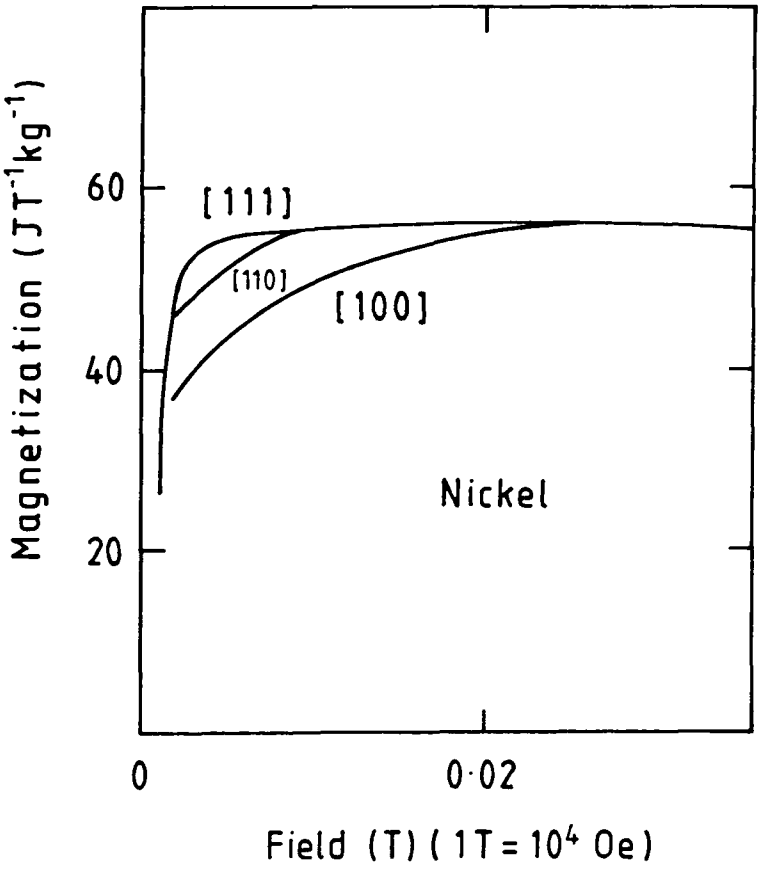

Fig. 3.7 Magnetization as a function of field in single crystals of nickel for different crystallographic direction (after Crangle, 1977).

3.5.2 Coercivity measurement

The results which are presented in Figures (3.8, 3.9) and Tables (3.4, 3.5) show that the coercivity is almost independent of temperature at low temperatures.

Since the coercivity is structure sensitive, the measurements can be used to obtain information about the pinning sites assuming to be uniformly distributed within the crystal. The relationship between the average distance which is between pinning lines along a Bloch wall, s, and coercivity, H_c, has been given by Friedel (1964). The equation may be written as

$$H_c \simeq \lambda \mu b/Sm_s$$

where,

μ is defined as a shear modulus and equal to 7.4×10^{11} ($dyne/cm^2$) in nickel.

λ is defined as a magnetostriction coefficient. In nickel λ_{111} is equal to 24.3×10^{-6}

b is defined as a Burgers vector.

It is equal to 3.523×10^{-10} m in nickel.

m_s is defined as a saturation magnetization.

It is equal to 55.4 J/T/Kg from Figure (3.5).

H_c is defined as the coercivity and equal to 149 Am^{-1}.

Thus on substitution we find

$$S \simeq 6.9 \times 10^{-6} \text{ m } (\pm 4\%)$$

It is known that μ and b are almost independent of temperature. m_s and λ vary little with temperature down to low temperatures as shown in Tables (3.6, 3.7), taken from

Table 3.4

T(k)	$H_c(KAm^{-1})$
291	0.147
4.2	0.149
20	0.139
45.3	0.135
70.1	0.137
100	0.139
145.2	0.147
190	0.159
235	0.152
292.8	0.163

Table 3.5

T(k)	$H_c(KAm^{-1})$
292	0.0712
4.2	0.0711
17	0.07785
30	0.109
60	0.1119
85	0.0736
125	0.0811
185	0.0845
235.5	0.0722
292	0.0700

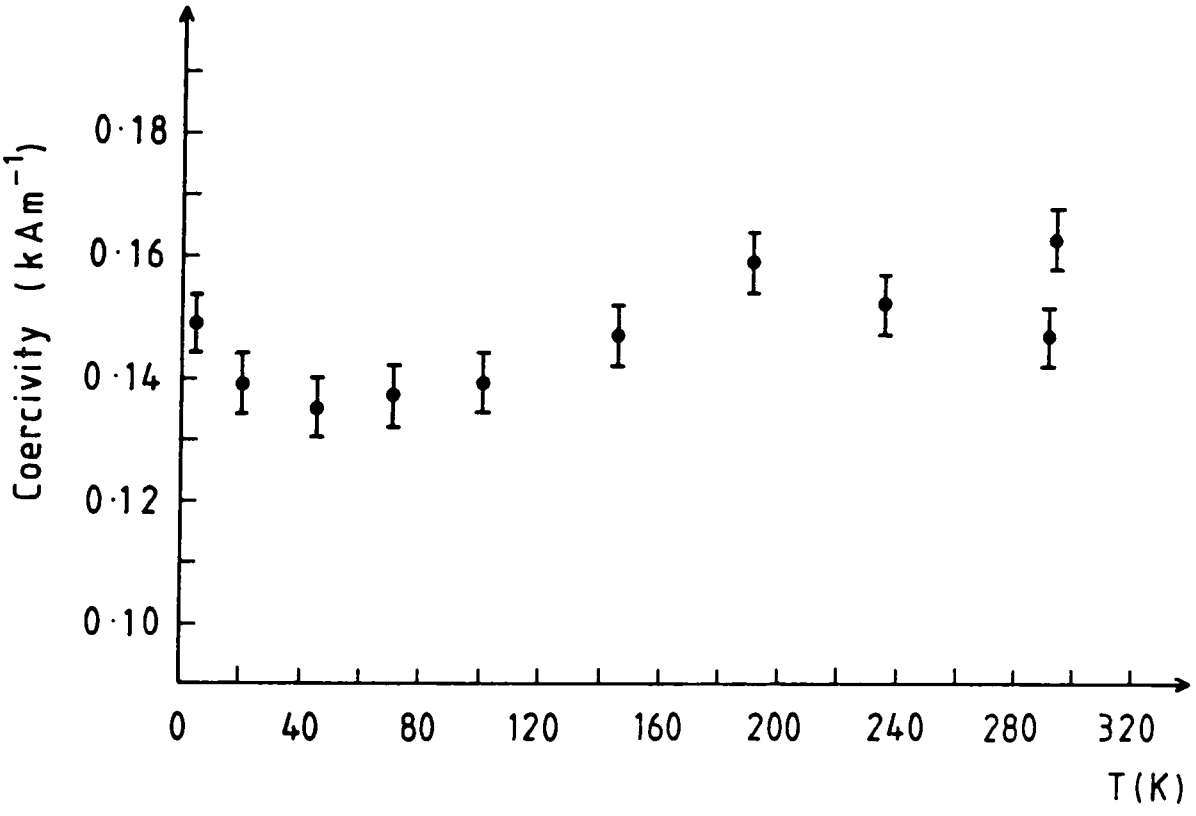

Fig. 3.8 The coercivity dependence of temperature on growth axis <111>

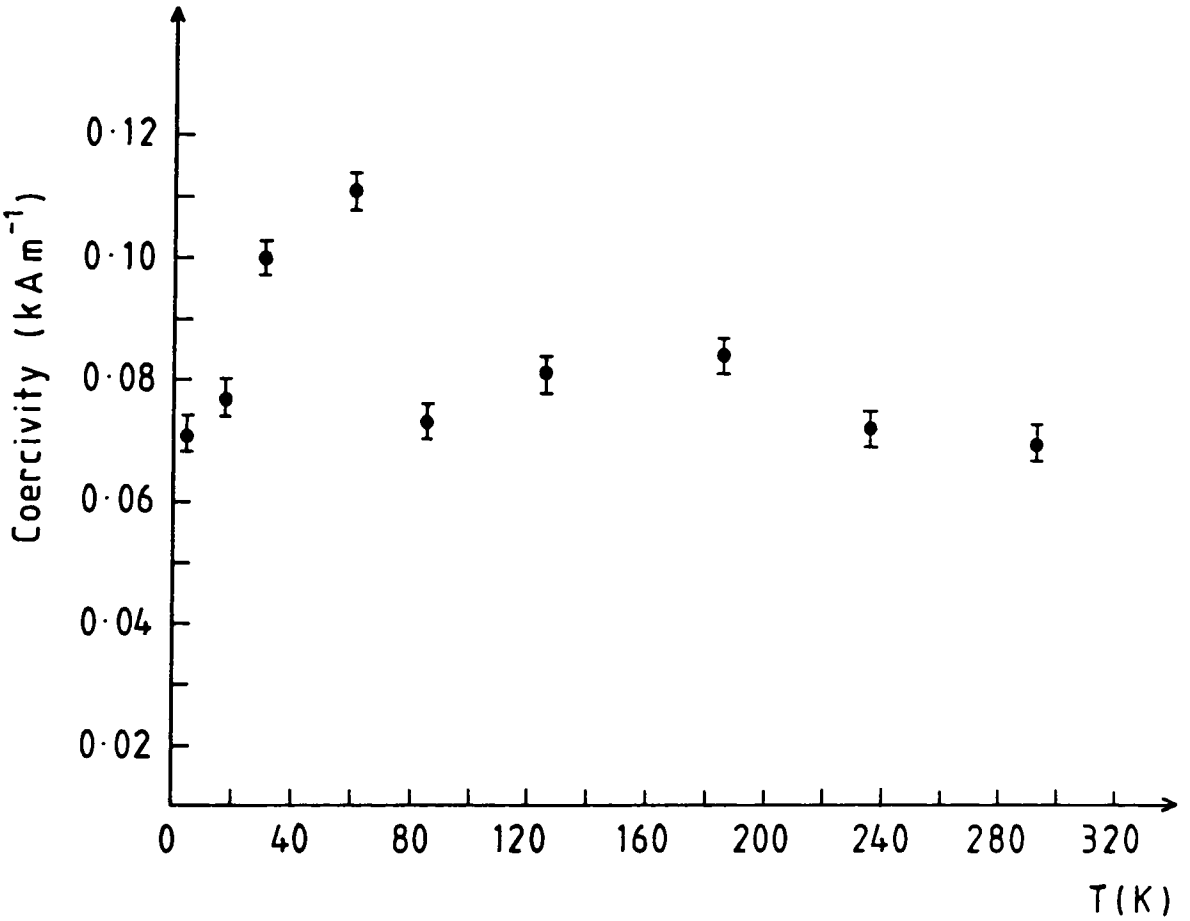

Fig. 3.9 The coercivity dependence of temperature on direction perpendicular on growth axis <111>

Table (3.6)

[100] Specimen

T(K)	$\lambda \times 10^{-6}$	m_s erg/oe/cm^3	$(\lambda/m_s) \times 10^{-6}$
112	45.7	499	0.0915
130	50.7	510	0.994
143	54.4	515	0.1056
153	55.0	519	0.1059
160	54.4	519	0.1048
173	54.8	518	0.1057
180	55.0	517	0.1063
199	54.4	514	0.1058
208	54.4	512	0.1062
213	54.4	512	0.1063

Table (3.7)

[111] Specimen

T(K)	$\lambda \times 10^{-6}$	m_s erg/oe/cm^3	$(\lambda/m_s) \times 10^{-6}$
119	22.3	523	0.0426
138	22.2	522	0.0425
165	21.6	510	0.0416
171	21.4	518	0.0413
196	21.2	515	0.0411
205	20.8	514	0.0404
217	20.4	512	0.0398
226	20.4	511	0.0309
243	20.2	507	0.0398
251	19.9	505	0.0394
262	19.6	502	0.0390
273	19.4	499	0.0388

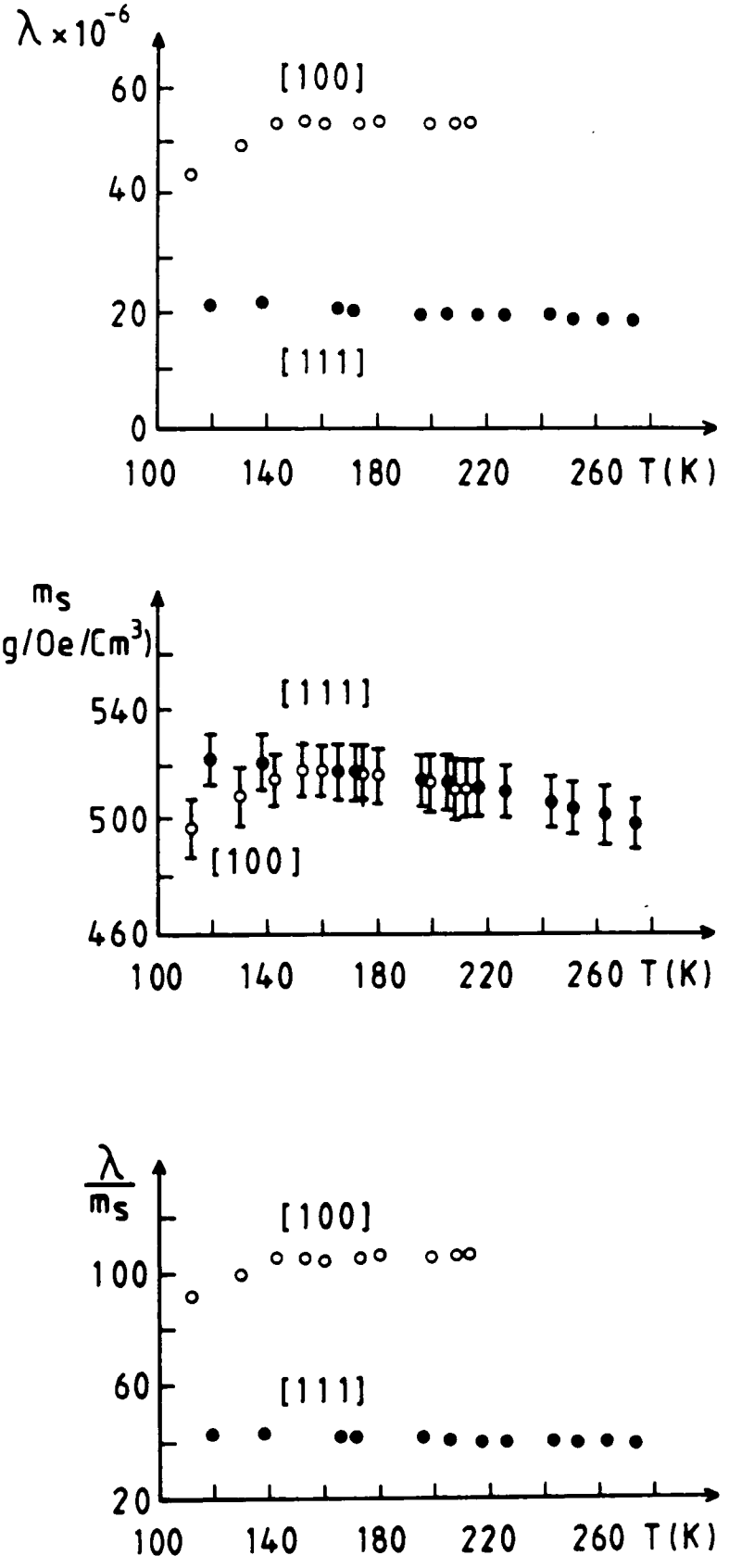

Fig. 3.10 λ, m_S and λ/m_S dependent on temperature in the [111] and [100] directions.

Hunt's thesis (1954). m_s/λ (Figure 3.10) is seen to have an even smaller variation with temperature.

The dislocation density could be estimated from previous calculation by

$$\text{Dislocation density} \simeq (1)^2/(6.862 \times 10^{-4})^2$$

$$\simeq 2 \times 10^6 \text{ cm}^{-2}$$

This probably over-estimates the dislocation density because the coercivity depends on inhomogeneities at the surface as well as internal strain. However, the independence of H_c on temperature is consistent with pinning of domain walls by dislocations. The dislocation density required is realistic.

3.6 Attempts at dislocation free growth and comparison with copper

In order to examine the effect of crystal cone angles, copper crystals with different crystal and shoulder radii, and consequently different angle, were grown.

Crystals were pulled from 99.998% pure copper by a seed crystal of orientation <110> and the growth conditions were similar to those used in growing nickel crystals. Tables (3.8-3.11) show the growth conditions while table (3.12) represents the geometrical parameters of the crystals. It is established that growing dislocation free copper (Sworn and Brown, 1972) and Silver (Tanner, 1973) single crystals could be achieved by use of a slow growth rate, long after heater and introduction of a very thin neck.

The aim of growing crystals with different cone angle is

to see how this affects the crystal perfection.

From Figure (3.11) it is clear that for small angle anomalous transmission was undetectable through the bulk of the crystal. Increasing the angle, dislocation lines -D- could be seen, and further increase shows a perfect region.

It is evident that in order to pull highly perfect copper crystals under these conditions a large crystal cone angle is required.

In the next chapter, the temperature gradient at the interface is computed and the effect of neck diameter and crystal cone angle on the temperature gradient is compared for both copper and nickel.

Table 3.8

The pulling, rotation and voltage used during growth

Crystal number one

Pulling mm/min	Rotation r.p.m.	volt (in R.F. generator)
2	2	169
2	2	161
2	2	161
2	2	162
2	2	163
2	2	164

Table 3.9

The pulling, rotation and voltage used during growth

Crystal number two

Pulling mm/min	Rotation r.p.m.	volt (in R.F. generator)
2	2	165
2	2	159
2	2	159
2	2	160
2	2	166
2	2	161

Table 3.10

The pulling, rotation and voltage used during growth

Crystal number three

Pulling mm/min	Rotation r.p.m.	volt (in R.F. generator)
2	2	174
2	2	174
2	2	169
2	2	170
2	2	170
2	2	170
2	2	171

Table 3.11

The pulling, rotation and voltage used during growth

Crystal number four

Pulling mm/min	Rotation r.p.m.	volt (in R.F. generator)
2	2	163
2	2	163
2	2	160
2	2	160
2	2	160

Table 3.12

Crystal number	Crystal angle	Crystal diameter mm	Crystal length mm	neck diameter mm	neck length mm
1	40^{o}	2	15	1	10
2	80^{o}	3	12	1	8
3	90^{o}	2	11	1	7
4	120^{o}	2.2	13	1	7

Fig. 3.11 Anomalous transmission topograph of copper single crystals.

(a) Crystal cone angle = 40°, no anomalous transmission occurs,

(b) Dislocation lines could be seen at 80°,

(c) Defects occurs at 90°, and

(d) At 120° dislocation free region could be seen. 200 reflection, MoKα radiation.

(b)

0.505mm

(c)

0.988mm

(d)

1.33mm

temperature distribution as a function of the length and the radial growth and assumes that the ambient temperature is constant over the length.

With the aid of such a model calculations have been performed for six elements silver, copper, nickel, silicon, aluminium and chromium. The first four elements have been analysed to compare with previous results, Alourfi (1986), while the last two represent low and high melting temperature materials.

4.2 Formulation of the model

In the modified model (Figure 4.2) we note that instead of the three constituents seed, neck and crystal used by Buckley-Golder and Humphreys (1977) (Figure 4.1) two more constituents were added namely seed shoulder and crystal shoulder. Each of them consists of three parts. Following Buckley-Golder (1977), we assume cylindrical symmetry and it is assumed that the crystal grows into a constant ambient temperature. Two heat transfer processes occur:-

1. Conduction up the crystal, and
2. Radiation from surfaces such as A,B,C,D,E,F,G and H in Figure (4.2). The basic heat transfer equation used is

$$C\ A\rho\ \frac{\partial T(z)}{\partial t} = K\ A\ \frac{\partial^2 T(z)}{\partial z^2} - h_R\ P\ (T(z) - T_A) \qquad (4.1)$$

This assumes that the temperature distribution is a function only of z and this neglects radiation loss from the tops of the cylindrical elements. The neglect of radial temperature gradients is justified because of the small diameter compared

with the length of the crystals, the high thermal conductivity and the use of a long after-heater. C and ρ are the specific heat capacity and density respectively for the element considered, T(z) is the temperature of the rod at a given point z in Figure (4.2), K is the thermal conductivity, h_R is the heat radiation coefficient, T_A is the ambient temperature and P is the circumference of the rod.

By looking at equation (4.1), it is observed that the left hand side represents the heat lost with time from Δz of rod, where Δz is an infinitesimal element. As for the conduction up the rod, it is represented in the first term of the right hand side of the equation. Radiation loss is accounted for in the second term of the right hand side.

In the time independent condition:-

$$\frac{\partial T(z)}{\partial t} = 0 \text{ equation (4.1) reduces to}$$

$$\frac{d^2T(z)}{dz^2} = n^2 \left[(T(z) - T_A)\right] \qquad (4.2)$$

where

$$n^2 = \frac{h_R P}{KA} = \frac{2B_i}{R^2}$$

and

$$B_i = \frac{h_R R_i}{K}$$

B_i is the Biot number and R is the radius of the rod.

The solution of equation (4.2) is

$$T(z) = T_A + \text{Cosh}\left[\frac{(2B_i)^{\frac{1}{2}}}{R_i} z\right]) \; A \; + \text{Sinh}\left[\frac{(2B_i)^{\frac{1}{2}}}{R_i} z\right] B \qquad (4.3)$$

where A and B are the integration constants and R_i is the diameter of the step i.

x_i is defined as $x_i = \frac{(2B_i)^{\frac{1}{2}}}{R_i}$

If we consider that the diameter of seed, neck and crystal are constant through their length whereas seed shoulder and crystal shoulder are approximated by a series of constant diameter steps, then

$$T_1 = T_A + Q_1C_{1z} + Q_2S_{1z} \quad (4.4a)$$

$$T_2 = T_A + Q_3C_{2z} + Q_4S_{2z} \quad (4.4b)$$

$$T_3 = T_A + Q_5C_{3z} + Q_6S_{3z} \quad (4.4c)$$

$$T_4 = T_A + Q_7C_{4z} + Q_8S_{4z} \quad (4.4d)$$

$$T_5 = T_A + Q_9C_{5z} + Q_{10}S_{5z} \quad (4.4e)$$

$$T_6 = T_A + Q_{11}C_{6z} + Q_{12}S_{6z} \quad (4.4f)$$

$$T_7 = T_A + Q_{13}C_{7z} + Q_{14}S_{7z} \quad (4.4g)$$

$$T_8 = T_A + Q_{15}C_{87} + Q_{16}S_{8z} \quad (4.4h)$$

$$T_9 = T_A + Q_{17}C_{9z} + Q_{18}S_{9z} \quad (4.4i)$$

The subscript 1 in T refers to the crystal, 2,3,4 refer to the crystal shoulder 5 refers to the neck, 6,7,8 refers to the seed shoulder and 9 refers to the seed. The constants Q_1 to Q_{18} were determined by the following boundary conditions:-

$Z = o,$

$$T_1 = T_m \quad (4.5a)$$

where T_m is the melting point.

$$Z = L_1,$$

$$T_1(L_1) = T_2(L_1) \tag{4.5b}$$

$$K\,A_1 \frac{dT_1(L_1)}{dZ} = K\,A_2 \frac{dT_2(L_1)}{dZ} + h_{Rc}(A_1 - A_2)\,[T_1(L_1) - T_A] \tag{4.5c}$$

$$Z = L_2\ ,$$

$$T_2(L_2) = T_3(L_2) \tag{4.5d}$$

$$K\,A_2 \frac{dT_2(L_2)}{dZ} = K\,A_3 \frac{dT_3(L_2)}{dZ} + h_{Rc}(A_2 - A_3)\,[T_2(L_2) - T_A] \tag{4.5e}$$

$$Z = L_3\ ,$$

$$T_3(L_3) = T_4(L_3) \tag{4.5f}$$

$$K\,A_3 \frac{dT_3(L_3)}{dZ} = K\,A_4 \frac{dT_4(L_3)}{dZ} + h_{Rc}(A_3 - A_4)\,[T_3(L_3) - T_A] \tag{4.5g}$$

$$Z = L_4\ ,$$

$$T_4(L_4) = T_5(L_4) \tag{4.5h}$$

$$K\,A_4 \frac{dT_4(L_4)}{dZ} = K\,A_5 \frac{dT_5(L_4)}{dZ} + h_{Rc}(A_4 - A_5)\,[T_4(L_4) - T_A] \tag{4.5i}$$

$$Z = L_5 ,$$

$$T_5(L_5) = T_6(L_5) \tag{4.5j}$$

$$K\ A_5 \frac{dT_5(L_5)}{dZ} = K\ A_6 \frac{dT_6\ (L_5)}{dZ} + h_{Rs}(A_6 - A_5)[T_5(L_5) - T_A] \tag{4.5k}$$

$$Z = L_6 ,$$

$$T_6(L_6) = T_7(L_6) \tag{4.5l}$$

$$K\ A_6 \frac{dT_6(L_6)}{dZ} = K\ A_7 \frac{dT_7(L_6)}{dZ} + h_{Rs}(A_7 - A_6)[T_6(L_6) - T_A) \tag{4.5m}$$

$$Z = L_7 ,$$

$$T_7(L_7) = T_8(L_7) \tag{4.5n}$$

$$K\ A_7 \frac{dT_7(L_7)}{dZ} = K\ A_8 \frac{dT_8(L_7)}{dZ} + h_{Rs}(A_8 - A_7)[T_7(L_7) - T_A] \tag{4.5o}$$

$$Z = L_8 ,$$

$$T_8(L_8) = T_9(L_8) \tag{4.5p}$$

$$K\ A_8 \frac{dT_8(L_8)}{dZ} = K\ A_9 \frac{dT_9(L_8)}{dZ} + h_{Rs}(A_9 - A_8)[T_8(L_8) - T_A] \tag{4.5q}$$

$$Z = L_9 \ ,$$

$$T_9(L_9) = T_A \qquad (4.5r)$$

As a result, the temperature T(z) is denoted at all points, as is the temperature gradient found by differentiating equations 4.4a to 4.4i.

4.3 Determination of the constants Q_1 to Q_{18}

Using equation (4.4a) with condition (4.5a), we obtain

$$T_m - T_A = Q_1. \qquad (4.6a)$$

If we define S_{ij} and C_{ij} as

$$S_{ij} = \sinh (x_i L_J)$$

$$C_{ij} = \cosh (x_i L_J)$$

equation (4.4a) and (4.4b) can be used with the conditions (4.5b) and (4.5c) to yield

$$Q_1 C_{11} + Q_2 S_{11} - Q_3 C_{21} - Q_4 S_{21} = 0 \qquad (4.6b)$$

and

$$(\xi_1 - \xi_5) Q_1 + (\xi_2 - \xi_6)\ Q_2 - \xi_3 Q_3 - \xi_4 Q_4 = 0 \qquad (4.6c)$$

where

$$\xi_1 = K\ A_1\ X_1\ S_{11},$$

$$\xi_2 = K\ A_1\ X_1\ C_{11},$$

$$\xi_3 = K\ A_2\ X_2\ S_{21},$$

$$\xi_4 = K\ A_2\ X_2\ C_{21},$$

$$\xi_5 = h_{Rc}(A_1 - A_2)\ C_{11},$$

and $$\xi_6 = h_{Rc}\ (A_1 - A_2)\ S_{11}.$$

From equation (4.4b), (4.4c) and conditions (4.5d), (4.5e), we get

$$Q_3C_{22} + Q_4S_{22} - Q_5C_{32} - Q_6S_{32} = 0 \qquad (4.6d)$$

and

$$(E_1 - E_5)\, Q_3 + (E_2 - E_6)\, Q_4 - E_3\, Q_5 - E_4\, Q_6 = 0 \qquad (4.6e)$$

where

$$E_1 = K\, A_2\, X_2\, S_{22},$$

$$E_2 = K\, A_2\, X_2\, C_{22},$$

$$E_3 = K\, A_3\, X_3\, S_{32},$$

$$E_4 = K\, A_3\, X_3\, C_{32},$$

$$E_5 = h_{Rc}\, (A_2 - A_3) C_{22},$$

and $E_6 = h_{Rc}\, (A_2 - A_3)\, S_{22}.$

From equations (4.4c), (4.4d) and the conditions (4.5f), (4.5g) the result is

$$Q_5C_{33} + Q_6S_{33} - Q_7C_{43} - Q_8S_{43} = 0 \qquad (4.6f)$$

and

$$(\gamma_1 - \gamma_5)Q_5 + (\gamma_2 - \gamma_6)Q_6 - \gamma_3\, Q_7 - \gamma_4\, Q_8 = 0 \qquad (4.6g)$$

where

$$\gamma_1 = KA_3\, X_3\, S_{33},$$

$$\gamma_2 = KA_3\, X_3\, C_{33},$$

$$\gamma_3 = KA_4\, X_4\, S_{43},$$

$$\gamma_4 = KA_4\, X_4\, C_{43},$$

$$\gamma_5 = h_{Rc}\, (A_3 - A_4)\, C_{33},$$

and $\gamma_6 = h_{Rc}\, (A_3 - A_4)\, S_{33},$

Equations (4.4d), (4.4e) and conditions (4.5h), (4.6i) lead to

$$Q_7C_{44} + Q_8S_{44} - Q_9C_{54} - Q_{10}S_{54} = 0 \qquad (4.6h)$$

and

$$(\alpha_1 - \alpha_5)Q_7 + (\alpha_2 - \alpha_6)Q_8 - \alpha_3Q_9 - \alpha_4Q_{10} = 0 \qquad (4.6i)$$

where

$$\alpha_1 = K\, A_4\, X_4\, S_{44},$$

$$\alpha_2 = K\, A_4\, X_4\, C_{44},$$

$$\alpha_3 = K\, A_5\, X_5\, S_{54},$$

$$\alpha_4 = K\, A_5\, X_5\, C_{54},$$

$$\alpha_5 = h_{Rc}\,(A_4 - A_5)\, C_{44},$$

and $$\alpha_6 = h_{Rc}\,(A_4 - A_5)\, S_{44}.$$

It is clear from equations (4.4e), (4.4f) and the conditions (4.5j), (4.5k), that

$$Q_9C_{55} + Q_{10}S_{55} - Q_{11}C_{65} - Q_{12}S_{65} = 0 \qquad (4.6j)$$

and

$$(\beta_1 - \beta_5)Q_9 + (\beta_2 - \beta_6)Q_{10} - \beta_3Q_{11} - \beta_4Q_{12} = 0 \qquad (4.6k)$$

where

$$\beta_1 = K\, A_5\, X_5\, S_{55},$$

$$\beta_2 = K\, A_5\, X_5\, C_{55},$$

$$\beta_3 = K\, A_6\, X_6\, S_{65},$$

$$\beta_4 = K\, A_6\, X_6\, C_{65},$$

$$\beta_5 = h_{Rs}\,(A_6 - A_5)\, C_{55},$$

and $$\beta_6 = h_{Rs}\,(A_6 - A_5)\, S_{55}.$$

Also equations (4.4f), (4.4g) and the conditions (4.5l), (4.5m), gives

$$Q_{11}\, C_{66} + Q_{12}\, S_{66} - Q_{13}\, C_{76} - Q_{14}\, S_{76} = 0 \qquad (4.6l)$$

and

$$(\delta_1-\delta_5)Q_{11} + (\delta_2 - \delta_6)Q_{12} - \delta_3Q_{13} - \delta_4Q_{14} = 0 \qquad (4.6m)$$

where

$$\delta_1 = K\, A_6\, X_6\, S_{66},$$

$$\delta_2 = K\, A_6\, X_6\, C_{66},$$

$$\delta_3 = K\, A_7\, X_7\, S_{76},$$

$$\delta_4 = K\, A_7\, X_7\, C_{76},$$

$$\delta_5 = h_{Rs}\,(A_7 - A_6)\, C_{66},$$

and $$\delta_6 = h_{Rs}\,(A_7 - A_6)\, S_{66}.$$

Consequently the results of equations (4.4g), (4.4h) and the conditions (4.5n), (4.5o), are

$$Q_{13}\, C_{77} + Q_{14}\, S_{77} - Q_{15}\, C_{87} - Q_{16}\, S_{87} = 0 \qquad (4.6n)$$

and

$$(\Gamma_1 - \Gamma_5)Q_{13} + (\Gamma_2 - \Gamma_6)Q_{14} - \Gamma_3\, Q_{15} - \Gamma_4\, Q_{16} = 0 \qquad (4.6o)$$

where

$$\Gamma_1 = K\, A_7\, X_7\, S_{77},$$

$$\Gamma_2 = K\, A_7\, X_7\, C_{77},$$

$$\Gamma_3 = K\, A_8\, X_8\, S_{87},$$

$$\Gamma_4 = K\, A_8\, X_8\, C_{87},$$

$$\Gamma_5 = h_{Rs}\,(A_8 - A_7)\, C_{77},$$

and $$\Gamma_6 = h_{Rs}\,(A_8 - A_7)\, S_{77}.$$

It follows from equations (4.4h), (4.4i) and the conditions (4.5p), (4.5q), that

$$Q_{15}C_{88} + Q_{16}S_{88} - Q_{17}C_{98} - Q_{18}S_{98} = 0 \qquad (4.6p)$$

and

$$(\Omega_1 - \Omega_5)Q_{15} + (\Omega_2 - \Omega_6)Q_{16} - \Omega_3 Q_{17} - \Omega_4 Q_{18} = 0 \qquad (4.6q)$$

where

$$\Omega_1 = K\, A_8\, X_8\, S_{88},$$

$$\Omega_2 = K\, A_8\, X_8\, C_{88}$$

$$\Omega_3 = K\, A_9\, X_9\, S_{98},$$

$$\Omega_4 = K\, A_9\, X_9\, C_{98},$$

$$\Omega_5 = h_{Rs}\,(A_9 - A_8)\, C_{88},$$

and $$\Omega_6 = h_{Rs}\,(A_9 - A_8)\, S_{88}.$$

Finally from equation (4.4i) and (4.5n), we get

$$Q_{17}\, C_{99} + Q_{18}\, S_{99} = 0 \qquad (4.6r)$$

The coefficients of the equations were written in the form of a matrix (Figure 4.3). The program listed in Appendix B was used to evaluate the coefficients. Basic parameters used in this calculation are listed in table 4.1.

4.4 Results

4.4.1 Varying the seed length

It is clear from the model that the seed was assumed to have a cylindrical geometry. Its length was increased by a factor of 2 from 6 mm to 12 mm and keeping other parameters constant (Table 4.2). It was found that this change has no effect on the absolute value of the temperature gradient at the interface ($z = 0$).

The heat loss by radiation was ignored because it is very small compared with heat loss by conduction. As the interface is a fixed point then increasing the seed length can lead only to a small reduction in the thermal gradient (Table 4.3).

By looking at the Figure (4.4) we see that generally a higher melting temperature leads to a higher temperature gradient. The exception is Silicon which interchanges with nickel and arises because of the significant different thermal properties of a semiconductor and a metal.

Convergence of the simulation has been examined by use of both 3 and 4 steps in the neck region as demonstrated in Table (4.4). There is no significant effect of changing from

3 to 4 steps which indicates that the solution has converged. Geometrical parameters used are listed in Table 4.5.

4.4.2 Varying the seed shoulder length

The shoulder diameter is kept constant for each step and the step length reduced - as in Table (4.6). This is equivalent to reducing length and increasing the angle of the slope of shoulder; little change occurs because there is no heat loss from the tops, see Figure (4.5) and table (4.7)

4.4.3 Varying the seed and seed shoulder radii

In this section the effect of changing both seed and shoulder radius is examined. The shoulder slope length is held constant. The seed radius was reduced and the shoulder radius reduced proportionally (Table 4.8). This does not maintain the same shoulder angle to different radius; the angle becoming smaller for small shoulder radii. Again, little change is found, presumably because the neck region acts as a "heat valve", (Figure 4.6 and Table 4.9).

4.4.4 Varying the crystal length

Increase in the grown crystal length (Table 4.10) leads to an increase in temperature gradient (Figure 4.7). This is both absolutely and proportionally larger for Ni and Cr than for Al, Ag and Cu (Table 4.11).

4.4.5 Varying the crystal shoulder length

Reducing the crystal shoulder length by factor 2 from 3 mm to 1.5 mm which is equivalent to increasing the crystal shoulder angle, reduced the temperature gradient. See Table (4.12) and Figure (4.8). Geometrical parameters used are listed in Table (4.13).

4.4.6 Varying the crystal and shoulder radii

This has by far the biggest effect. On increasing the crystal diameter, the proportional increase in shoulder radii means that for the larger diameter crystal, the shoulder angle becomes large. Thus the rapid increase in diameter in the shoulder region (Table 4.14) appears to be beneficial. This is done in the growth of Silicon, partly, this is to give constant diameter crystals and as large a region as possible to be cut for wafers (Figure 4.9). However, as well as this for economic reason it may also help to reduce the thermal gradient. See Figure (4.10) and Table (4.15).

Murthy and Aubert (1981) reported that dislocation free silicon could be grown by use of flaired bulges in the neck. X-ray topographs show that the dislocation density in region 1 is greater than that in region 3 (Figure 4.11). Calculation of temperature gradient using our model shows no difference between single or multiple necks (Figures 4.12, 4.13). For low dislocation density crystals, we believe one should aim for very rapid increases in the diameter of the crystal below the neck. Tables 4.16 and 4.17 show the temperature gradient for single and multiple necks and the geometrical parameters used in the calculations.

4.4.7 Varying the neck length

Introducing a long neck before growing Cu, Al and Ag crystals reduced the temperature gradient. However, it is seen from table (4.18) that increasing the neck length by a factor 2 from 3 mm to 6 mm has only a small

effect on the absolute value of the temperature gradient in Ni, Cr and Si crystals. This is confirmed in Figure 4.14. Geometrical parameters used in the calculations are listed in Table 4.19.

4.4.8 Varying the neck radius

Reducing the neck radius by a factor 2 Table 4.20) reduces significantly the temperature gradient for Al, Cu, Ag. However for Ni, Cr and Si while the absolute change in temperature gradient (Table 4.21) is similar to Al, Cu and Ag, the proportional is very much lower. The curves of Figure (4.15) do not extrapolate to the origin for Ni, Cr and Si.

These results agree with experimental results of Zasimchuck et al. (1981) and Sworn and Brown (1972) in their work. They claimed that the dislocation density in copper single crystal is reduced by reducing the neck radius. The same result was found by Tanner (1973) in his work on silver single crystal.

4.4.9 A comparison between the previous and present models

The data presented by Alourfi (1986) show a similar conclusion to that obtained by the present model. The biggest effect occurs when the crystal radius increases. This is done by keeping the crystal shoulder constant. Thus the crystal cone angle is constant. The only factor variable is crystal radius. Figure (4.16) shows that under these conditions the same relation exists for both models. The difference in temperature gradient value is related to the presence of the crystal shoulder in the current model, a

factor absent in the previous model. Again by looking to other geometrical parameters such as neck length, (Figure 4.17) little difference is found between the models.

4.4.10 The relation between thermal conductivity and temperature gradient

The temperature gradient as a function of thermal conductivity is shown in Figure (4.18). It is shown that temperature gradient does not depend simply on the thermal conductivity. The relation between them could not be represented simply because the different materials have different properties such as melting point, ambient temperature and density.

4.5 Conclusion

The results obtained from the previous simulation for seed, neck and crystal are similar to those obtained by Buckley-Golder and Humphreys (1979) and recently by Alourfi (1986) . Here, the crystal shoulder and seed shoulder are introduced for the first time in this model to the best of the researcher's knowledge. However, in concluding, we can state that the best method for growing low dislocation density crystals under a high radiation condition are:-

(1) The seed shoulder should be short.

(2) The crystal length should be small in order to reduce the temperature gradient.

(3) Neck radius should be small while the neck length should be increased.

(4) Thus in order to reduce the temperature gradient the

crystal diameter should be large and the rate of increase of diameter in the neck should also be large. The neck angle will therefore be very large. The results indicate why it has proved impossible to grow dislocation-free nickel crystals by use of a thin neck. Results for growth of copper confirm that higher perfection crystals can be obtained when the crystal shoulder cone angle is large.

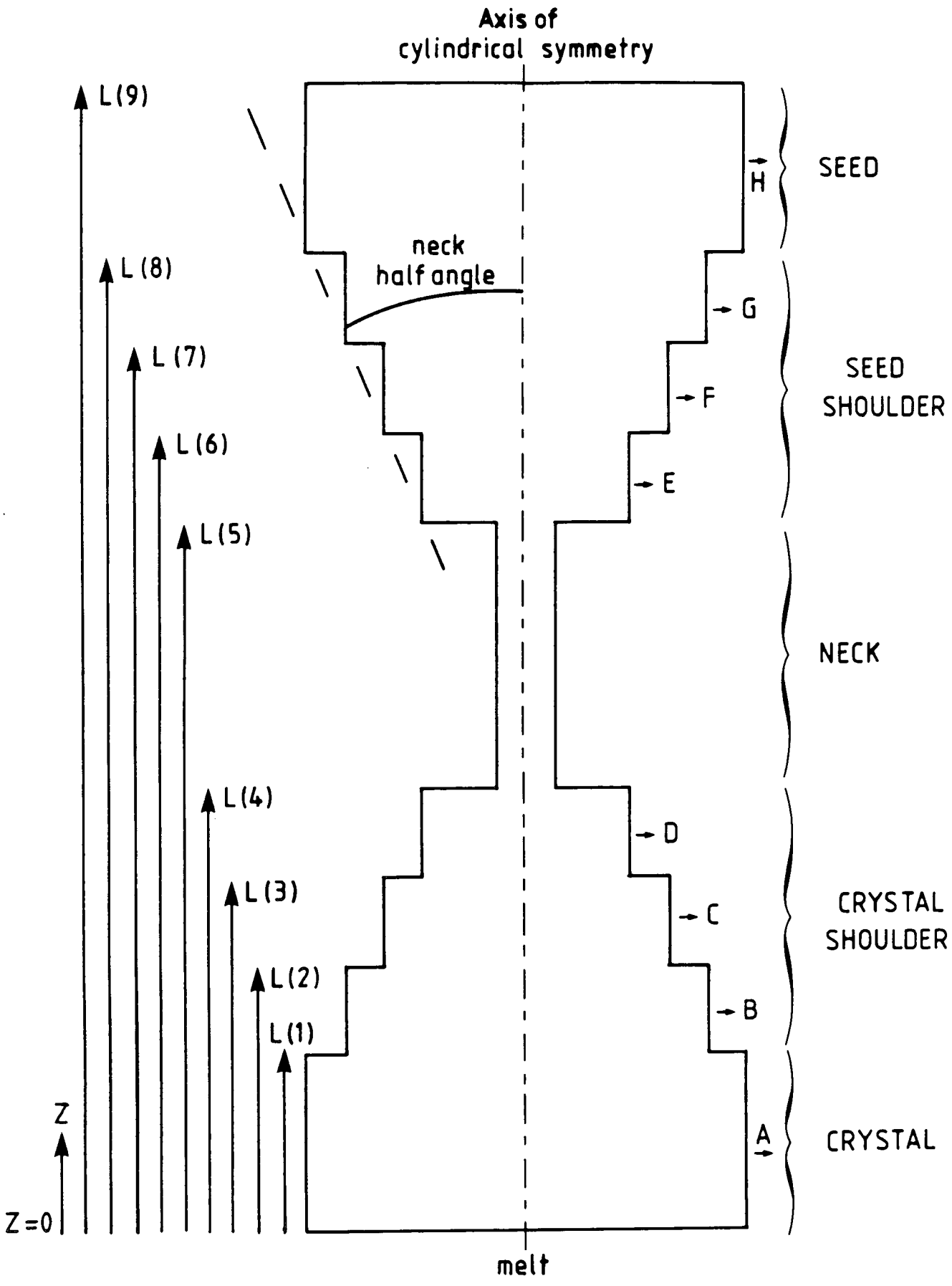

Fig. 4.2 Crystal growth model, see the text.

Fig. 4.3

1																	
C_{11}	S_{11}	$-C_{21}$	$-S_{21}$														
$\xi_1-\xi_5$	$\xi_2-\xi_6$	$-\xi_3$	$-\xi_4$														
		C_{22}	S_{22}	$-C_{32}$	$-S_{32}$												
		$\varepsilon_1-\varepsilon_5$	$\varepsilon_2-\varepsilon_6$	$-\varepsilon_3$	$-\varepsilon_4$												
				C_{33}	S_{33}	$-C_{43}$	$-S_{43}$										
				$\gamma_1-\gamma_5$	$\gamma_2-\gamma_6$	$-\gamma_3$	$-\gamma_4$										
						C_{44}	S_{44}	$-C_{54}$	$-S_{54}$								
						$\alpha_1-\alpha_5$	$\alpha_2-\alpha_6$	$-\alpha_3$	$-\alpha_4$								
								C_{55}	S_{55}	$-C_{65}$	$-S_{65}$						
								$\beta_1-\beta_5$	$\beta_2-\beta_6$	$-\beta_3$	$-\beta_4$						
										C_{66}	S_{66}	$-C_{76}$	$-S_{76}$				
										$\delta_1-\delta_5$	$\delta_2-\delta_6$	$-\delta_3$	$-\delta_4$				
												C_{77}	S_{77}	$-C_{87}$	$-S_{87}$		
												$\Gamma_1-\Gamma_5$	$\Gamma_2-\Gamma_6$	$-\Gamma_3$	$-\Gamma_4$		
														C_{88}	S_{88}	$-C_{98}$	$-S_{98}$
														$\Omega_1-\Omega_5$	$\Omega_2-\Omega_6$	$-\Omega_3$	$-\Omega_4$
																C_{99}	S_{99}

Table 4.1

The Basic Parameters used in this calculation

Element	K (w/mm/C)	T_m (C)	T_A (C)	E at 0.65 μ	Bi(crystal) (low radiation)	X 2 → Bi(crystal) (high radiation)
Al	0.092	660.4	599.0	0.10	1.816 E-4	3.632 E-4
Ag	0.377	961.9	872.0	0.05	5.075 E-5	1.015 E-4
Cu	0.352	1083.0	983.0	0.10	1.437 E-4	2.875 E-4
Ni	0.0819	1453.0	1318.0	0.45	5.695 E-3	1.139 E-2
Cr	0.066	1857.0	1684.0	0.35	1.028 E-2	2.056 E-2
Si	0.032	1410.0	1279.0	0.4	1.201 E-2	2.403 E-2

Table 4.2

Geometrical parameters used in Figure 4.4. L is the variable plotted. It is equal to 6, 8, 10 and 12.

Section	Radius (mm)	Length (mm)
Crystal	1.0	3.0
crystal shoulder 1	0.9	1.0
crystal shoulder 2	0.8	1.0
crystal shoulder 3	0.7	1.0
neck	0.2	3.0
seed shoulder 1	0.7	1.0
seed shoulder 2	0.8	1.0
seed shoulder 3	0.9	1.0
seed	2.0	L

Table 4.3

Increasing seed length from 6 mm to 12 mm (high radiation condition)

Element	$\frac{dT_c}{dZ}(Z=0)$	$\frac{dT_c}{dZ}(Z=0)$	percentage change in $\frac{dT_c}{dZ}(Z=0)$
	6 mm	12 mm	
Aℓ	0.901	0.890	1.220
Ag	1.095	1.079	1.461
Cu	1.396	1.378	1.289
Ni	13.926	13.922	0.028
Cr	27.623	27.622	0.003
Si	23.365	23.365	0.0

Table 4.4

Changing seed steps from 4 to 3 steps

Element	$\frac{dT_c}{dZ}$ (Z=0)	$\frac{dT_c}{dZ}$ (Z=0)	percentage change in $\frac{dT_c}{dZ}$ (Z=0)
	4 steps	3 steps	
Al	0.901	0.917	1.744
Ag	1.095	1.119	2.144
Cu	1.396	1.421	1.759
Ni	13.926	13.937	0.078
Cr	27.623	27.630	0.025
Si	23.365	23.369	0.017

Table 4.5

Geometrical Parameters used in the calculation seed shoulder 1 equal zero when we change to 3 steps

Section	Radius (mm)	Length (mm)
crystal	1.0	3.0
crystal shoulder 1	0.9	1.0
crystal shoulder 2	0.8	1.0
crystal shoulder 3	0.7	1.0
neck	0.2	3.0
seed shoulder 1	0.7	1.0
seed shoulder 2	0.8	1.0
seed shoulder 3	0.9	1.0
seed	2.0	6.0

Table 4.6

Geometrical parameters used in Figure 4.5. S is the variabhle plotted. It is equal to 0.25, 0.5, 0.75 and 1

Section	Radius (mm)	Length (mm)
crystal	1.0	3.0
crystal shoulder 1	0.9	1.0
crystal shoulder 2	0.8	1.0
crystal shoulder 3	0.7	1.0
neck	0.2	3.0
seed shoulder 1	0.7	S
seed shoulder 2	0.8	S
seed shoulder 3	0.9	S
seed	2.0	6.0

Table 4.7

Reducing seed shoulder length from 3 mm to 1.5 mm (high radiation condition)

Element	$\frac{dT_c}{dZ}$ (Z=0)	$\frac{dT_c}{dZ}$ (Z=0)	percentage change in $\frac{dT_c}{dZ}$ (Z=0)
	3 mm	1.5 mm	
Al	0.901	0.919	1.997
Ag	1.095	1.123	2.557
Cu	1.396	1.426	2.148
Ni	13.926	13.939	0.093
Cr	27.623	27.631	0.028
Si	23.365	23.370	0.021

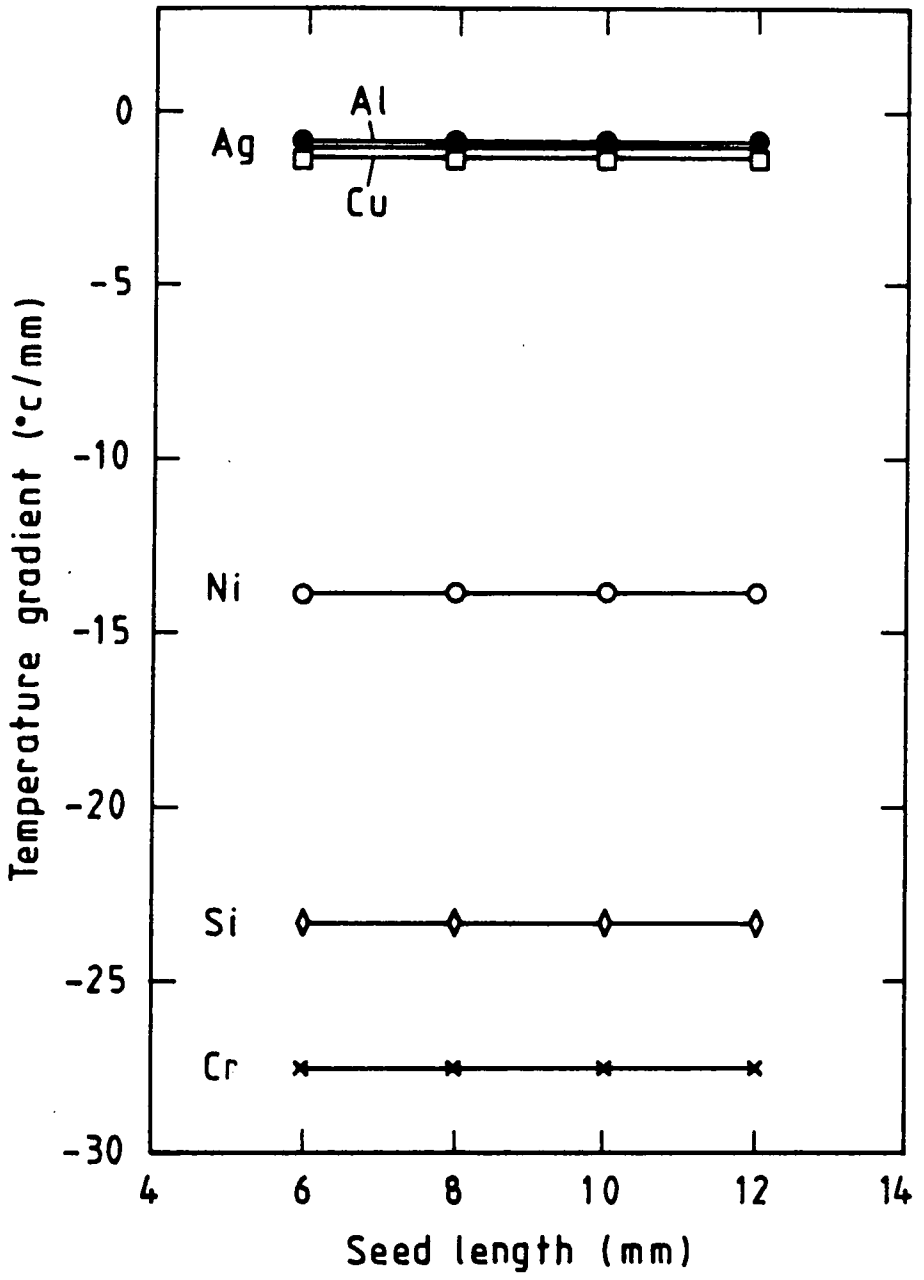

Fig. 4.4 Increasing the seed length from 6, 8, 10 and finally to 12 mm.

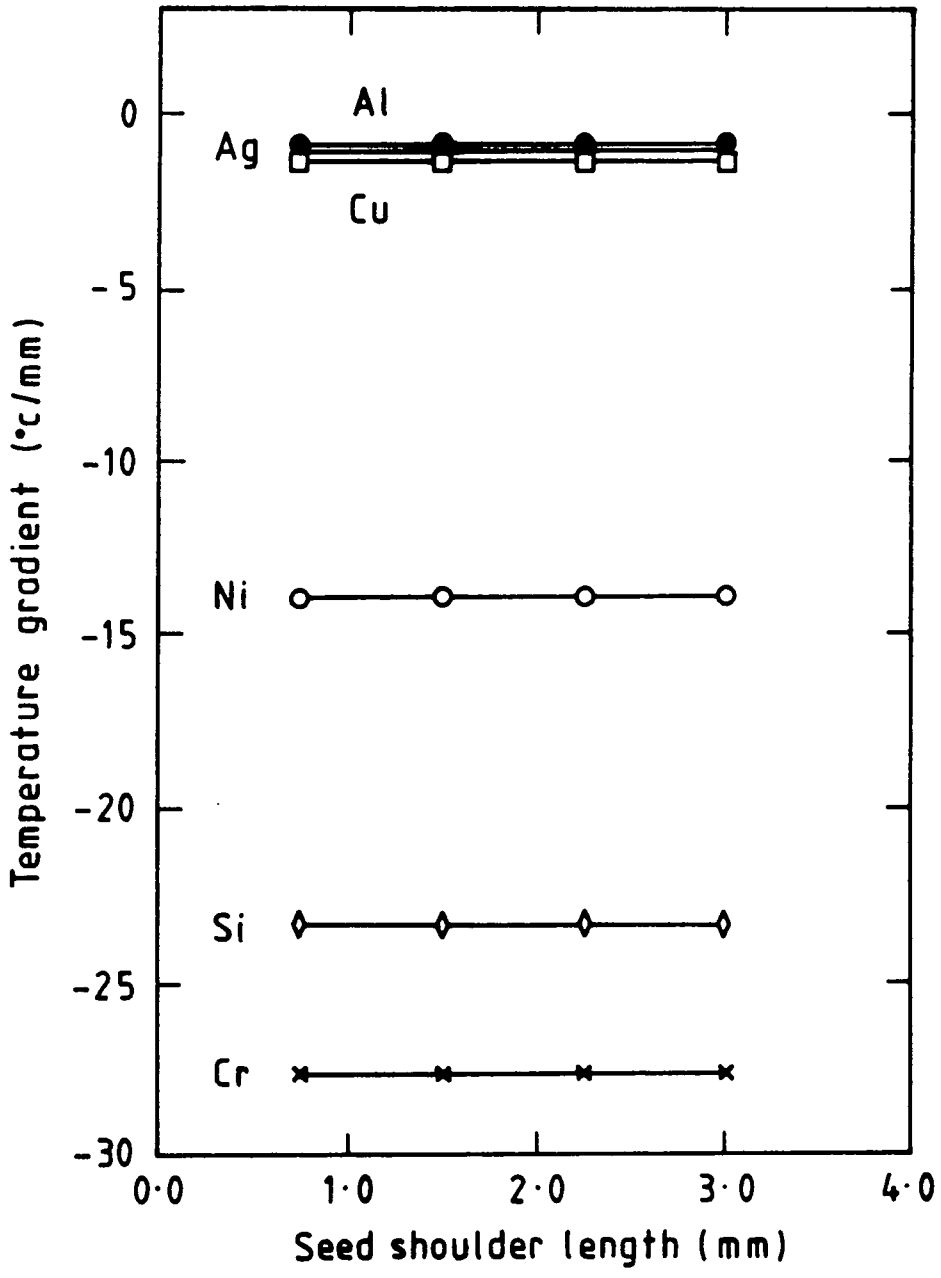

Fig. 4.5 Increasing the seed shoulder length from 0.75, 1.5, 2.25 and finally to 3 mm.

Table 4.8

Geometrical parameters used in calculation, r is the variable It is equal to 0.5, 0.75, 1 and 1.5

Section	Radius (mm)	Length (mm)
crystal	1.0	3.0
crystal shoulder 1	0.9	1.0
crystal shoulder 2	0.8	1.0
crystal shoulder 3	0.7	1.0
neck	0.2	3.0
seed shoulder 1	0.7r	1.0
seed shoulder 2	0.8r	1.0
seed shoulder 3	0.9r	1.0
seed	2.0r	6.0

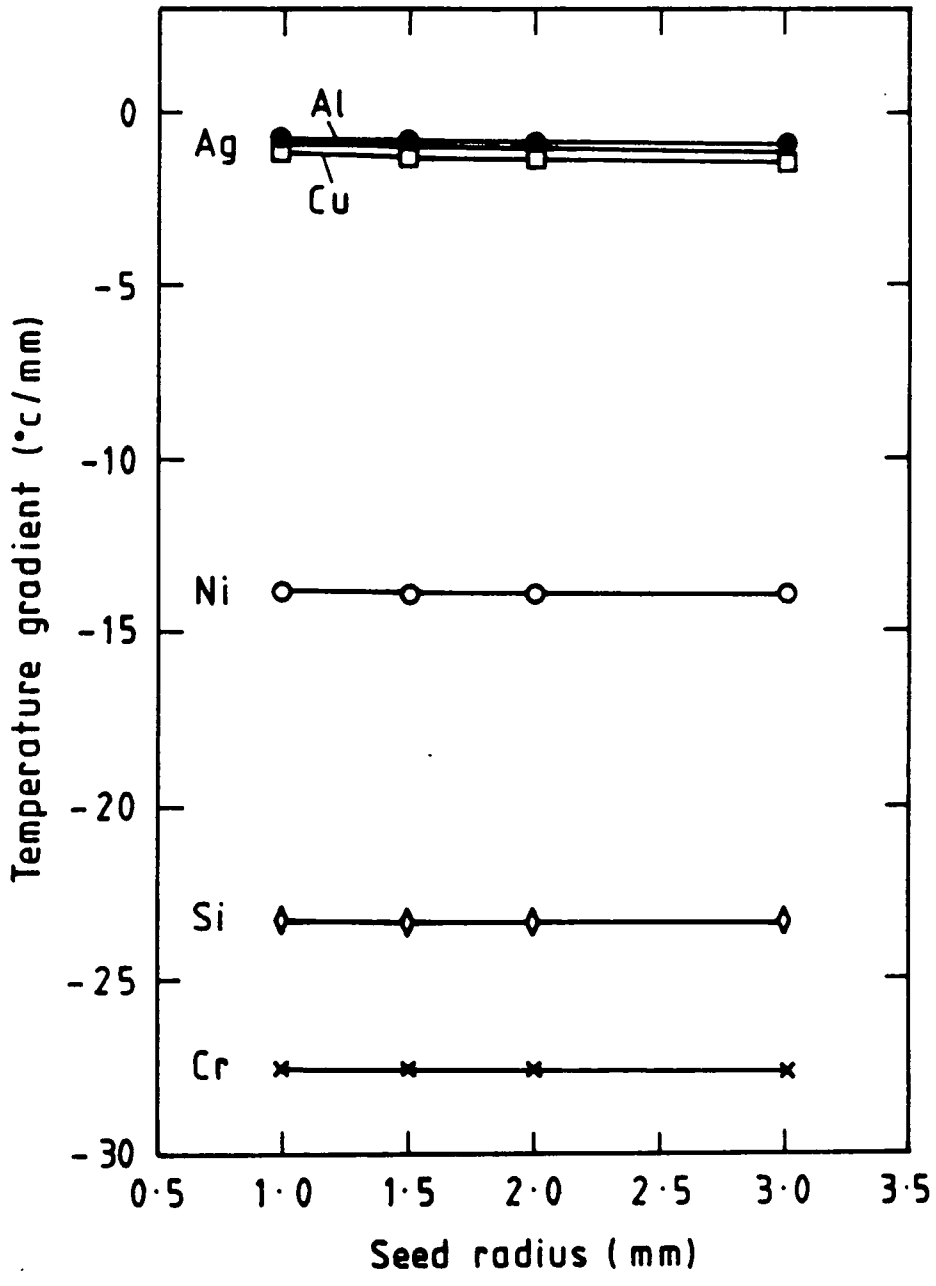

Fig. 4.6 Increasing seed radius. r is equal to 1, 1.5, 2 and 3 mm.

Table 4.9

Reducing seed and shoulder radii by factor 2 (high radiation condition)

Element	$\frac{dT_c}{dZ}$ (Z=0)	$\frac{dT_c}{dZ}$ (Z=0)	Percentage change in $\frac{dT_c}{dZ}$ (Z=0)
	r=2	r=1	
Al	0.901	0.785	12.874
Ag	1.095	0.920	15.981
Cu	1.396	1.205	13.681
Ni	13.926	13.848	0.560
Cr	27.623	27.580	0.155
Si	23.365	23.341	0.102

Table 4.10

Geometrical parameter used in Figure 4.7. L is the variable plotted. It is equal to 3, 4, 5 and 6

Section	Radius (mm)	Length (mm)
crystal	1.0	L
crystal shoulder 1	0.9	1.0
crystal shoulder 2	0.8	1.0
crystal shoulder 3	0.7	1.0
neck	0.2	3.0
seed shoulder 1	0.7	1.0
seed shoulder 2	0.8	1.0
seed shoulder 3	0.9	1.0
seed	2.0	6.0

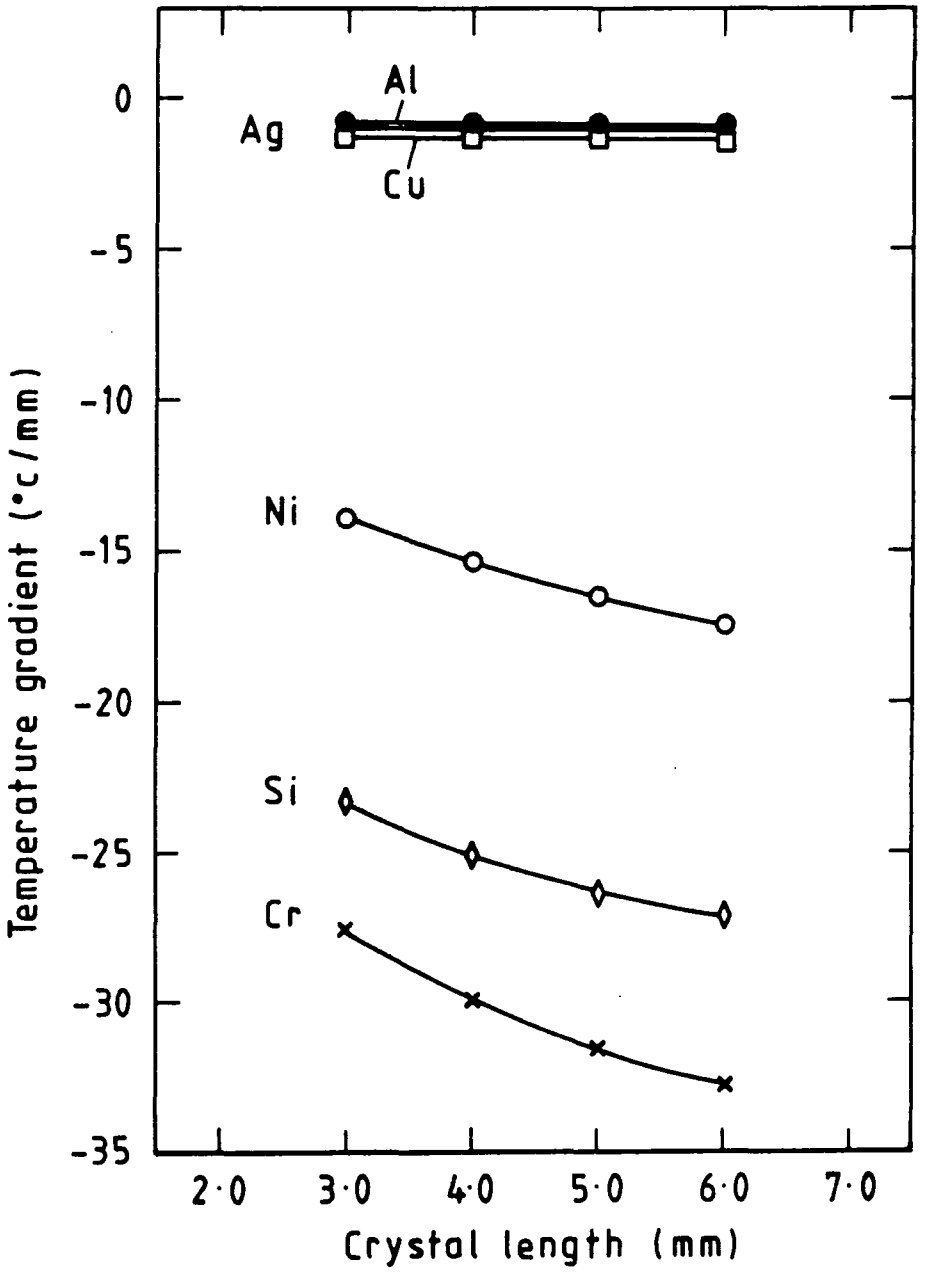

Fig. 4.7 Increasing the crystal length from 3, 4, 5 and finally to 6 mm.

Table 4.11

Increasing crystal length by factor 2 from 3 mm to 6mm (high radiation condition)

Element	$\frac{dT_c}{dZ}$ (Z=0)	$\frac{dT_c}{dZ}$ (Z=0)	percentage change in $\frac{dT_c}{dZ}$ (Z=0)
	3 mm	6 mm	
Al	0.901	0.991	9.988
Ag	1.095	1.109	1.278
Cu	1.396	1.505	7.808
Ni	13.926	17.497	25.642
Cr	27.623	32.697	18.368
Si	23.365	27.180	16.327

Table 4.12

Reducing crystal shoulder length by factor 2 (high radiation condition)

Element	$\frac{dT_c}{dZ}$ (Z=0)	$\frac{dT_c}{dZ}$ (Z=0)	percentage change in $\frac{dT_c}{dZ}$ (Z=0)
	3mm	1.5mm	
Al	0.901	0.874	2.996
Ag	1.095	1.104	0.821
Cu	1.396	1.367	2.077
Ni	13.926	11.907	14.498
Cr	27.623	24.204	12.377
Si	23.365	20.656	11.594

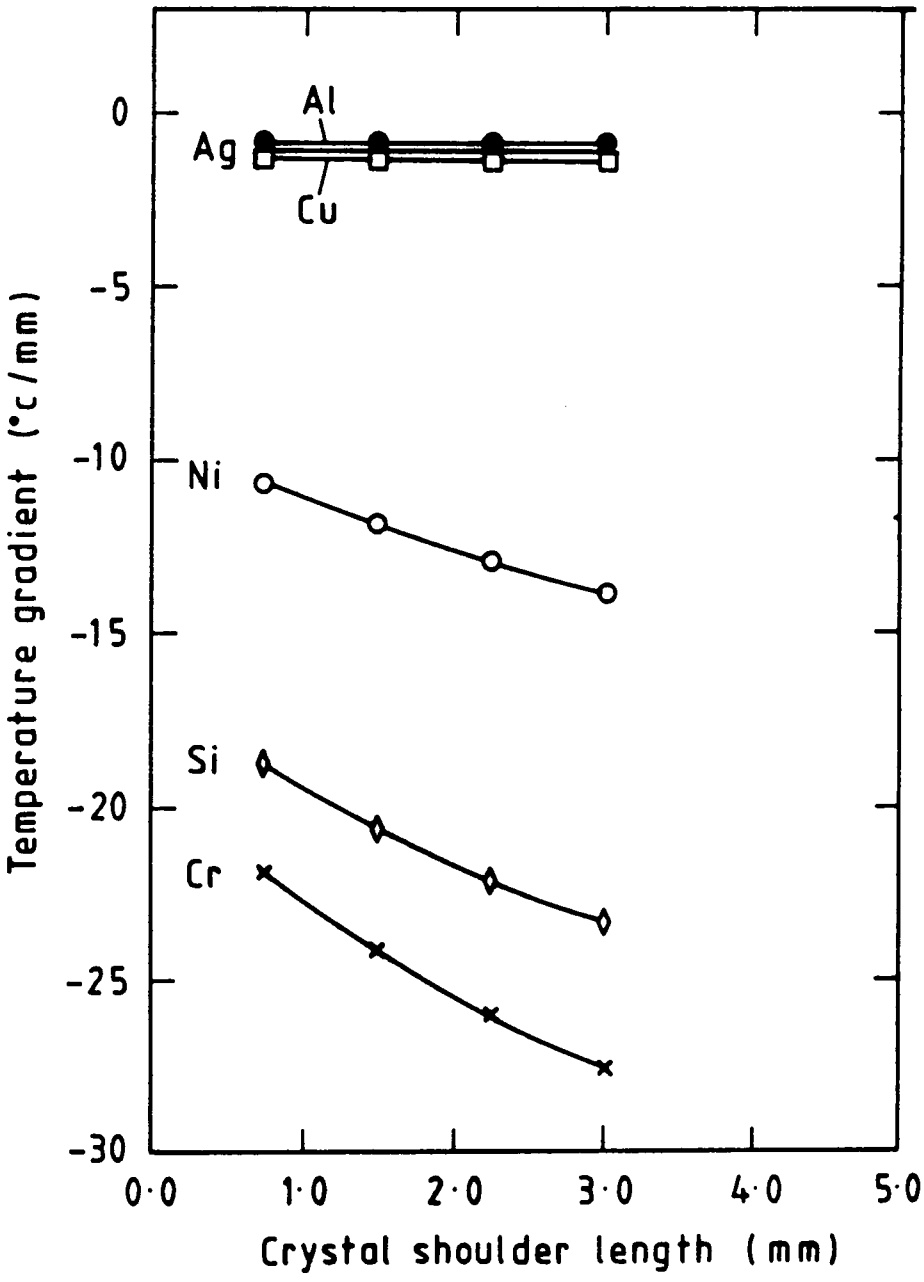

Fig. 4.8 Increasing crystal shoulder length from 0.75, 1.5, 2.25 and finally to 3 mm.

Table 4.13

Geometrical parameters used in Figure 4.8. S is the variable plotted. it is equal to 0.25, 0.50, 0.75 and 1

Section	Radius (mm)	Length (mm)
crystal	1.0	3
crystal shoulder 1	0.9	S
crystal shoulder 2	0.8	S
crystal shoulder 3	0.7	S
neck	0.2	3
seed shoulder 1	0.7	1.0
seed shoulder 2	0.8	1.0
seed shoulder 3	0.9	1.0
seed	2.0	6.0

Table 4.14

Geometrical parameters used in the calculation. r is the variable. It is equal to 1, 1.5, 2, 3, and 4.

Section	Radius (mm)	Length (mm)
crystal	1.0r	3.0
crystal shoulder 1	0.9r	1.0
crystal shoulder 2	0.8r	1.0
crystal shoulder 3	0.7r	1.0
neck	0.2	3.0
seed shoulder 1	0.7	1.0
seed shoulder 2	0.8	1.0
seed shoulder 3	0.9	1.0
seed	2.0	6.0

Fig. 4.9 Photograph of Silicon single crystals. It was grown by rapid increase in the diameter.

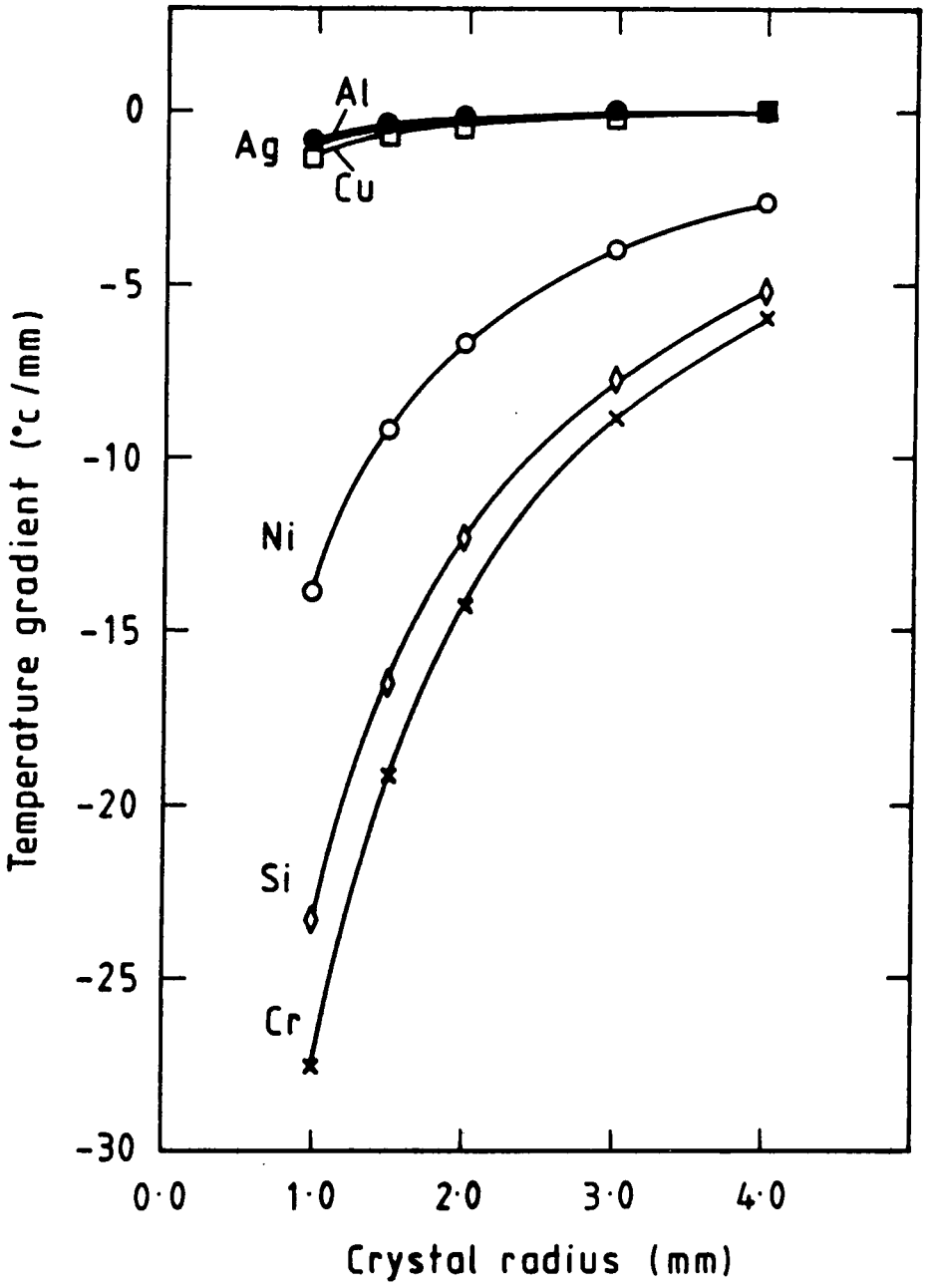

Fig. 4.10 Increasing crystal radius. r is equal to 1, 1.5, 2, 3 and 4 mm.

Table 4.15

Increasing the crystal and shoulder radii by factor 2 (high radiation condition)

Element	$\frac{dT_c}{dZ}$ (Z=0)	$\frac{dT_c}{dZ}$ (Z=0)	percentage change in $\frac{dT_c}{dZ}$ (Z=0)
	r=1	r=2	
Al	0.901	0.283	68.590
Ag	1.095	0.310	71.689
Cu	1.396	0.427	69.412
Ni	13.926	6.741	51.594
Cr	27.623	14.381	47.938
Si	23.365	12.419	46.847

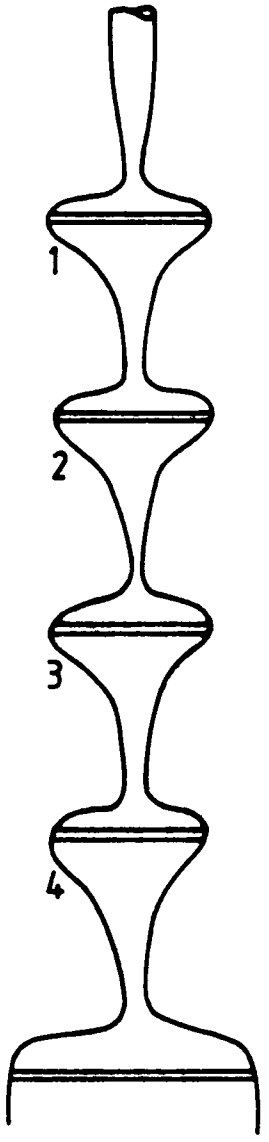

Fig. 4.11 Diagram shows growth procedure used to grow silicon single crystals (after Murthy and Aubert, 1981).

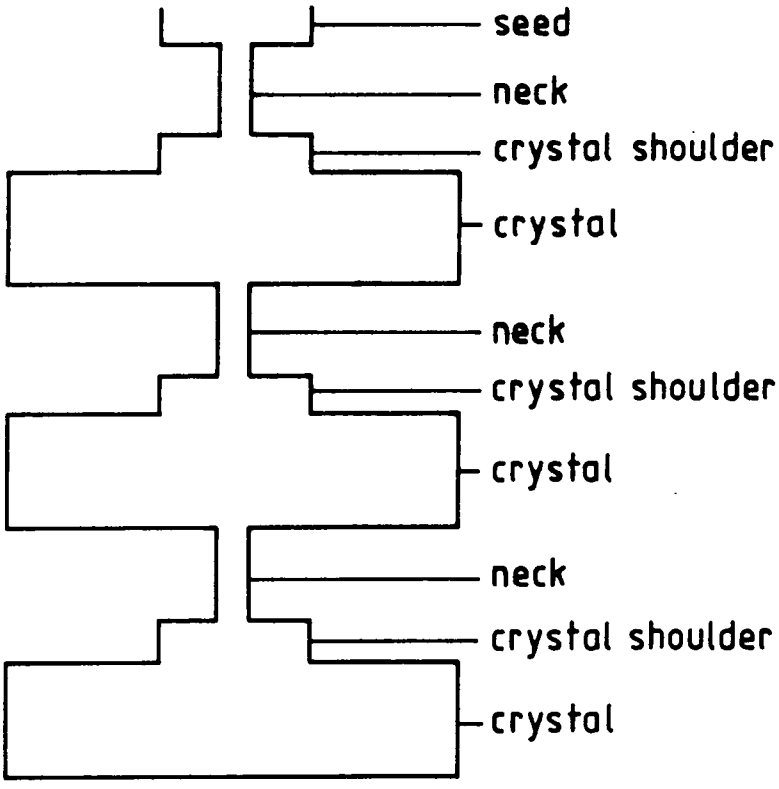

Fig. 4.12 Crystal growth model with multiple necks.

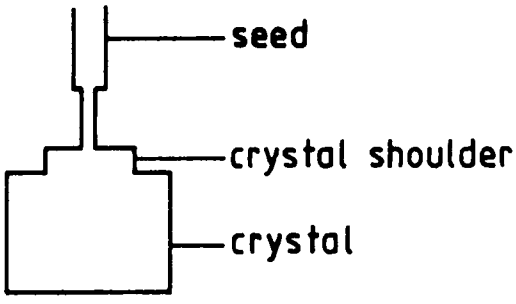

Fig. 4.13 Crystal growth model with single neck.

Table 4.16

crystal radius	single neck	multiple neck
mm	$\frac{dT_c}{dZ}$ (Z=0)	$\frac{dT_c}{dZ}$ (Z=0)
1	19.80	19.76
2	7.97	7.96
3	3.99	4.00

Table 4.17

Geometrical parameters used in the calculation. R is equal to 1, 2 and 3. Sections 4, 5, 6, 7, 8 and 9 go to zero with single neck model.

Section		Radius (mm)	Length (mm)
crystal	(1)	R	3.0
crystal shoulder	(2)	0.9	1.0
neck	(3)	0.2	3.0
crystal	(4)	1.0	3.0
crystal shoulder	(5)	0.9	1.0
neck	(6)	0.2	3.0
crystal	(7)	1.0	3.0
crystal shoulder	(8)	0.9	1.0
neck	(9)	0.2	3.0
seed	(10)	2.0	6.0

Table 4.18

Increasing the neck length by factor 2 from 3 mm to 6 mm (high radiation condition)

Element	$\frac{dT_c}{dZ}$ (Z=0)	$\frac{dT_c}{dZ}$ (Z=0)	percentage change in $\frac{dT_c}{dZ}$ (Z=0)
	3 mm	6 mm	
Al	0.901	0.601	33.296
Ag	1.095	0.641	41.461
Cu	1.396	0.902	35.386
Ni	13.926	13.737	1.357
Cr	27.623	27.522	0.365
Si	23.365	23.309	0.239

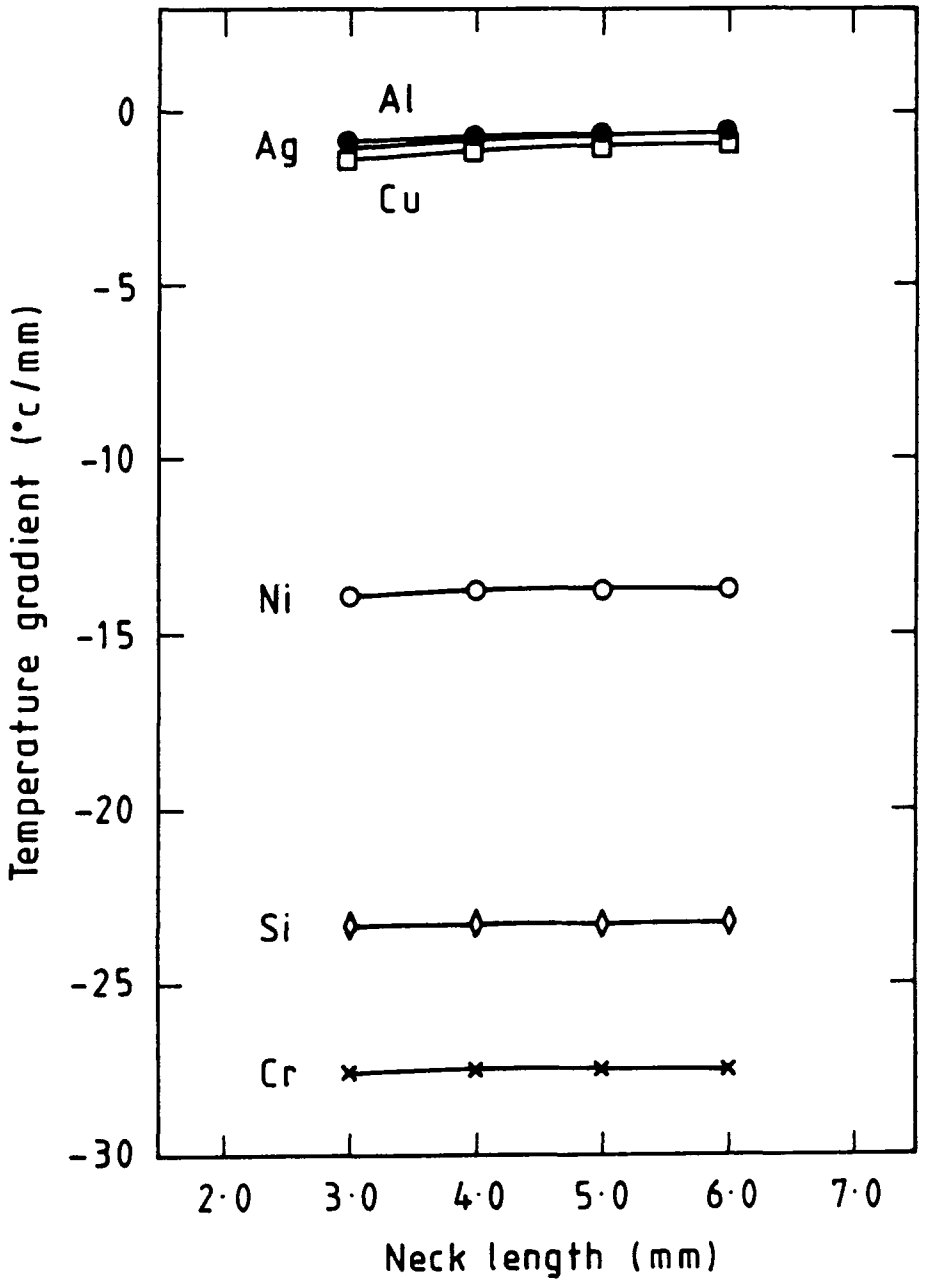

Fig. 4.14 Increasing neck length from 3, 4, 5 and finally to 6 mm.

Table 4.19

Geometrical parameter used in Figure 4.13. L is the variable plotted. It is equal to 3, 4, 5 and 6.

Section	Radius (mm)	Length (mm)
crystal	1.0	3.0
crystal shoulder 1	0.9	1.0
crystal shoulder 2	0.8	1.0
crystal shoulder 3	0.7	1.0
neck	0.2	L
seed shoulder 1	0.7	1.0
seed shoulder 2	0.8	1.0
seed shoulder 3	0.9	1.0
seed	2.0	6

Table 4.20

Geometrical parameter used in Figure 4.14. R is the variable plotted. It is equal to 0.1, 0.12, 0.17 and 2.0

Section	Radius (mm)	Length (mm)
crystal	1.0	3.0
crystal shoulder 1	0.9	1.0
crystal shoulder 2	0.8	1.0
crystal shoulder 3	0.7	1.0
neck	R	3.0
seed shoulder 1	0.7	1.0
seed shoulder 2	0.8	1.0
seed shoulder 3	0.9	1.0
seed	2.0	6.0

Table 4.21

Reducing the neck radius by factor 2 from 2 mm to 1 mm (high reduction condition)

Element	$\frac{dT_c}{dZ}$ (Z=0)	$\frac{dT_c}{dZ}$ (Z=0)	percentage change in $\frac{dT_c}{dZ}$ (Z=0)
	0.2 mm	0.1 mm	
Al	0.901	0.413	54.162
Ag	1.095	0.375	65.753
Cu	1.396	0.599	57.091
Ni	13.926	13.136	5.672
Cr	27.623	26.832	2.863
Si	23.365	22.818	2.341

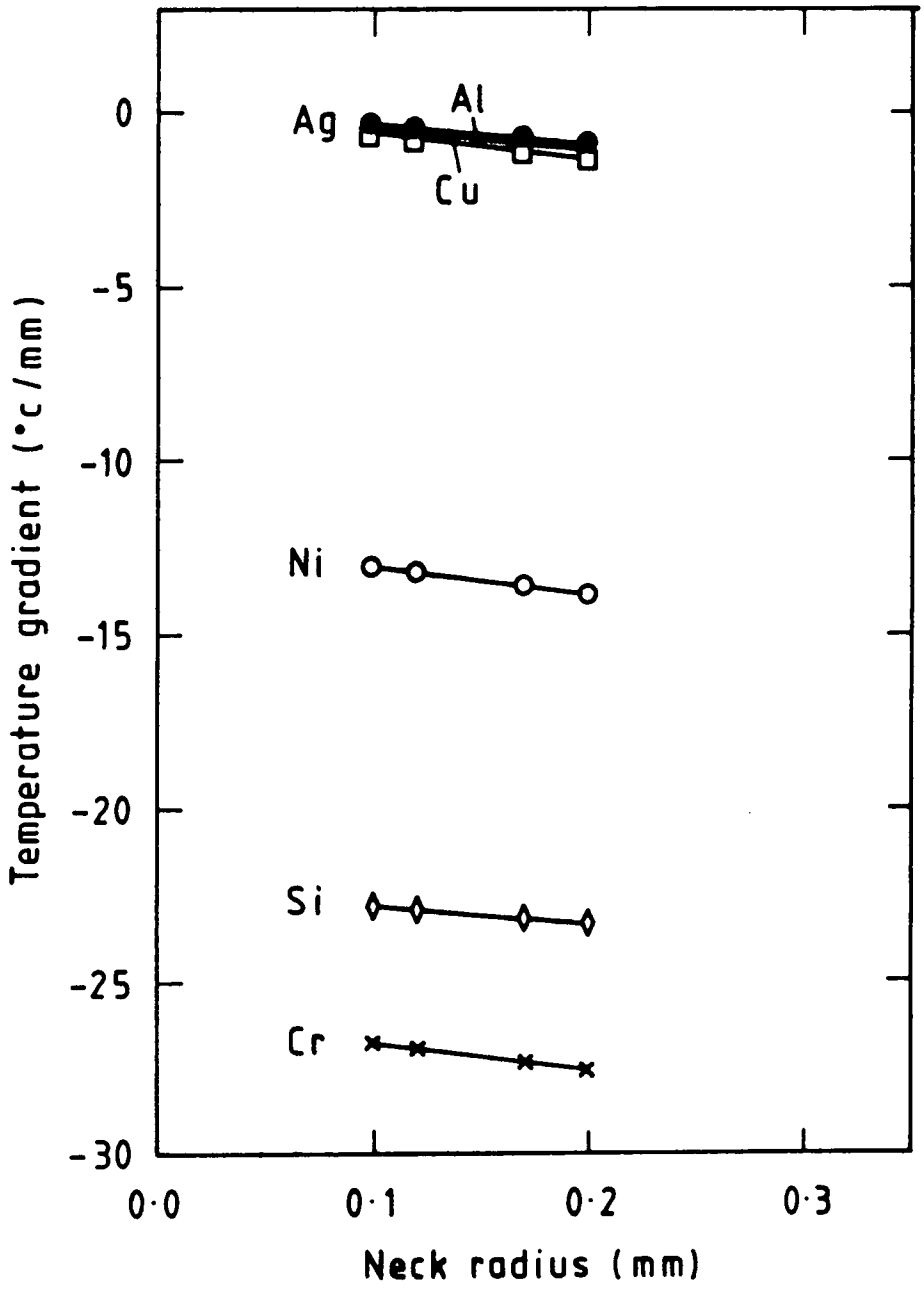

Fig. 4.15 Increasing neck radius from 0.1, 0.12, 0.17 and finally to 2 mm.

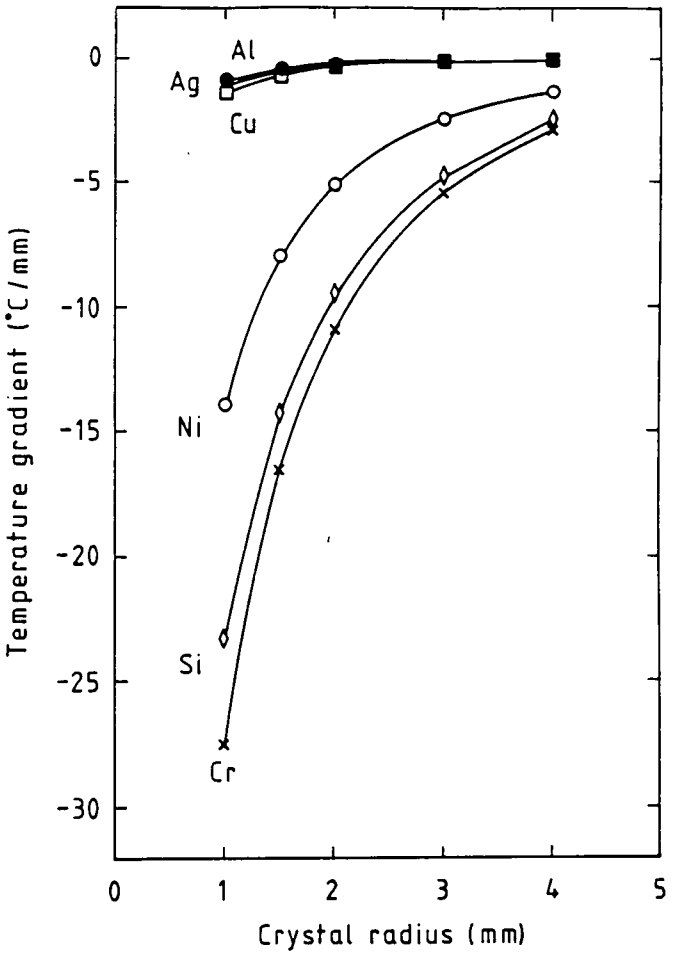

(a)

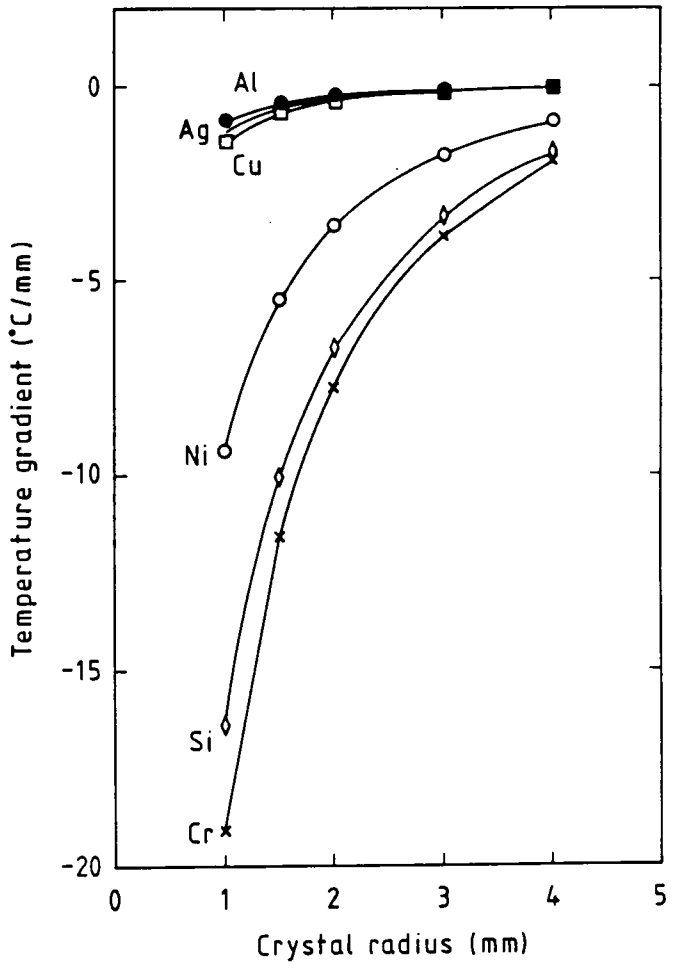

(b)

Fig. 4.16 Comparison between current (a) and previous (b) models at different crystal radius

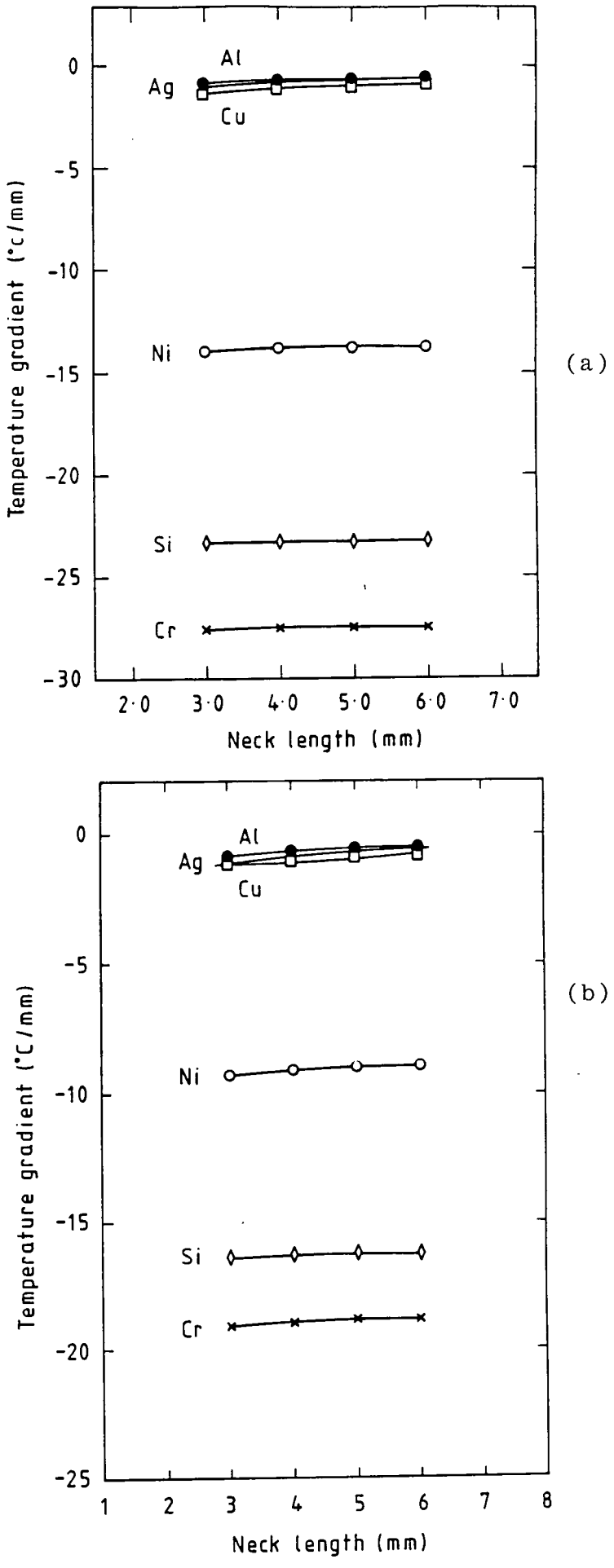

Fig. 4.17 Comparison between current (a) and previous (b) models at different neck lengths.

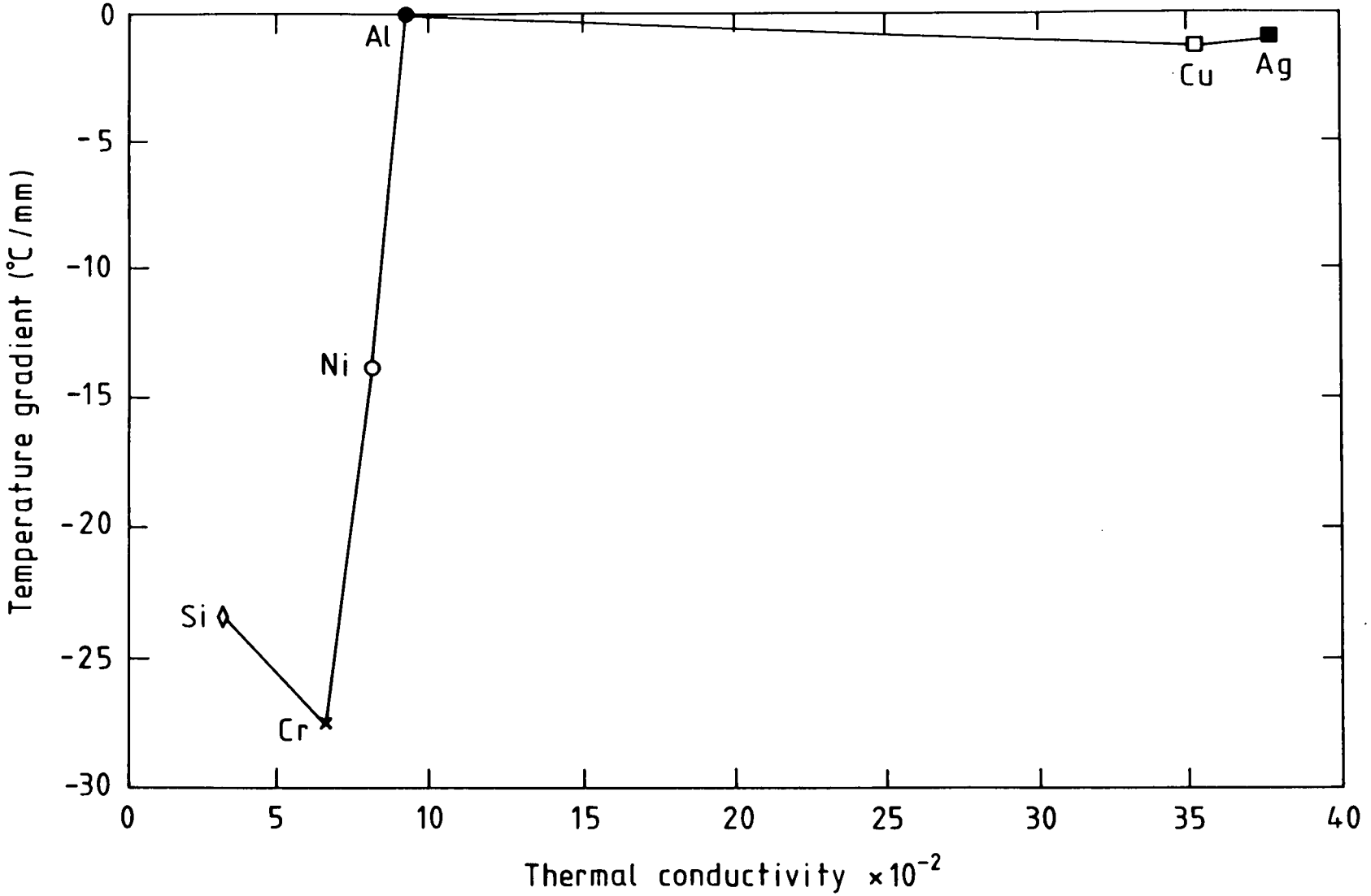

Fig. 4.18 The relation between thermal conductivity and temperature gradient.

CHAPTER FIVE

DOMAIN WALL MOTION IN HAEMATITE OBSERVED IN REAL TIME

5.1 Introduction

The original aim had been to study domain wall motion of domains in nickel in real time using synchrotron radiation. Pilot experiments to examine the feasibility of using the TV system at Daresbury were undertaken on α-Fe_2O_3.

Haematite (α - Fe_2O_3) is a weak ferromagnet at room temperature. Its magnetic properties have been studied by neutron diffraction by Shull et al. (1951) and Nathans et al. (1964).

The domain structure of α - Fe_2O_3 has been observed by Labushkin et al. (1978). Recently an extensive study of the behaviour of the domain structure was carried out using X-ray topography at Daresbury Laboratory by Clark et al. (1983) and Tanner et al. (1988).

Pilot experiments to study domain wall movement in flux growth crystals of haematite under a magnetic field have been performed at the Synchrotron Radiation Source at Daresbury Laboratory.

5.2 Experimental procedure

The crystals used in this experiment are thin basal plane platelets with an area of 0.33 cm^2 to 0.79 cm^2. They were grown from PbO - PbF_2 flux by B.M. Wanklyn at the

Clarendon Laboratory, Oxford. Since they are very fragile and brittle no attempts were made to cut them.

Topographs were taken using white synchrotron radiation on Station 7.6 at Daresbury Laboratory. The magnetic field was horizontal and all topographs were taken in transmission using the $30\bar{3}0$ reflection. The topographs were recorded on Ilford L4 25 μm thick nuclear plates with a 3 minute exposure time, as well as in real time on the TV imaging system. While the best quality resolution X-ray topographs are obtained from nuclear plates, there is a demand for live topograph to study dynamic processes. It also helps to reduce the long time required for exposure and development. There exist two approaches to permit rapid viewing and recording real time topographs, namely direct and indirect methods (Green, 1977). In the direct method X-ray topographic images are converted into electrical signals. TV tubes are susceptible to radiation damage and thus life time is short. As for the indirect method X-ray topographic images are converted into visible light by a fluorescent screen (Figure 5.1). The latter could be used with conventional X-ray source while the former required high intensity X-ray generator it is more expensive but has the highest resolution.

The camera on station 7.6 is a direct conversion device and was used to observe in real time the movement of domains as a function of magnetic field. All motion is controlled by stepping motors and all are under complete local computer

control. TV images were recorded on Sony Umatic videotape and a comparison between the videotape and the nuclear plate has been made. Figures (5.2) obtained at 150, 300 and zero field are good examples of this comparison.

5.3 Static experiments

Stripe patterns can be seen in Figure (5.3), showing a portion of the domain wall for the first crystal. As synchrotron radiation has a continuous wavelength beam, both domains appear in the image. When a parallel planar boundary is extended through the sample, the X-rays diffracted by the upper domain will not be diffracted by the lower one. Each domain can be treated as an independently diffracting crystal. The contrast on the right hand side of the image is much stronger than the rest of the image because it is thinner. The interaction between the magnetization and the local strain inside the crystal is seen here to be strong. No dislocations can be seen and significant strain content is present, maybe due to flux included inside the crystal.

Parallel domains were observed, very similar to those obtained by Tanner et al. (1988). They noted that the images were between 100 and 200 μm wide, the interaction with a twin boundary was very strong and could be removed from the sample by application of a weak field. Figure (5.4) shows schematically their interpretation for these parallel domains. The results here are consistent with these earlier observations.

In a zero magnetic field 6 domains per cm were observed on both TV monitor and nuclear plate. However at 120mA,

although 12 domains were observed in 1 cm on the nuclear plate image, only one was seen on the TV monitor. (The corresponding actual widths of domains were 1.6mm at zero field, and 0.9 mm (nuclear plate) and 10 mm (TV) at 120mA). The difference is due to the fact that the fine domain structure cannot be seen from the TV monitor as the domains have rather low contrast. Because resolution and defect contrast are related, where the intensity is low, closely spaced defects with low contrast will not be revealed in real-time topography. The number of domains in a given length of crystal and width of an individual domain are measured as a function of field, Table (5.1) and Figure (5.5). As the field increases the number of domains decreases as it is measured from the TV. This inverse relation was not seen by Tanner et al. (1988), due to the fact that when the measurements were made from nuclear plates, the fine structure was counted. Again the low contrast means that the closely spaced domain boundaries are not detected. Clearly care must be taken when using real time imaging for such measurements.

The domains in the second crystal (Figure 5.6) are highly mobile as the field increases. Also the domains are long, wide and here the interaction is very weak. The lines (S) are related to the surface structure (Figure 5.7), while in the first crystal there is no correlation with surface morphology, Figure (5.6). The domain interaction with the rotation twin boundary is very clear. When the crystal is

rotated through 90^{o} to image with $11\bar{2}0$ reflection, the twin boundary appears (Figure 5.8). No change was observed in the topographs as the current increased. The only intensity changes seen are due to the movement of the crystal by the magnetic field gradient. No magnetic structure is visible at any field.

From the previous measurements, we declare that as the magnification factor is equal to 18.0, the resolution is between 46 and 92 μm. The resolution has been found by other workers to approach 20μm when the defect contrast is high. At station 9.4, the TV detector has sufficient sensitivity and resolution for a wide range of real time topography experiments.

Table 5.1

Current mA	Domain wall width per 2 cm	Nos. of Domain per 2 cm
40	5	7
50	7	6
60	12	4
80	14	3
90	19	2
100	21	1

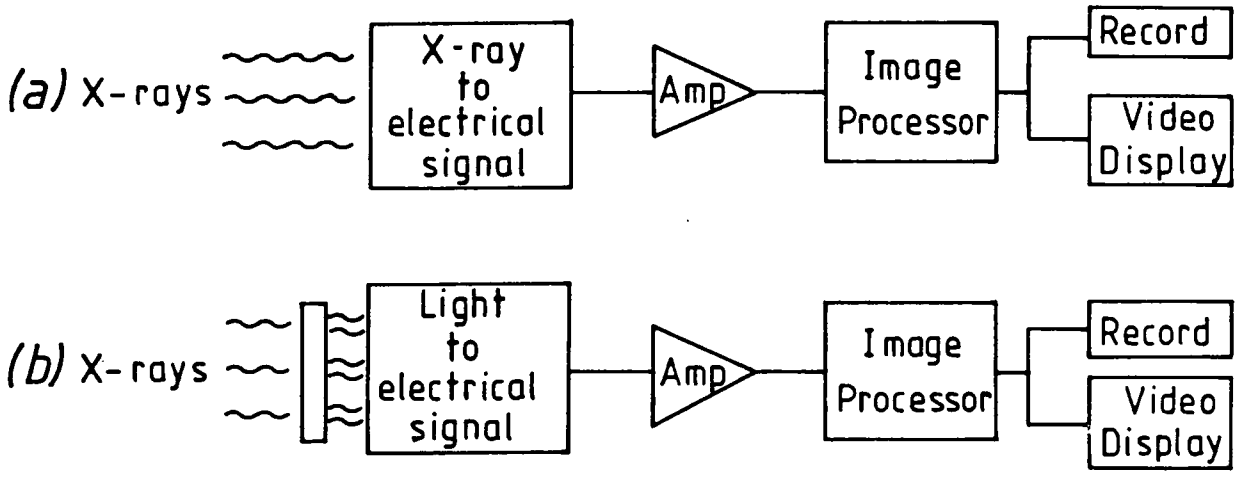

Fig. 5.1 (a) Direct conversion of X-rays.

(b) In direct conversion of X-rays (after Tanner and Cringean, 1987).

(a)

(b)

(c)

Fig. 5.2 Crystal structure as it appears in the TV monitors,
(a) At 150 mA,
(b) At 300 mA,
(c) At zero field.

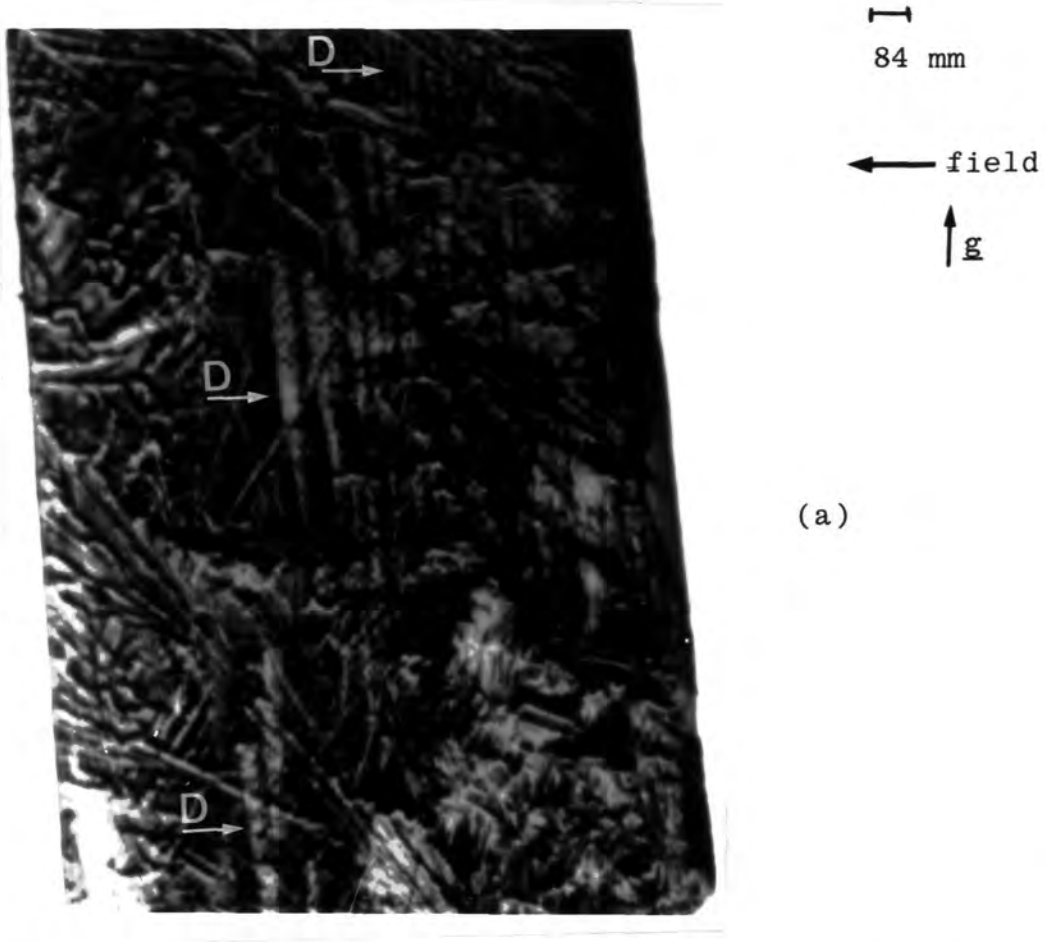

(a)

Fig. 5.3 Synchrotron X-ray topographs of α-Fe_2O_3 showing domain walls in $30\bar{3}0$ reflection (a) zero field, (b) field of 120 mA, (c) field of -100 mA, (d) field of -150 mA, (e) crystal in field of -300 mA and (f) crystal in field of -1200 mA.

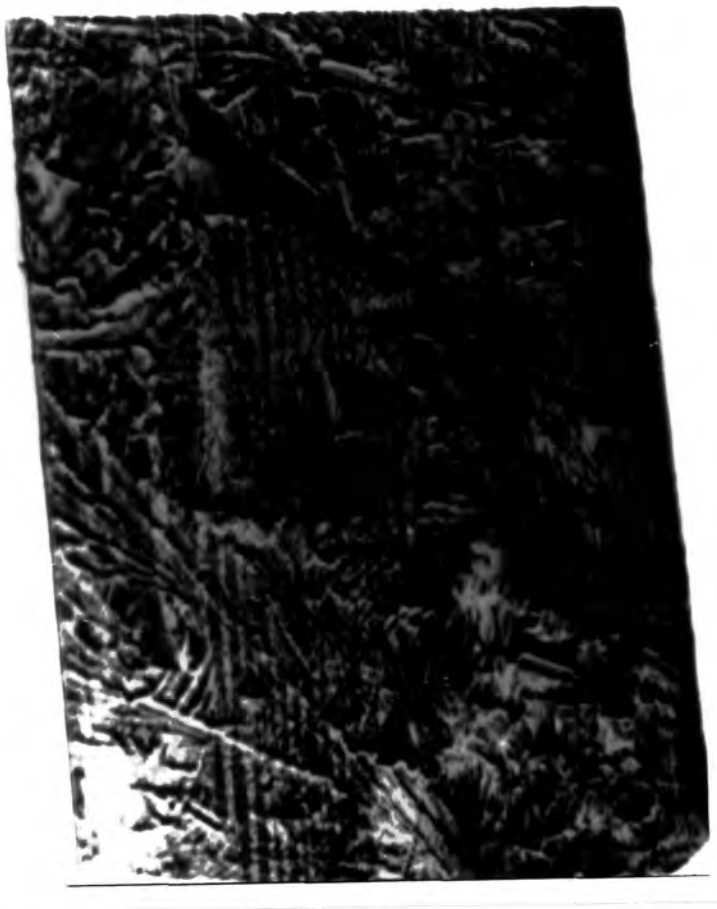

(b)

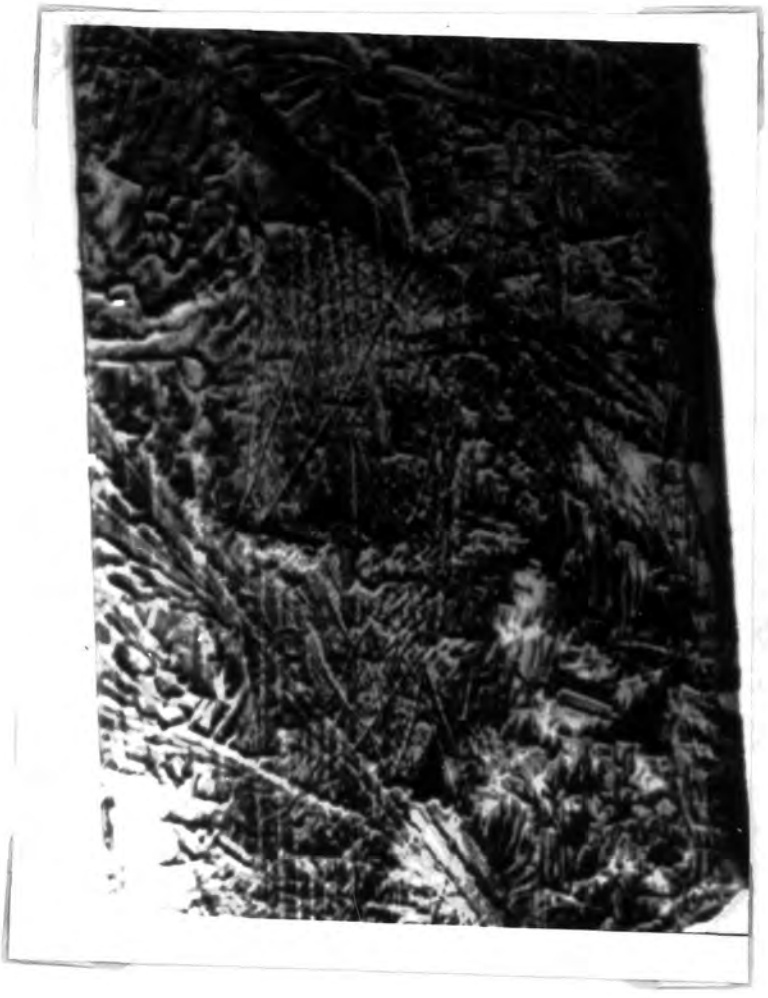

(c)

(d)

(e)

(f)

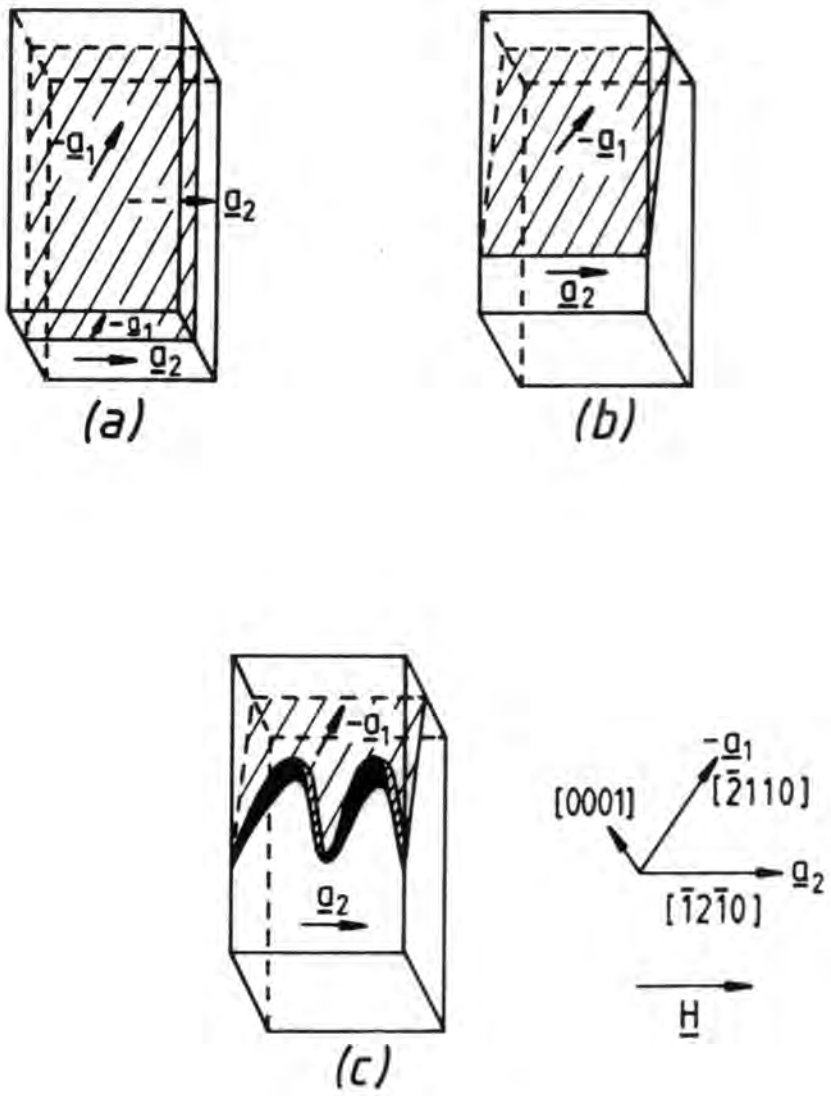

Fig. 5.4 Interpretation of the interdigital domain structure

(a) at zero field,

(b) movement of domain under application of magnetic field

(c) development of interdigital structure (after Tanner et al., 1988).

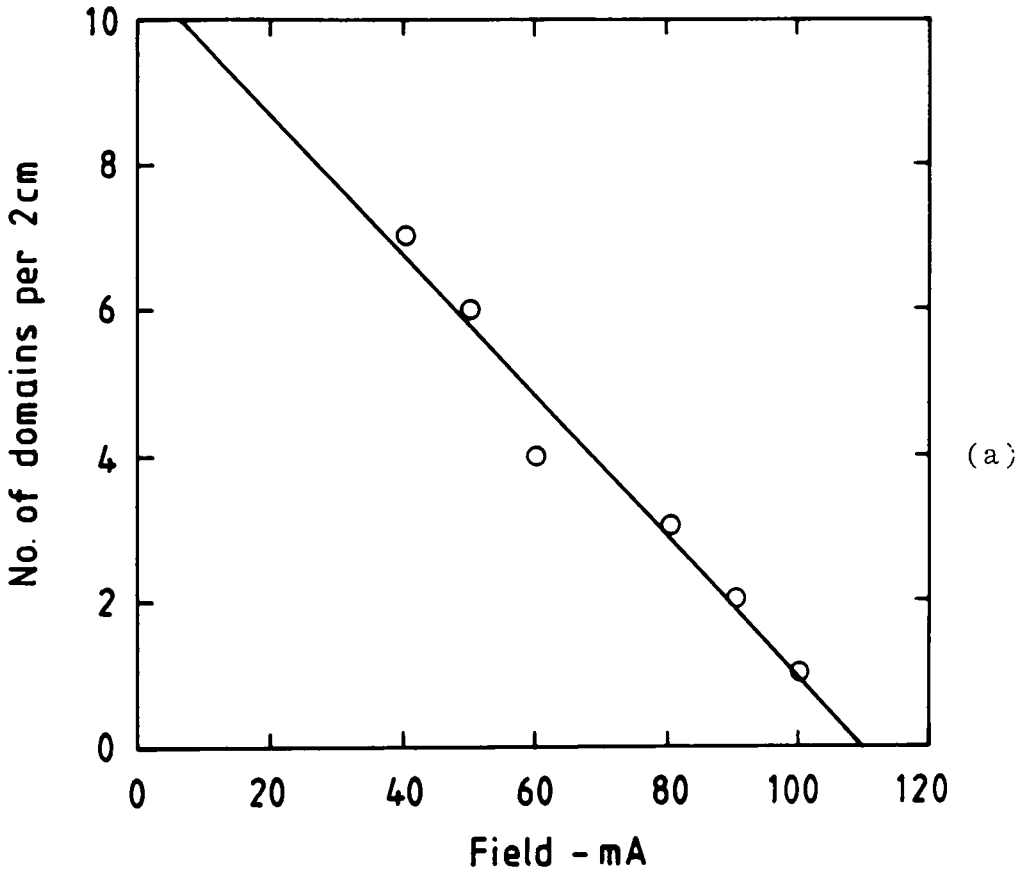

(a)

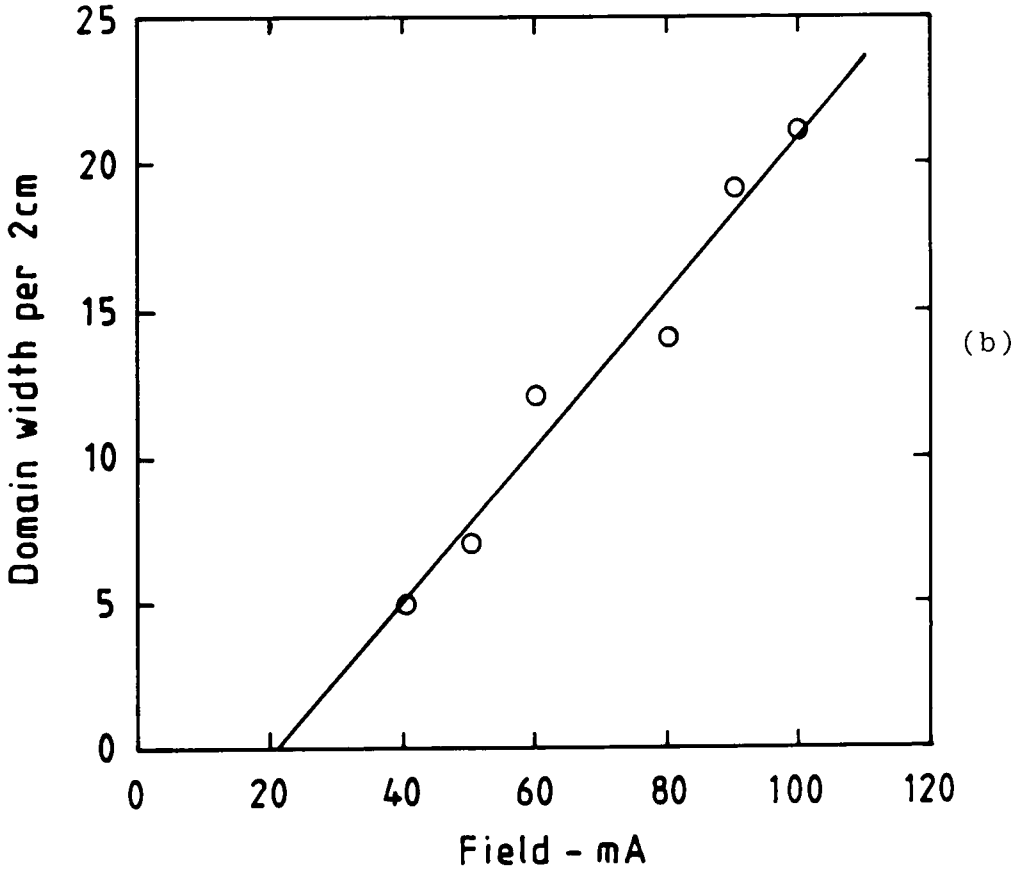

(b)

Fig. 5.5 (a) Number of domains as a function of field
(b) Domain width as function of field

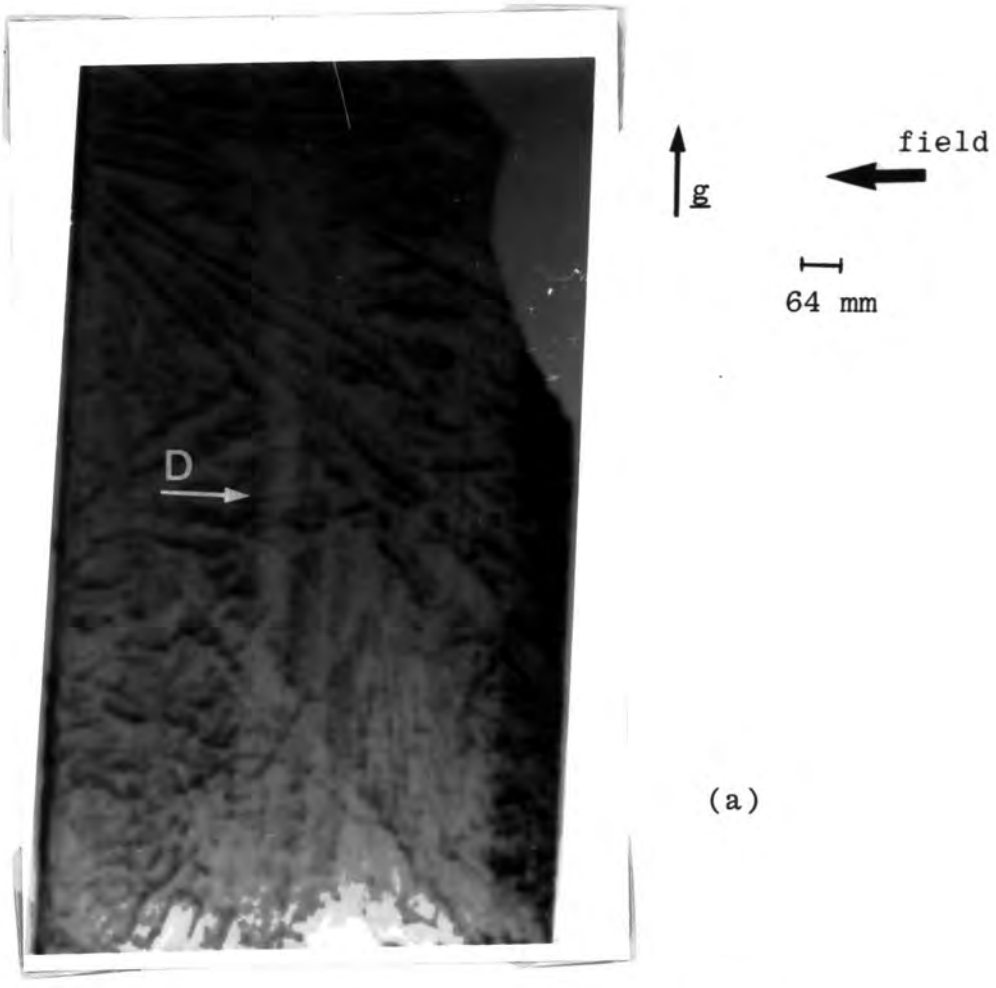

Fig. 5.6 White-radiation topographs of the second crystal, (a) zero field, b = 80 mA, c = 100 mA and d = -80 mA and e = -100 mA.

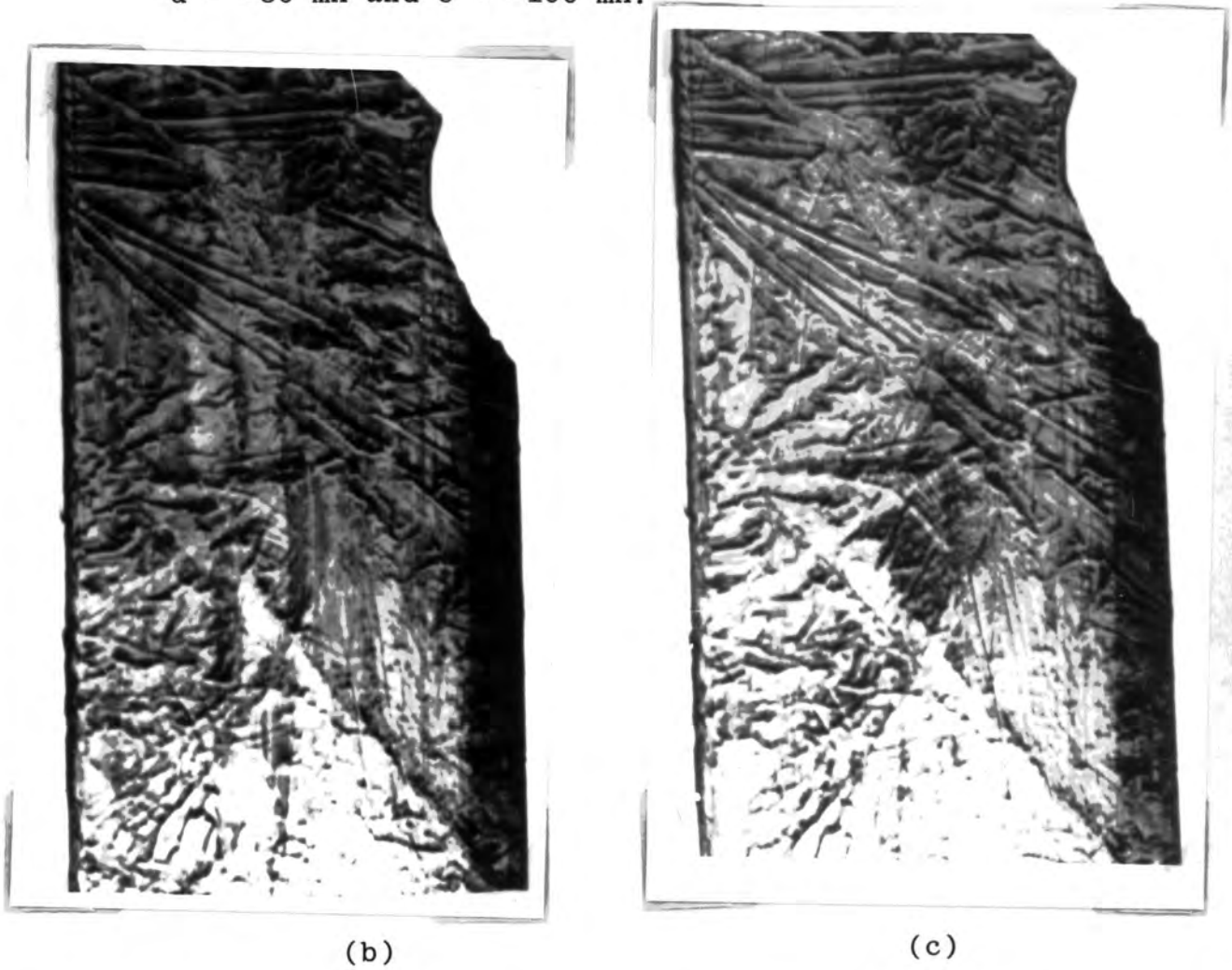

(d)

(e)

(a)

Fig. 5.7 Photograph of the crystal
(a) first crystal, and
(b) second crystal.

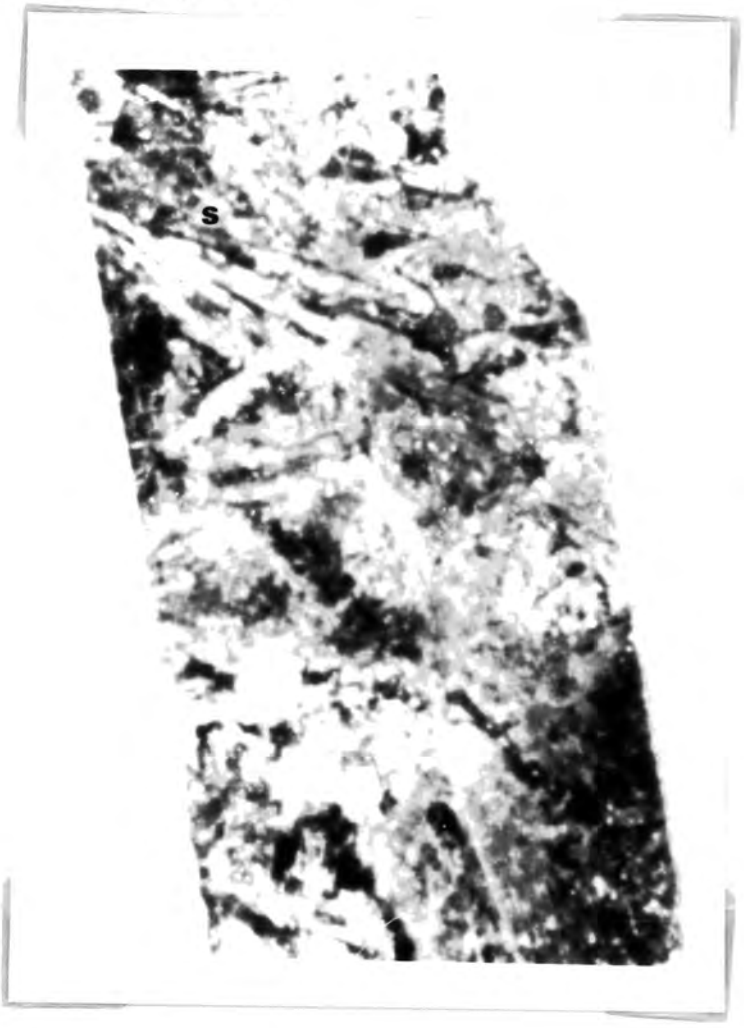

(b)

(a)

Fig. 5.8 Topograph of the second sample after it rotated through 90°, (a) = 0.4 Amp, (b) = 0.8 Amp, (c) =-0.4 Amp, (d) = -0.8 Amp, (e) = 2 Amp, and (f) = 2.3 Amp.

(b)

(c)

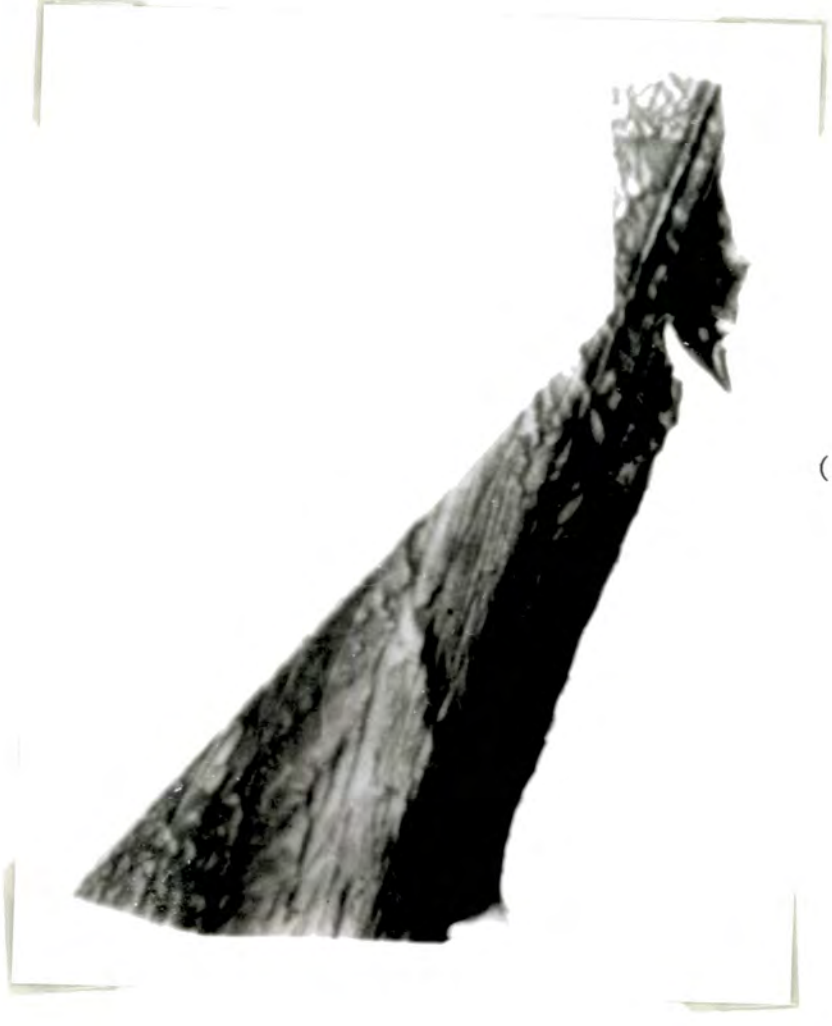

(d)

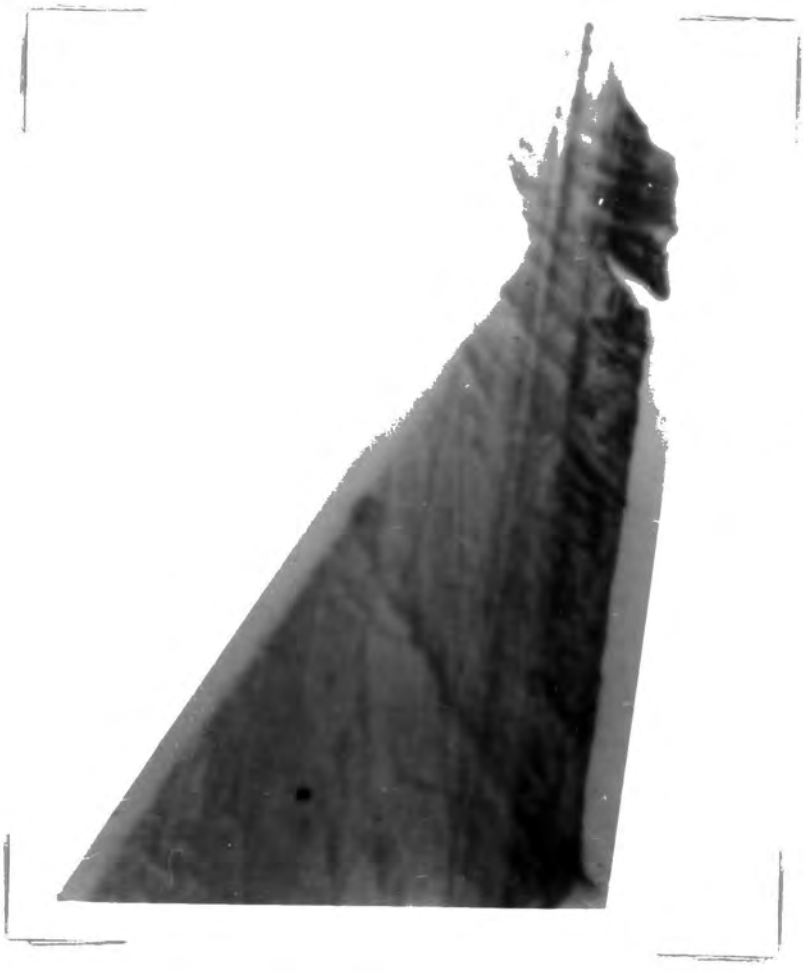

(e)

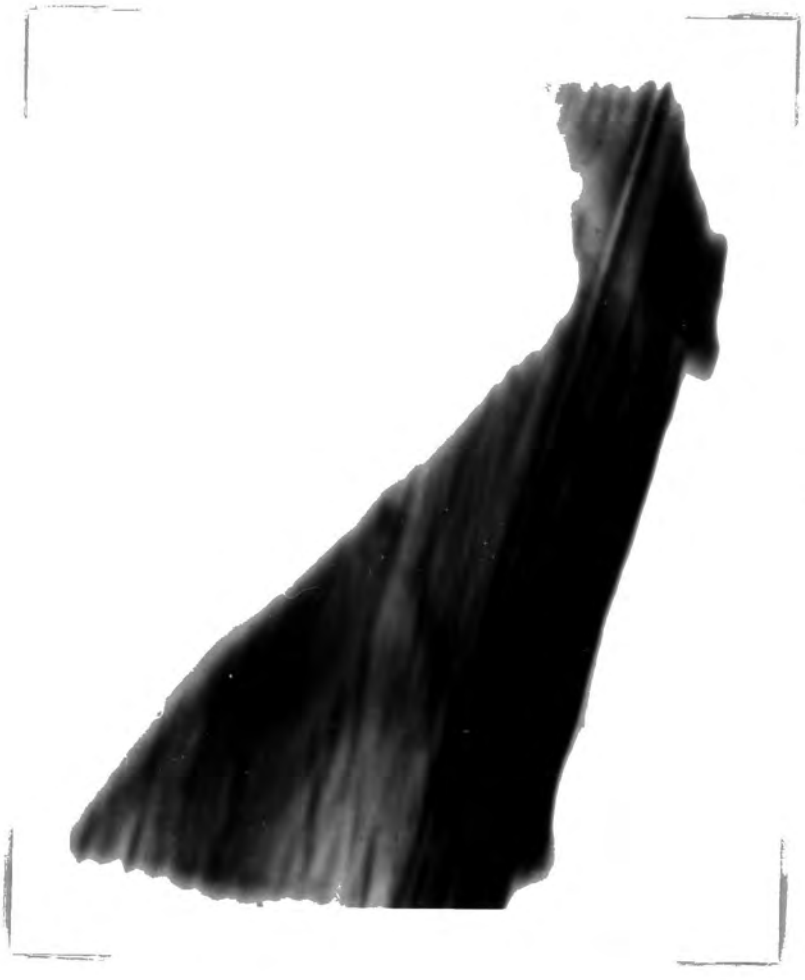

(f)

CHAPTER SIX

CONCLUSIONS

Nickel and copper crystals have been grown by the Czochralski technique in attempts to obtain dislocation-free crystals. X-ray topographs of nickel single crystals grown by this technique show high perfection but not zero dislocation density.

Domain motion in nickel under an applied magnetic field has been observed by Lang topography. Similar structures of domains reappear after the magnetic field has been removed.

Magnetization measurements show that the saturation depends on the orientation, and that the coercivity is independent of temperature at low temperature. Anomalous transmission topographs of copper crystals show dislocated and dislocation free regions.

In order to explain the unsuccessful attempt to grow dislocation free nickel crystals by reducing the neck radius, the model developed by Buckley-Golder and Humphreys has been extended. The effects of geometrical dimensions of the crystal, neck, seed and neck angle have been examined. As it has been found experimentally in copper and silver, reducing the neck radius has the effect of producing zero dislocation density. This condition is not however, applicable to growth of nickel single crystals. It is suggested that for low dislocation density growth of nickel single crystals, there should be a rapid increase in the crystal diameter around the

neck region. This technique has been reported by Murthy and Aubert (1981) who claims that dislocation free silicon can be grown by the use of flaired bulges in the neck. Simulation of this technique indicated that this method helps to reduce dislocation density. The technique should be applied to grow nickel in order to minimize the temperature gradient while it is assumed it will reduce the dislocation density. Further attempts to produce a nickel single crystal as free as possible from dislocation is important for the study of how the internal strain effects magnetic and mechanical properties.

APPENDIX A

Calibration for the coil used in domains movement experiment

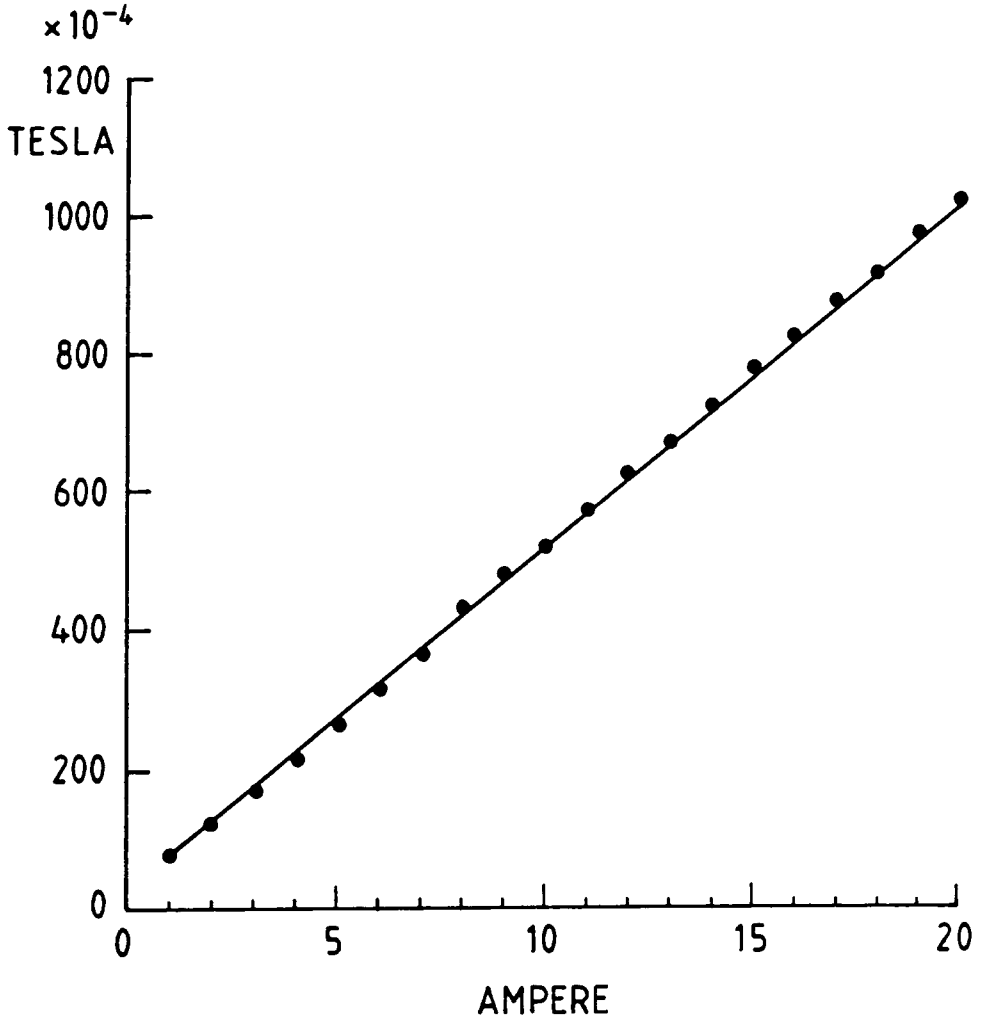

APPENDIX B

```
 10 REM  ************************************************************************
 20 REM                          MAIN PROGRAMME
 30 REM  ************************************************************************
 40 N=18:M=9
 50 DIM S(M,M),C(M,M),AX(N,N),BX(N),ST(M),INDEX(N,2),E$(10),TM(10),TS(10)
 60 DIM PIVOT(N),IPIVOT(N),A(M),R(M),L(M),XLL(M),HR(10),K(10),TA(10)
 70 DIM CONS(2,N),B(2,M),X(2,N),Z(200),TZ(2,100),DTZ(2,100),EM(10),TEST(N)
 80 @%=0:C%=37:FACTOR=2.0:CLS
 90 REM  ************************************************************************
100 REM                       Reading Input Parameters
110 REM  ************************************************************************
120 READ NELEM
130 FOR I=1 TO NELEM:READ E$(I),EM(I),K(I),TM(I),TA(I):NEXT
140    FOR I=1 TO M
150         READ XLL(I),R(I),ST(I)
160         A(I)=PI*R(I)^2
170         MX=MX+XLL(I)
180         L(I)=MX
190    NEXT I
200 REM  ************************************************************************
210 REM                       Changing Input Parameters
220 REM  ************************************************************************
230 PROCSELECT
240 PRINT:PRINT TAB(25);"SPACE BAR TO CONTINUE ":AA=GET
250 @%=0
260 PROCCHANGE
270 @%=0
280 PRINT:PRINT TAB(30);"PLEASE WAIT"
290 REM  ************************************************************************
300 REM                       Calculate the Biot Numbers
310 REM  ************************************************************************
320   FOR J=1 TO 2:FOR I=1 TO M
330         IF J=1 THEN HR=HRL
340         IF J=2 THEN HR=HRH
350         B(J,I)=HR*R(I)/K
360         X(J,I)=SQR(2*B(J,I))/R(I)
370   NEXT I:NEXT J
380 REM  ************************************************************************
390   FOR Q=1 TO 2
400  IF Q=1 THEN HR=HRL
410 IF Q=2 THEN HR=HRH
420   PROCCALC
430   NEXT Q
440 GOTO 460
450  PRINT TAB(20);"SPACE PAR TO CONTINUE ":AA=GET
460 CLS:PRINT:PRINT
470 PRINT TAB(20,4);" P   .....   DATA for  TM, TA, K, EM, HR"
480 PRINT TAB(20,6);" D   .....   DATA for  Radius, Length, Area"
490 PRINT TAB(20,8);" B   .....   Biot Numbers"
500 PRINT TAB(20,10);" C   .....   Constants"
510 PRINT TAB(20,12);" T   .....   Temperature Distribution "
520 PRINT TAB(20,14);" A   .....   ALL DATA"
530 PRINT TAB(20,16);" S   .....   STORE DATA IN A DISK FILE"
540 PRINT TAB(20,18);" E   .....   END"
550 A$=GET$:@%=0
560 IF A$="C" OR A$="c" THEN CLS:PROCT1:GOTO 450
570 IF A$="A" OR A$="a" THEN CLS:PROCT1:PROCT2:PROCT3:@%=0:PROCT4:PROCT5:GOTO 450
580 IF A$="C" OR A$="a" THEN CLS:PROCT1:GOTO 450
590 IF A$="T" OR A$="t" THEN CLS:PROCT2:GOTO 450
```

```
600 IF A$="B" OR A$="b" THEN CLS:PROCT3:GOTO 450
610 IF A$="E" OR A$="e" THEN 660
620 IF A$="D" OR A$="d" THEN CLS:PROCT4:GOTO 450
630 IF A$="P" OR A$="p" THEN CLS:PROCT5:GOTO 450
640 IF A$="S" OR A$="s" THEN CLS:PROCSTORE:GOTO 450
650 VDU7:GOTO 550
660 END
670 REM  *****************************************************************
680 REM                       END OF MAIN PROGRAMME
690 REM  *****************************************************************
700 DEF PROCT4
710 REM  *****************************************************************
720 PRINT TAB(10);"-------------------------------------------------------"
730PRINT TAB(10);"INDEX";TAB(20);"RADIUS";TAB(29);"LENGTH";TAB(40);"STEP";TAB(49);"Z
740PRINT TAB(10);"-------------------------------------------------------"
750 PRINT
760 FOR I=1 TO 4
770 PRINT TAB(0);"Crystal";:@%=0:PRINT TAB(11);"(";I;")";
780 @%=&20209:PRINT TAB(20);R(I);TAB(29);XLL(I);TAB(40);ST(I);TAB(48);L(I);
790 @%=&20409:PRINT TAB(58);A(I)
800 NEXT I
810 PRINT
820 I=5
830 PRINT TAB(0);"Neck ";:@%=0
840 PRINT TAB(11);"(";I;")";
850 @%=&20209:PRINT TAB(20);R(I);TAB(29);XLL(I);TAB(40);ST(I);TAB(48);L(I);
860 @%=&20409:PRINT TAB(58);A(I)
870PRINT
880 FOR I=6 TO 9
890 PRINT TAB(0);"Seed";:@%=0:PRINT TAB(11);"(";I;")";
900 @%=&20209:PRINT TAB(20);R(I);TAB(29);XLL(I);TAB(40);ST(I);TAB(48);L(I);
910 @%=&20409:PRINT TAB(58);A(I)
920 NEXT I
930 PRINT
940PRINT TAB(10);"-------------------------------------------------------"
950 ENDPROC
960 REM  *****************************************************************
970 DEF PROCCHANGE
980 REM  *****************************************************************
990 CLS:FOR I=1 TO 5:PRINT:NEXT
1000 PROCT4
1010 PRINT:PRINT:INPUT"                    INDEX  to be changed or ZERO to continue ";J
1020 IF J<0 OR J>9 THEN VDU7:GOTO 1010
1030 IF J=0 THEN 1130
1040 PRINT:PRINT
1050 PRINT TAB(5);"Old value for RADIUS is  ";R(J);TAB(40);
1060 INPUT"       Enter new value  ";R(J)
1070 PRINT TAB(5);"Old value for LENGTH is  ";XLL(J);TAB(40);
1080 INPUT"       Enter new value  ";XLL(J)
1090 PRINT TAB(5);"Old value for STEP is  ";ST(J);TAB(40);
1100 INPUT"       Enter new value  ";ST(J)
1110MX=0:FOR I=1 TO M:A(I)=PI*R(I)^2:MX=MX+XLL(I):L(I)=MX:NEXT I
1120 GOTO 990
1130ENDPROC
1140 REM  *****************************************************************
1150 DEF  PROCCALC
1160 REM  *****************************************************************
1170   FOR I=1 TO M:FOR J=1 TO M
1180        X1=X(Q,I)*L(J)
1190        PROCEXP
```

```
1200         C(I,J)=C:S(I,J)=S
1210    NEXT J:NEXT I
1220 FOR I=1 TO N:FOR J=1 TO N:AX(I,J)=0:NEXT J:NEXT I
1230 BX(1)=TM-TA:FOR I=2 TO N:BX(I)=0:NEXT I
1240:
1250 AX(1,1)=1
1260 :
1270 AX(2,1)=C(1,1): AX(2,2)=S(1,1): AX(2,3)=-C(2,1): AX(2,4)=-S(2,1)
1280 :
1290 AX(3,1)=K*A(1)*X(Q,1)*S(1,1)-HR*(A(1)-A(2))*C(1,1)
1300 AX(3,2)=K*A(1)*X(Q,1)*C(1,1)-HR*(A(1)-A(2))*S(1,1)
1310 AX(3,3)=-K*A(2)*X(Q,2)*S(2,1): AX(3,4)=-K*A(2)*X(Q,2)*C(2,1)
1320 :
1330 AX(4,3)=C(2,2): AX(4,4)=S(2,2): AX(4,5)=-C(3,2): AX(4,6)=-S(3,2)
1340 :
1350 AX(5,3)=K*A(2)*X(Q,2)*S(2,2)-HR*(A(2)-A(3))*C(2,2)
1360 AX(5,4)=K*A(2)*X(Q,2)*C(2,2)-HR*(A(2)-A(3))*S(2,2)
1370 AX(5,5)=-K*A(3)*X(Q,3)*S(3,2): AX(5,6)=-K*A(3)*X(Q,3)*C(3,2)
1380 :
1390 AX(6,5)=C(3,3): AX(6,6)=S(3,3): AX(6,7)=-C(4,3): AX(6,8)=-S(4,3)
1400 :
1410 AX(7,5)=K*A(3)*X(Q,3)*S(3,3)-HR*(A(3)-A(4))*C(3,3)
1420 AX(7,6)=K*A(3)*X(Q,3)*C(3,3)-HR*(A(3)-A(4))*S(3,3)
1430 AX(7,7)=-K*A(4)*X(Q,4)*S(4,3): AX(7,8)=-K*A(4)*X(Q,4)*C(4,3)
1440 :
1450 AX(8,7)=C(4,4): AX(8,8)=S(4,4): AX(8,9)=-C(5,4): AX(8,10)=-S(5,4)
1460 :
1470 AX(9,7)=K*A(4)*X(Q,4)*S(4,4)-HR*(A(4)-A(5))*C(4,4)
1480 AX(9,8)=K*A(4)*X(Q,4)*C(4,4)-HR*(A(4)-A(5))*S(4,4)
1490 AX(9,9)=-K*A(5)*X(Q,5)*S(5,4): AX(9,10)=-K*A(5)*X(Q,5)*C(5,4)
1500 :
1510 AX(10,9)=C(5,5): AX(10,10)=S(5,5): AX(10,11)=-C(6,5): AX(10,12)=-S(6,5)
1520 :
1530 AX(11,9)=K*A(5)*X(Q,5)*S(5,5)-HR*(A(6)-A(5))*C(5,5)
1540 AX(11,10)=K*A(5)*X(Q,5)*C(5,5)-HR*(A(6)-A(5))*S(5,5)
1550 AX(11,11)=-K*A(6)*X(Q,6)*S(6,5): AX(11,12)=-K*A(6)*X(Q,6)*C(6,5)
1560 :
1570 AX(12,11)=C(6,6):AX(12,12)=S(6,6): AX(12,13)=-C(7,6): AX(12,14)=-S(7,6)
1580 :
1590 AX(13,11)=K*A(6)*X(Q,6)*S(6,6)-HR*(A(7)-A(6))*C(6,6)
1600 AX(13,12)=K*A(6)*X(Q,6)*C(6,6)-HR*(A(7)-A(6))*S(6,6)
1610 AX(13,13)=-K*A(7)*X(Q,7)*S(7,6): AX(13,14)=-K*A(7)*X(Q,7)*C(7,6)
1620 :
1630 AX(14,13)=C(7,7): AX(14,14)=S(7,7): AX(14,15)=-C(8,7): AX(14,16)=-S(8,7)
1640 :
1650 AX(15,13)=K*A(7)*X(Q,7)*S(7,7)-HR*(A(8)-A(7))*C(7,7)
1660 AX(15,14)=K*A(7)*X(Q,7)*C(7,7)-HR*(A(8)-A(7))*S(7,7)
1670 AX(15,15)=-K*A(8)*X(Q,8)*S(8,7): AX(15,16)=-K*A(8)*X(Q,8)*C(8,7)
1680 :
1690 AX(16,15)=C(8,8): AX(16,16)=S(8,8): AX(16,17)=-C(9,8):AX(16,18)=-S(9,8)
1700 :
1710 AX(17,15)=K*A(8)*X(Q,8)*S(8,8)-HR*(A(9)-A(8))*C(8,8)
1720 AX(17,16)=K*A(8)*X(Q,8)*C(8,8)-HR*(A(9)-A(8))*S(8,8)
1730 AX(17,17)=-K*A(9)*X(Q,9)*S(9,8): AX(17,18)=-K*A(9)*X(Q,9)*C(9,8)
1740 :
1750 AX(18,17)=C(9,9): AX(18,18)=S(9,9)
1760 PROCMATRIX
1770 REM   FOR I=1 TO NX:CONS(Q,I)=BX(I):NEXT I
1780 :
1790 :
```

```
1800 Z%=0
1810 FOR Z=0 TO L(1) STEP ST(1)
1820 Z%=Z%+1:X1=X(Q,1)*Z:PROCEXP:Z(Z%)=Z
1830 TZ(Q,Z%)=TA+CONS(Q,1)*C+CONS(Q,2)*S
1840 DTZ(Q,Z%)=CONS(Q,1)*S*X(Q,1)+CONS(Q,2)*C*X(Q,1)
1850 NEXT Z
1860 IF Q=2 THEN TS(1)=Z%
1870 FOR Z=L(1) TO L(2) STEP ST(2)
1880 Z%=Z%+1:X1=X(Q,2)*Z:PROCEXP:Z(Z%)=Z
1890 TZ(Q,Z%)=TA+CONS(Q,3)*C+CONS(Q,4)*S
1900 DTZ(Q,Z%)=CONS(Q,3)*S*X(Q,2)+CONS(Q,4)*C*X(Q,2)
1910 NEXT Z
1920 IF Q=2 THEN TS(2)=Z%
1930 FOR Z=L(2) TO L(3) STEP ST(3)
1940 Z%=Z%+1:X1=X(Q,3)*Z:PROCEXP:Z(Z%)=Z
1950 TZ(Q,Z%)=TA+CONS(Q,5)*C+CONS(Q,6)*S
1960 DTZ(Q,Z%)=CONS(Q,5)*S*X(Q,3)+CONS(Q,6)*C*X(Q,3)
1970 NEXT Z
1980 IF Q=2 THEN TS(3)=Z%
1990 FOR Z=L(3) TO L(4) STEP ST(4)
2000 Z%=Z%+1:X1=X(Q,4)*Z:PROCEXP:Z(Z%)=Z
2010 TZ(Q,Z%)=TA+CONS(Q,7)*C+CONS(Q,8)*S
2020 DTZ(Q,Z%)=CONS(Q,7)*S*X(Q,4)+CONS(Q,8)*C*X(Q,4)
2030 NEXT Z
2040 IF Q=2 THEN TS(4)=Z%
2050 FOR Z=L(4) TO L(5) STEP ST(5)
2060  Z%=Z%+1:X1=X(Q,5)*Z:PROCEXP:Z(Z%)=Z
2070 TZ(Q,Z%)=TA+CONS(Q,9)*C+CONS(Q,10)*S
2080 DTZ(Q,Z%)=CONS(Q,9)*S*X(Q,5)+CONS(Q,10)*C*X(Q,5)
2090 NEXT Z
2100 IF Q=2 THEN TS(5)=Z%
2110 FOR Z=L(5) TO L(6) STEP ST(6)
2120 Z%=Z%+1:X1=X(Q,6)*Z:PROCEXP:Z(Z%)=Z
2130 TZ(Q,Z%)=TA+CONS(Q,11)*C+CONS(Q,12)*S
2140 DTZ(Q,Z%)=CONS(Q,11)*S*X(Q,6)+CONS(Q,12)*C*X(Q,6)
2150 NEXT Z
2160 IF Q=2 THEN TS(6)=Z%
2170 FOR Z=L(6) TO L(7) STEP ST(7)
2180 Z%=Z%+1:X1=X(Q,7)*Z:PROCEXP:Z(Z%)=Z
2190 TZ(Q,Z%)=TA+CONS(Q,13)*C+CONS(Q,14)*S
2200 DTZ(Q,Z%)=CONS(Q,13)*S*X(Q,7)+CONS(Q,14)*C*X(Q,7)
2210 NEXT Z
2220 IF Q=2 THEN TS(7)=Z%
2230 FOR Z=L(7) TO L(8) STEP ST(8)
2240 Z%=Z%+1:X1=X(Q,8)*Z:PROCEXP:Z(Z%)=Z
2250 TZ(Q,Z%)=TA+CONS(Q,15)*C+CONS(Q,16)*S
2260 DTZ(Q,Z%)=CONS(Q,15)*S*X(Q,8)+CONS(Q,16)*C*X(Q,8)
2270 NEXT Z
2280 IF Q=2 THEN TS(8)=Z%
2290 FOR Z=L(8) TO L(9) STEP ST(9)
2300 Z%=Z%+1:X1=X(Q,9)*Z:PROCEXP:Z(Z%)=Z
2310 TZ(Q,Z%)=TA+CONS(Q,17)*C+CONS(Q,18)*S
2320 DTZ(Q,Z%)=CONS(Q,17)*S*X(Q,9)+CONS(Q,18)*C*X(Q,9)
2330 NEXT Z
2340 IF Q=2 THEN TS(9)=Z%
2350 ENDPROC
2360 REM  ***************************************************************
2370 REM
2380 REM    Matrix inversion with solution of NX linear equations
2390 REM
```

```
2400 REM  ************************************************************
2410 DEF PROCMATRIX
2420 FOR I=1 TO N:TEST(I)=0:NEXT I
2430 FOR KK=1 TO N
2440 PIVOT=-1E+20
2450 FOR I=1 TO N
2460 J=I
2470FOR I1=1 TO N
2480IF TEST(I1)=J THEN 2520
2490NEXT I1
2500XX=AX(I,J)
2510 IF XX>PIVOT THEN PIVOT=XX:IX=I:JX=J
2520 NEXT I
2530TEST(KK)=IX
2540AX(IX,JX)=1/AX(IX,JX)
2550FOR L1=1 TO N:FOR M1=1 TO N
2560IF L1=IX OR M1=IX THEN 2580
2570 AX(L1,M1)=AX(L1,M1)-AX(L1,JX)*AX(IX,M1)/PIVOT
2580 NEXT M1
2590 NEXT L1
2600 FOR I=1 TO N
2610 J=JX
2620 IF I=J THEN 2640
2630 AX(I,J)=AX(I,J)/PIVOT
2640 NEXT I
2650 FOR J=1 TO N
2660 I=IX
2670 IF I=J THEN 2690
2680 AX(I,J)=-AX(I,J)/PIVOT
2690 NEXT J
2700 C%=C%-1:PRINT TAB(34,28);"          ";TAB(34,28);C%
2710NEXT KK
2720 FOR I=1 TO N
2730 S=0
2740 FOR J=1 TO N
2750 S=S+AX(I,J)*BX(J)
2760 NEXT J
2770 CONS(Q,I)=S
2780 NEXT I
2790ENDPROC
2800 REM  ************************************************************
2810 DEF PROCEXP
2820 REM  ************************************************************
2830 C=(EXP(X1)+EXP(-X1))/2
2840 S=(EXP(X1)-EXP(-X1))/2
2850 ENDPROC
2860 REM  ************************************************************
2870 DEF PROCT1
2880 REM  ************************************************************
2890 PRINT TAB(10);"----------------------------------------"
2900 PRINT TAB(18);"Low Radiation      High Radiation "
2910 PRINT TAB(10);"----------------------------------------":PRINT
2920 FOR I=1 TO N
2930  @%=0:PRINT TAB(10);"C";I;
2940  @%=&20509:PRINT TAB(20);CONS(1,I);TAB(40);CONS(2,I)
2950 NEXT I:PRINT
2960 PRINT TAB(10);"----------------------------------------"
2970 ENDPROC
2980 REM  ************************************************************
2990 DEF PROCT2
```

```
3000 REM  ********************************************************************
3010 PRINT TAB(1);"----------";TAB(20);"------------------";TAB(50);"----------------
3020  PRINT TAB(1);"  z (mm) ";TAB(25);" Tz (C)";TAB(50);"     DTz (C/mm)"
3030 PRINT TAB(20);" Low          High";TAB(52);"Low          High"
3040 PRINT TAB(1);"----------";TAB(20);"------------------";TAB(50);"----------------
3050 FOR I=1 TO TS(9):D1=Z(I):D2=Z(I+1)
3060 @%=&20109:PRINT TAB(3);Z(I);TAB(21);TZ(1,I);TAB(30);TZ(2,I);
3070 @%=&20409:PRINT TAB(50);DTZ(1,I);TAB(62);DTZ(2,I)
3080 IF D1=D2 THEN PRINT
3090 NEXT I
3100 PRINT TAB(1);"----------";TAB(20);"------------------";TAB(50);"----------------
3110ENDPROC
3120 REM  ********************************************************************
3130 DEF PROCT3
3140 REM  ********************************************************************
3150 PRINT TAB(5);"-------------------------------------------------"
3160 PRINT TAB(31);"BIOT NUMBERS"
3170 PRINT TAB(5);"-------------------------------------------------"
3180 PRINT TAB(20)" Low Radiation";TAB(40);"High Radiation"
3190 PRINT TAB(5);"                 -------------      ---------------"
3200 @%=&10509
3210 FOR I=1 TO 4:PRINT TAB(5);"Crystal   ";TAB(22);B(1,I);TAB(42);B(2,I):NEXT
3220 PRINT
3230 PRINT TAB(5);"Neck      ";TAB(22);B(1,5);TAB(42);B(2,5)
3240 PRINT
3250 FOR I=6 TO 9:PRINT TAB(5);"Seed      ";TAB(22);B(1,I);TAB(42);B(2,I):NEXT
3260 PRINT TAB(5);"-------------------------------------------------"
3270ENDPROC
3280 REM  ********************************************************************
3290DEF PROCSELECT
3300 REM  ********************************************************************
3310CLS:FOR I=1 TO 6:PRINT:NEXT
3320PRINT TAB(15);"Data are avialable for the following elements"
3330 PRINT:PRINT
3340FOR I=1 TO NELEM
3350PRINT TAB(25);I;"  .........      ";E$(I)
3360 PRINT
3370 NEXT
3380PRINT
3390INPUT "             Type the number of the element to be considered  ";NE
3400 PRINT:PRINT TAB(25);
3410 INPUT"Factor for high radiation";FACTOR
3420E$=E$(NE):K=K(NE):EM=EM(NE):TM=TM(NE):TA=TA(NE)
3430 RHU=5.66956E-14:REM W/mm^2/deg^4
3440 T1=TM+273.150:T2=TA+273.150
3450 HRL=RHU*EM*(T1^3+T1^2*T2+T1*T2^2+T2^3):REM W/mm^2/C
3460 HRH=HRL*FACTOR
3470 PROCT5
3480ENDPROC
3490 REM  ********************************************************************
3500DEF PROCT5
3510 REM  ********************************************************************
3520FOR I=1 TO 2:PRINT:NEXT
3530PRINT TAB(1);" Element";TAB(20);"TM";TAB(30);"TA";TAB(40);"Emissivity";TAB(58);"T
3540PRINT TAB(20);"(C)";TAB(30);"(C)";TAB(61);"(W/mm/C)":PRINT
3550PRINT TAB(1);E$;TAB(20);TM;TAB(30);TA;TAB(43);EM;TAB(60);K
3560PRINT:@%=&10509
3570PRINT TAB(3);"Heat-Radiation Coefficient  HR (LOW RADIATION)  = ";HRL;"  (W/mm^2/
3580PRINT TAB(20);"Factor for high radiation  =  ";FACTOR:PRINT:@%=&10509
3590PRINT TAB(3);"Heat-Radiation Coefficient  HR (HIGH RADIATION) = ";HRH;"  (W/mm^2/
```

```
3600ENDPROC
3610 DEF PROCSTORE
3620*SPOOL <DATA>
3630PROCT5
3640FOR I=1 TO 3:PRINT:NEXT I
3650PROCT4
3660FOR I=1 TO 3:PRINT:NEXT I
3670PROCT3
3680FOR I=1 TO 3:PRINT:NEXT I
3690PROCT1
3700FOR I=1 TO 3:PRINT:NEXT I
3710PROCT2
3720*SPOOL
3730ENDPROC
3740:
3790:
3800 REM  ***************************************************************
3830 REM         (1)  Element
3840 REM         (2)  Emissivity                 EM (at 0.65 micron)
3850 REM         (3)  Thermal Conductivity       K (W/mm/C)
3860 REM         (4)  Melting Temperature        TM (C)
3870 REM         (5)  Ambient Temperature        TA (C)
3880 DATA 6
3885 DATA "ALUMINIUM  AL",0.1,0.092,660.4,599.0
3890 DATA "Copper   Cu",0.1,0.352,1083,983
3900 DATA "Silicon  Si",0.4,0.032,1410,1279
3910 DATA "Nickel   Ni",0.45,0.0819,1453,1318
3920 DATA "Silver   Ag",0.05,0.377,961.9,872
3925 DATA "CHROMIUM Cr",0.35,0.066,1857,1684
3930 REM  ***************************************************************
3940 REM             DATA FOR CRYSTAL (LENGTH,RADIUS, STEP)
3950 DATA  3,1,1
3960 DATA  1,.9,.5
3970 DATA  1,.8,.5
3980 DATA  1,.7,.5
3990 REM             DATA FOR NECK (LENGTH, RADIUS, STEP)
4000 DATA  3,.2,1
4010 REM             DATA FOR SEED (LENGTH, RADIUS, STEP)
4020 DATA  1,.7,.5
4030 DATA  1,.8,.5
4040 DATA  1,.9,.5
4050 DATA  6,2,1
4060 REM  ***************************************************************
```

REFERENCES

Alourfi, M.S., (1986), M.Sc. Thesis, Durham University.

Aust, K.T., (1963), Page 452 in "The art and science of growing crystals", John Wiley 7 Sons Inc., London.

Authier, A., (1967), Adv. X-ray Anal. 10, 9.
(1970), in "Advances in Structure Research by Diffraction Methods", 3, 1. (ed. Briell and Mason.
(1978), in "Diffraction and Imaging Techniques in Material Science", 2, 715, North-Holland Publishing Co., Oxford.

Badrick, A.S.T. and Puttick, K.E. (1971), Phil. Mag., 23, 585.

Batterman, B. and Cole, H. (1964), Rev. Mod. Phys. 36, 681.

Brandle, C.D. (1980), Ch. 7 in "Crystal Growth", Pergamon press.

Brice, J.C. (1968), J. Crystal Growth, 2, 395.

Buckley-Golder, I.M., (1977), D. Phil. Thesis, Oxford University.

Buckley-Golder, I.M. and Humphreys, C.J. (1979), Phil. Mag. A. 39, 41.

Calverley, A., Davis, M. and Levew, R.F. (1957), J. Sci. Instrum., 34, 142.

Clark, G.F., Goddard, P.A., Nicholson, J.R.S., Tanner, B.K. and Wanklyn, B.M., (1983), Phil. Mag. B. 47, 307.

Crangle, J. (1977), "The magnetic properties of Solids", Edward Arnold, London.

Dash, W.C., (1959), J. Appl. Phys., 30, 459.

Deguchi, Y. and Kamigaki, N., Kashiwaya, K. and Kino, T. (1978), Japanese J. Appl. Phys. 17, 611.

Elbaum, C., (1960), Phil. Mag., 5, 669.

Esin, V.D., Krivonosova, A.S. and Fedorov, T.C., (1981), J. Crystal Growth, 52, 385.

Fehmer, H. and Uelhoff, W., (1972), J. Crystal Growth, 13/14, 257.

Fisher, G.R. and Barnes, P., (1984), J. Appl. Cryst. 17, 231.

Friedel, J. (1964), "Dislocations", Pergamon Press, New York.

Gow, K.V. and Chalmers, B. (1951), British J. Appl. Phys., 2, 300.

Green, J.R. (1977), Adv. X-ray Anal. 20, 221.

Hayashi, S., One, S. and Komatsu, H., (1983), J. Crystal Growth, 61, 698.

Hoon, S.R. and Willcock, S.N.M. (1988), J. Phys. E., 21, 772.

Hunt, G.H. (1954), Ph.D. Thesis, Durham University.

Jones, D.W., (1974), in "Crystal Growth Theory and Technique", 1, 233, Plenum press.

Jourdan, C., Rome-Talbot, D. and Gastaldi, J., (1972), Phil. Mag., 26, 1053.

Jourdan, C. and Gastaldi, (1979), Scripta Metallurgica, 13, 55.

Keck, P.H., Green, M. and Polk, M.L., (1953), J. Appl. Phys., 24, 1479.

Kittel, C. (1949), Rev. Mod. Phys., 21, 541.

Kohada, H., Yamada, K., Nakanish, H., Kobayashi, O., Saka, J. and Keigo, H. (1985), J. Crystal Growth, 71, 813.

Kuriyama , M., Boettinger, W.J. and Burdette, H.C., 1977, Adv. X-ray Anal. 20, 245.

Labushkin, V.G., Seleznev, V.N., Faleev, N.N. and Figin, V.A., (1978), Sov. Phys. Solid St., 20, 891.

Lang, A., (1958), J. Appl. Phys., 29, 597.
(1959), Acta Cryst. 29, 249.
(1963), Brit. J. Appl. Phys. 14, 904.
(1978), in "Diffractiona nd Imaging Technique in Material Science", 2, 623, North Holland Publishing Co., Oxford.

MacCormack, I.B., and Tanner, B.K., (1978), J. Appl. Cryst., 11, 40.

Murthy, M.R.L.N. and Aubert, (1981), J. Crystal Growth, 52, 391.

Nathans, R., Pickart, S.J., Alperin, H.A. and Brown, P.J. (1964), Phys. Rev. 136, 1641.

Nes, E., and Nøst, B., (1966), Phil. Mag., 13, 855.

Nøst, B., (1965), Phil. Mag., 11, 183.

Nøst, B. and Sorensen, G., (1966), Phil. Mag., 13, 1705.

Okkerse, B. (1959), Philips Tech. Rev., 21, 340.

Osaka, J., Kohada, H. and Kobayashi, T. (1984), Japanese J. Appl. Phys., 23, L195.

Paige, D.M. (1983), Ph.D. Thesis, Durham.

Polcarova, M. (1969), IEEE Transaction on Magnetics, 5, 536.

Polcarova, M. and Lang, A. (1962), Appl. Phys. Lett., 1, 13.

Shull, C.G., Strauser, W.A. and Wollan, E.O., (1951), Phys. Rev. 83, 333.

Stephenson, J.D., Kelha, V., Telli, M. and Tuomi, T., (1979), Phys. Stat. Sol. (a), 51, 93.

Sworn, C.H. and Brown, T.E. (1972), J. Crystal Growth, 15, 195.

Tanner, B.K., (1973), Z. Natur. 28a, 676.
(1976), "X-ray Diffraction Topography", Pergamon press.
(1977), Ch. 6 in "Surface and defect properties of solids", Billing and Sons Limited, London.

Tanner, B.K., Midgley, D. and Sefa, M. (1977), J. Appl. Cryst. 10, 281.

Tanner, B.K. and Bowen, D.K. (1980), eds. "Characterization of crystal growth defects by X-ray methods", Plenum Press, New York.

Tanner, B.K. and Cringean, J.K., (1987), Prog. Crystal Growth and Charact., 14, 403.

Tanner, B.K., Clark, G.F. and Safa, M., (1988), Phil. Mag. B., 57, 361.

Tetsue Inoue, (1976), Tran. JIM., 17, 227.

Van der Hart, A., and Uelhoff, W., (1981), J. Crystal Growth, 51, 251.

Wernick,, J.H. and Davies (1956), J. Appl. Phys., 27, 149.

Zasimchuk, I.K., Ovsienko, D.E. and Fomin, A.V., (1981), J. Crystal Growth, 52, 376.

Zulehner, W. (1983), J. Crystal Growth, 65, 189.